5-19-2010

A Multi-Wilkinson Power Divider Based Complex Reflection Coefficient Detector

James Roger Cooper
University of South Florida

A Multi-Wilkinson Power Divider Based Complex Reflection Coefficient Detector

by

James Roger Cooper

A thesis submitted in partial fulfillment
of the requirements for the degree of
Master of Science in Electrical Engineering
Department of Electrical Engineering
College of Engineering
University of South Florida

Major Professor: Thomas Weller, Ph.D.
Arthur David Snider, Ph.D.
Gokhan Mumcu, Ph.D.

Date of Approval:
May 19, 2010

Keywords: complex impedance, reflection detector, vector sensor, phase mixing, microstrip, permittivity, microwave, Wilkinson power divider, vector addition

I would like to dedicate this work to Michael Anthony Cooper, Matthew David Cooper, Joshua Aaron Cooper, and Josiah Samuel Cooper. I learned trigonometry from you, Mike. I learned complex numbers from you, Matt. I learned squares and square roots from you, Josh. I learned long division from you, Joe. If it were not for you taking the time to teach me when I was young, I would not have learned the joy I get from math today. You have made me who I am and gotten me to where I am today. This thesis is part yours.

Acknowledgments

I would like to thank Dr. Thomas M. Weller, Dr. James Leffew, and Dr. David Arthur Snider for their guidance and encouragement which helped me to grow both in my field and in maturity.

I would also like to thank all my friends among the 412 WAMI group, among the STARS fellows, and among the LifeQuest Community who helped me keep perspective and sanity.

Thanks to the National Science Foundation and the University of South Florida's Students, Teachers and Resources in Science (STARS) Fellowship for their financial support. Thanks to Rogers Corporation for supplying some of the materials necessary for completing this research.

Special thanks to Priscilla and David Cooper, Jim and Joy McInnes, and Bruce and Pam Blagg, who have each done their part in forming who I am today.

Finally, not enough thanks or gratitude can be given to Jennifer Lee Cooper, my beautiful and amazing wife, who has supported and put up with me for the past 3 years.

Table of Contents

List of Tables

List of Figures

A Multi-Wilkinson Power Divider Based

Complex Reflection Coefficient Detector

James Roger Cooper

Abstract

In the field of applied electromagnetics, there is always a need to create new methods for electrical characterization of materials, systems, devices, etc. Many applications need small and/or inexpensive equipment in performing these characterizations. The current method for making measurements of electrical properties at frequencies above 300 MHz, the transmission/reflection method, has severe limitations in these areas due large size and high price of the necessary equipment for making them. Therefore, presented herein is the conceptualization, design and analysis of a complex reflection coefficient detector which is relatively small, lightweight, and inexpensive.

A reflection coefficient detector is a device designed to isolate and compare a driving signal against a reflected signal. The reflection of the second signal is caused by a mismatch between the device's output impedance and a load's input impedance. By comparing the driving, or transmitted, signal and the reflected signal, the reflection coefficient at the boundary can be calculated. This coefficient can be used to calculate a load's input impedance, or a material's permittivity when combined with an attached probe's characteristics.

The reflection coefficient detector presented is built using microstrip and surface mount components. This makes the device comparably cheap. Its design is based upon five Wilkinson Power Dividers which lends itself to be scaled down for implementation in on-chip, and other micro- and nano- scale systems.

The accuracy and functionality of the device will be demonstrated through the use of S-Parameters measurements and CAD simulations. Through this, it will be shown that the device is a practical form of making measurements in applications which are otherwise restricted to certain limitations. In closing, applications, alternative designs and future advancements of the complex reflection coefficient detector will be discussed.

I. Introduction

A. Background

The electrical properties, such as permittivity and characteristic impedance, of a material, device or system can be invaluable pieces of information to know for a wide range of purpose. These purposes can include checking dielectrics for imperfections before implementing into a system; tracking changes, such as blood pressure, sodium concentration or other characteristics in biological systems[1]; or testing a transceiver's efficiency in a wireless system. Currently, the most effective way to measure a material's or a device's electrical properties is to treat the subject under test as a load with some impedance.

When making impedance measurements, there are several available options. The I-V method and Auto-Balancing bridge method give highly accurate measurements for a wide range of impedances [2]. Because of this and their relative simplicity, they are used in many applications[3]. However, both of these methods have two severe limitations. First, even in special designs of these methods, such as the RF I-V method, the accuracy drops significantly after 300 MHz [2] due to the size large electrical size of the components, leaving the designs to only be used at lower frequencies. Second, the methods require expensive equipment, such as oscilloscopes, for making measurements of complex impedances. The Auto-Balancing bridge and Resonance methods both solve

the complex impedance problem, and because of this are often used in making complex measurements[4]. However, they are still limited in their functionality at higher frequencies.

For complex impedance measurements in higher frequencies, the most practical method is the transmission/reflection, or network analysis, method. This method makes use of electromagnetic reflections on the boundary between the measurement device and an unknown load. By calculating the reflection coefficient at the boundary, the impedance of the unknown load can be derived. This method can work at a wide range of frequencies, but it is limited by the relatively large and expensive network analyzers necessary to perform it.

B. Motivation

In situations where electrical characteristic measurements are needed for high frequencies it is not always practical to use the network analyzers currently necessary for the transmission/reflection method. This equipment can be large, heavy and very expensive. Limited situations can include times where it is necessary to measure several different devices or materials simultaneously. In this case it could be very costly to have an individual network analyzer for each material or device. It can include situations where it is necessary to place impedance sensors on or in systems that need to be small and/or mobile; systems that cannot handle the size or weight of network analyzers. Sometimes there might be power limitations that do not allow for 120V AC source. In

such cases, a method is needed for making impedance measurements using cheap and/or compact means.

Therefore, presented herein is a method and design for making high frequency impedance measurements that is both compact and inexpensive. This method will utilize the transmission/reflection method without the usage of a network analyzer; and Wilkinson Power Dividers. It is built using microstrip board and surface mount resistors. This allows for a very cheap construction. The prototype will make use of a low dielectric microstrip board and a relatively low frequency of 2.5 GHz in order to keep the board large and easy to fabricate. However, by increasing the frequency, changing the dielectric constant, and changing the substrate design the device can be made many times smaller without decreasing its functionality or increasing its resource consumption.

C. Thesis Overview

Chapter II covers the previous designs of impedance measurement devices. Low frequency methods are covered first, followed by high frequency methods. Also, the issue of complex impedance versus real impedance will be covered.

Chapter III covers the novel design of the thesis. It will cover the device in two physical parts: first covering how the excitation and reflection signals are isolated; then covering how the isolated signals are mixed and measured to give the values necessary for calculating the reflection coefficient. It will conclude with the mathematics which will be used for calculating the complex impedance; and the computational hardware necessary for making those calculations.

Chapter IV will cover the design and analysis of an equation based model for a Wilkinson Power Divider Based Reflection Coefficient Detector. In this chapter, certain innate problems, which are found in the device's design, will be covered along with proposed solutions and corrections.

Chapter V will cover the design and analysis of two CAD simulation models for the Wilkinson Power Divider Based Reflection Coefficient Detector. The first will be an ideal transmission line model; and the second will be a parasitic microstrip transmission line model.

Chapter VI will cover and analyze the results of the first prototype. It will make comparisons to the equation-based model, ideal transmission line model and the parasitic microstrip model.

Chapter VII will conclude the thesis with possible designs and applications of the Wilkinson Power Divider Based Reflection Coefficient Detector. It will also cover future work that can be done with the device.

D. References Cited

[1] S Gabriely, R W Lau, C Gabriel, “The dielectric properties of biological tissues: II. Measurements in the frequency range 10 Hz to 20 GHz”, Physics in Medicine and Biology, vol. 41, no. 11, pp. 2251–2269, November 1996, ISSN 0031-9155

[2] Agilent Technologies, “Agilent Technologies Impedance Measurement Handbook”, December 2003, © 2000 Agilent Technologies 5950-3000, pp. 2-1 to 2-4

[3] L Angrisani, A Baccigalupi, A Pietrosanto, “A digital signal-processing instrument for impedance measurement”, IEEE Transactions on Instrumentation and Measurement, vol. 45, issue 6, pp. 930-934, December 1996, ISSN 0018-9456

[4] S M Huangt, A L Stottf, R G Greenf and M S Beck, “Electronic transducers for industrial measurement of low value capacitances”, Journal of Physics E: Scientific Instruments, vol. 21, no. 3, March 1988, pp. 242-250, ISSN 0022-3735

II. Previous Methods and Designs for Impedance Measurement

A. Impedance Measurement Methods and Designs

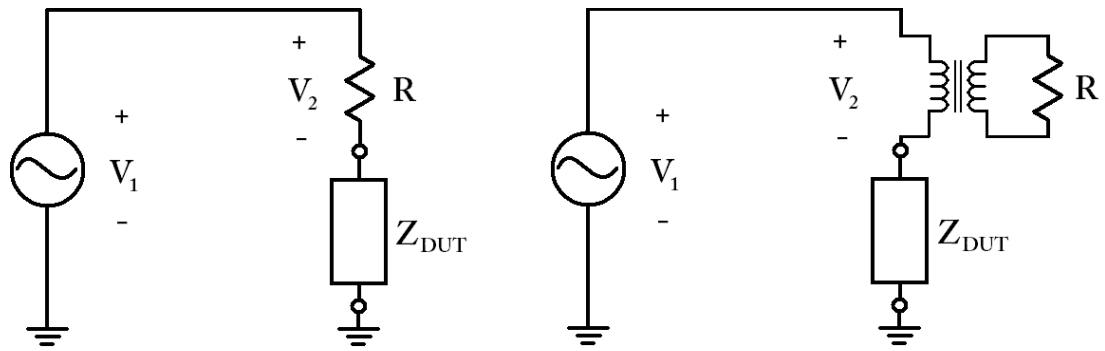

Figure 2-1 TWO BASIC I-V METHOD CIRCUITS General circuit diagram for using the I-V method to find an unknown impedance of ZDUT. (left) the simplified configuration and (right) the high accuracy configuration.

There are many options when making impedance measurements. For DC and low frequencies, the most simple is the IV method. This method is versatile and is used in many applications. This method uses a known resistance placed in series with an unknown impedance. Figure 2-1 shows two possible circuit designs for this method. If the value of the resistor, the voltage across the resistor, and the driving voltage are all known then the unknown impedance can be found by using

$$Z_{DUT} = R \times \left(\frac{V_1}{V_2} - 1\right) \quad \text{(e2.1)}$$

where R is the known resistor value, V_1 is the driving voltage, V_2 is the voltage across the known resistor, and Z_{DUT} is the unknown impedance. This method is exceptionally accurate across a wide range of impedances, especially when a transformer is used with the known resistor.

This method is limited, however, to lower frequencies due to the use of lumped element components and transformer, neither of which perform well in higher frequency ranges. The normal range is from DC to 300 MHz for the circuit design on the left, and up to 300 MHz* for the circuit design on the right in figure 2-2. The Bridge method, Resonance method, RF I-V method and Auto-Balancing Bridge method all have the same limitation in that they break down in the microwave range[2].

*For the transformer design, the lowest operating frequency is based upon the lowest functioning frequency for the transformer.

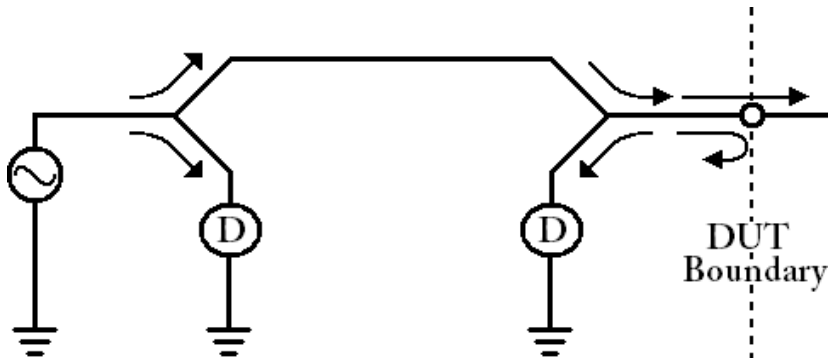

Figure 2-2 TRANSMISSION/REFLECTION METHOD A simple diagram of the Transmission reflection method being implemented. Pictured are a driving signal (left), two power splitters and two power detectors (center), and a boundary (right) which is usually connected to a probe or cable going to a material or device under test, MUT or DUT.

For higher frequencies, the most common method is the Network Analysis, or Transmission/Reflection, method [1][2]. In this method, a signal is transmitted to a DUT*. At the interface boundary, where the impedance detector connects to the DUT, part of the signal is reflected back due to a mismatch between the impedance detector's output impedance and the DUT's input impedance. This can be seen in figure 2-2, where the dotted line represents the boundary. The arrows represent the paths taken by the transmitted signal and the measured part of the reflected signal. The reflected signal is equal to

$$V_{in} \times \frac{Z_{bound} - Z_0}{Z_{bound} + Z_0} = V_{refl} \quad \text{(e2.2)}$$

*The DUT can either a device connected to the detector by a transmission line, or it can be a probe interface between the detector and a material being measured.

where V_{in} is the signal being sent to the boundary, Z_0 is the output impedance of the impedance detector, Z_{bound} is the input impedance of the DUT, and V_{refl} is the amount of the signal being reflected back. The ratio between V_{in} and V_{refl} is known as the reflection coefficient, denoted as Γ. It is calculated by

$$\frac{V_{refl}}{V_{in}} = \Gamma \tag{e2.3}$$

Since the output impedance is known, and the reflection is what is being measured, then the DUT's input impedance can be found by rewriting e2.2 and e2.3 as

$$Z_0 \times \left(\frac{1+\Gamma}{1-\Gamma}\right) = Z_{bound} \tag{e2.4}$$

While the drawback of the I-V method is frequency limitation, the drawback of the network analysis method is the equipment involved in making the measurements. In order to make them a network analyzer, such as those sold by Agilent and Anritsu, is needed. These network analyzers can range in cost from a few thousand dollars, up to several hundred thousand dollars depending upon frequency range, accuracy, and functionality. They are also of a considerable size, upwards from .2 m^3, and weight, upwards from 10 pounds. As stated in chapter I, this can be a major drawback in certain systems where cheap, small and/or light equipment is necessary for making the measurements.

B. Magnitude and Phase Detector Design

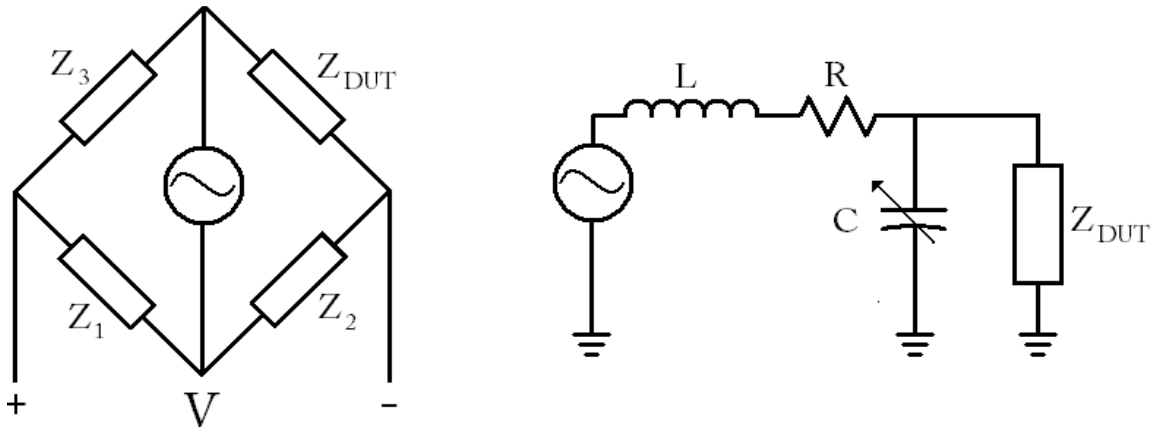

Figure 2-3 BRIDGE AND RESONANCE METHOD CIRCUITS Schematics of possible setups for the bridge method (left) and resonant method (right). Both methods are good when calculating complex impedances.

The I-V and Auto-Balancing bridge methods are simple designs which can easily return the value of an unknown resistance. Both require the use of two voltmeters, or a single two input voltmeter, which can be very cheap even for multiple decimal points of accuracy. If being controlled by a digital system such as a computer or micro-controller, the two methods could even be implemented through the use of A-to-D converters. These converters can also be cheap, starting around $7* for one of a few decimal points of accuracy.

*Price based on an AD7195: 4.8 KHZ, ULTRALOW NOISE, 24-BIT SIGMA-DELTA ADC as posted on www.analog.com as of 2010-03-16

However, when making complex impedance measurements, not just resistance measurements, it is necessary to know both the magnitude and the phase of the voltages. For this, a device such as an oscilloscope or other relatively expensive, large and/or heavy piece of equipment is needed. This is where the Bridge method and resonant method are very useful. Both methods employ the use of complex impedances, inductive and/or capacitive, as the known values.

The bridge method uses three known impedances in a combination of parallel and series with the unknown impedance, as shown in figure 2-3 (left). When the three known impedances are properly matched with the unknown there should be no voltage drop between the plus and minus terminals. When this happens the unknown impedance can be found by using

$$\frac{Z_2 \times Z_3}{Z_1} = Z_{DUT} \qquad \text{(e2.5)}$$

The resonant method, pictured in figure 2-3 (right), uses a series R-L with a tunable capacitor in order to match resonance with the unknown complex impedance. Neither method requires more than a simple voltmeter for calculating the unknown impedance.

The transmission/reflection method naturally incorporates the measurement of a complex impedance. Both V_{trans} and V_{refl} are traditionally found by using a directional coupler which isolates a proportional portion of each signal. The magnitude is found by taking the magnitudes of each signal and putting them into e2.3. The phase is traditionally calculated by taking the isolated signal portions and putting them through a

mixer. This will return a DC value which is related to the phase between V_{trans} and V_{refl}. This phase is the same as the phase of the reflection coefficient, Γ. Putting together the magnitude and the phase of the reflection into e2.4 will give the complex value of the impedance.

In using the transmission/reflection method, the part of the network analyzer which handles the isolation and mixing is known as the reflection coefficient detector. Figure 2-2 shows picture of an impedance detector, which is a reflection coefficient detector with power detectors and signal sources attached. The rest of a network analyzer is the signal generation, signal detection, central processing and user/device I/O, along with redundancy detectors in order to improve accuracy.

In order to build an impedance detector using the transmission/reflection method, a reflection coefficient detector must be built. In order to build a lightweight, low-cost, and low-profile alternative to a network analyzer it is necessary to build a lightweight, low-cost, and low-profile reflection coefficient detector. Chapter III will cover the conceptualization and design of such a device; and its analysis will be the focus of the rest of the thesis.

C. References Cited

[1] Agilent Technologies, “Agilent Technologies Impedance Measurement Handbook”, December 2003, © 2000 Agilent Technologies 5950-3000, pp. 2-1 to 2-4

[2] Agilent Technologies, “Agilent 8 Hints for Successful Impedance Measurements”, June 2000, © 2000 Agilent Technologies 5968-1947E, p. 2

III. A Multi-Wilkinson Power Divider Based Complex Reflection Coefficient Detector

The goal of this thesis is to present a method and design for high frequency impedance detection which is small, light weight and cost efficient. In order to do this, the transmission/reflection method will be implemented without the use of a network analyzer. Presented herein is the conceptualization and design of a circuit which will be used in place of a network analyzer as an impedance measurement device.

The mathematical techniques used to make the measurements will also be addressed in this chapter. The performance analysis of the ideal, simulated, and fabricated circuits will be covered in later chapters.

Until this device is placed inside a system, it is not an impedance detector. Instead, its primary function is as a reflection coefficient detector, or RCD. It is later in the processing stage that the reflection value is used to calculate electrical properties such as impedance.

The RCD is comprised of two sections. The first is for connecting to the driving signal source and the probing point. This section is also for isolating a portion of both the transmitted signal and the reflected signal for measurement. Herein it will be denoted as the isolation section of the RCD. The second section is for mixing, measuring and comparing the two isolated signal portions. Herein it will be denoted as the measurement and comparison section of the RCD.

A. Isolation

Figure 3-1 shows three basic designs for the isolation section of a reflection detector circuit. In the presented design the isolation will be done using two Wilkinson power dividers. The choice of Wilkinsons is due to recent research which shows both miniaturization[1][2] and wide bandwidth potential in these dividers[3][4]. It is also ideal as there is a high level of isolation between the two output ports. This is means that there will be very little signal leakage between the ports if a load mismatch is found at either port.

The first Wilkinson acts to equally split the excitation signal into two signals. One signal is sent towards the measurement and comparison section; the other signal to the second Wilkinson. The second Wilkinson sends the signal to the probing port where part of it will be reflected back from the material/device under test. This will be due to a mismatch in the output impedance of the detector and the input impedance of the material/device under test. A portion of the reflected signal will be sent to the measurement and comparison section, while the other portion is sent back to the driving source. This latter signal portion can be ignored as it will be mostly eaten up in the resistance of the excitation signal source. Figure 3-2 shows the isolation section with arrows representing the path of the signals.

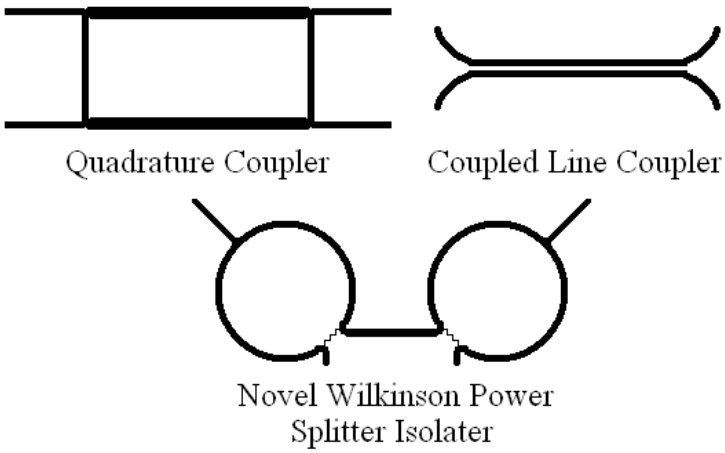

Figure 3-1 THREE DIRECTIONAL COUPLERS Three different circuit layouts for an isolation section. Each layout includes an input port, through port, isolated port and coupled port.

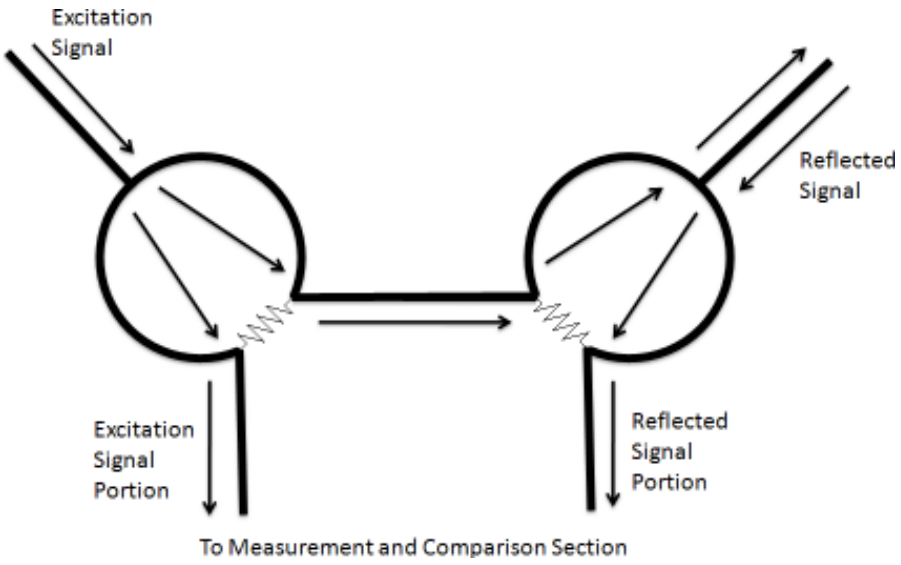

Figure 3-2 WILKINSON-BASED DIRECTIONAL COUPLER A circuit diagram of the two-Wilkinson isolation section. The arrows show the flow of a signal initiating at the excitation port and traveling to the measurement and comparing section of the detector.

B. Detection

Figure 3-3 shows the measurement and comparison section of the RCD circuit. Its purpose is to split and combine the isolated portions of the excitation and reflected signals coming from the isolation section. This is to find their magnitudes and the phase shift between them.

First the incoming signals are split into two parts, which is done by the two upper Wilkinsons power dividers. After the split, half of each signal portion is sent towards detectors; the portion of the excitation signal on the left, and the portion of the reflection signal on the right. By comparing these two signals the magnitude of the reflection coefficient can be calculated.

The center Wilkinson is used to combine a portion of the two signals coming from the upper Wilkinsons. The combined signal is sent to another detector. This combined signal, along with the portions of the excitation and reflected signals, is used to calculate the phase of the reflection coefficient.

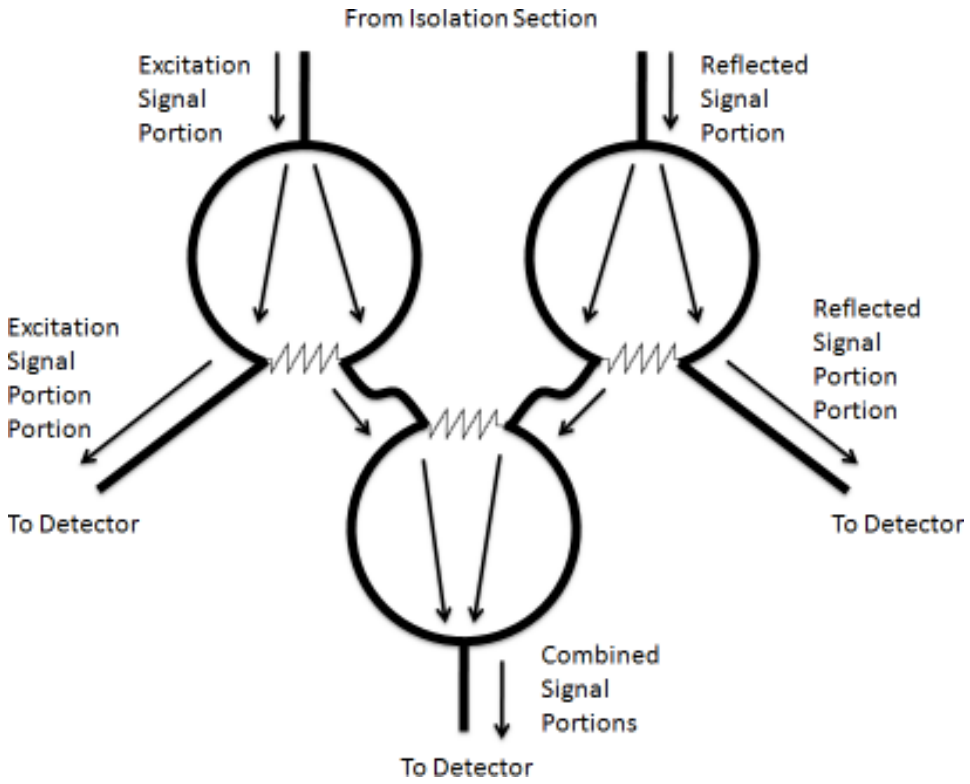

Figure 3-3 WILKINSON-BASED MEASUREMENT AND COMPARISON The circuit layout for the measurement and comparison section of the detector. This design consists of three Wilkinson power dividers which send a portion of the excitation signal, a portion of the reflected signal and a combination of these two signals to a set of detectors.

C. Magnitude and Phase Calculation

The magnitude of the reflection coefficient is found by comparing the magnitude of the excitation signal portion to that of the reflected signal portion. This can be done by using e2.3 where V_{refl} is the reflected portion, and V_{in} is the excitation portion. However, since the reflected signal traveled though two more arms of Wilkinson power dividers, each of which have at least -3 dB of gain, then the excitation signal in the equation needs

to be corrected. The correction factor should be equal to the loss of the two arms and interconnecting line. This extra path traveled can be seen in figure 3-2 where the signal to be reflected first travels to the right, then up one arm of the Wilkinson, gets reflected, and then travels down another arm of the Wilkinson to get to the measurement and comparison section. This correction will be further covered in chapter IV.

The phase of the reflection coefficient is found using the magnitudes of the portion of the excitation signal, the portion of the reflected signal, the combined signal portions, and the law of cosines.

$$a^2 + b^2 - 2\,a\,b \times \cos\Phi = c^2 \qquad \text{(e3.1)}$$

where a and b represent the magnitude of the excitation signal and reflected signal portions, respectively, c represents the magnitude of the combined signal portions, and Φ represents a phase shift between the signal portions.

The signals traveling out of each port are all sine waves with a time invariant peak amplitude and phase. Because of this, each signal can be thought of as a phasor. In figure 3-3, the central Wilkinson combines, or sums, the two signal portions, or phasors, and gives a unique signal with its own phase and peak amplitude. Since phasors work in a complex plane, instead of along a scalar line, the resulting signal will have a peak amplitude which is related to the peak amplitude and phase of the two signal portion portions. Figure 3-4 shows how both the magnitude and the phase play a role in the addition of phasors.

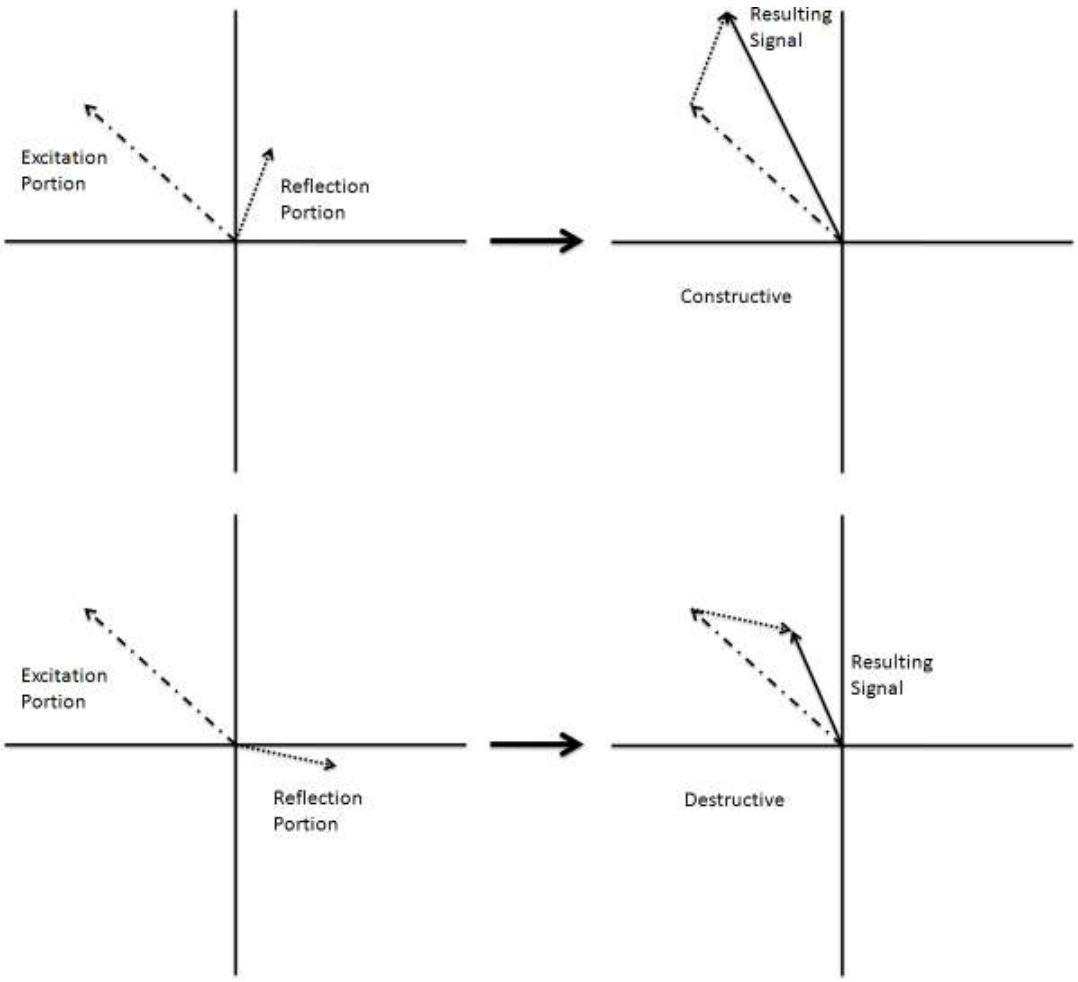

Figure 3-4 PHASOR MATH Two examples of phasor addition. The Excitation signal portion and reflected signal portion are added together, resulting in a signal with a unique phase and peak amplitude. On the top is a representation of constructive addition; the bottom shows destructive.

The two original phasors and the resulting phasor can be thought of as creating a triangle, as shown in figure 3-5. The angle, ϕ, is the angle between the excitation signal and the reflected signal portions. The angle of the resulting signal, ϕ', has a phase which

is the compliment of ϕ. This angle can be found taking e3.1 and rewriting it in terms of ϕ,

$$\Phi = \cos^{-1}\left(\frac{a^2 + b^2 - c^2}{2\,a\,b}\right) \quad \text{(e3.2)}$$

If *a* is considered to be the magnitude of the portion of the excitation signal, *b* is considered to be the magnitude of the portion of the reflection signal, and *c* is considered to be the magnitude of the combination of the portions, then

$$\Phi = 180 - \cos^{-1}\left(\frac{a^2 + b^2 - c^2}{2\,a\,b}\right) \quad \text{(e3.3)}$$

shows the phase shift between the two portions, or the phase of the reflection coefficient.

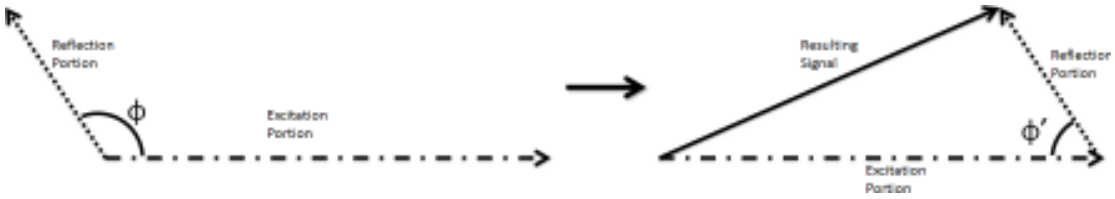

Figure 3-5 EXCITATION, REFLECTION, AND COMBINATION TRIANGLES A representation of the phasors from figure 3.C1 left being represented as a triangle. The phase, Φ, is the compliment of the phase between the two phasors, a and b. This phase can be found if the magnitudes of a, b and c are known.

In figure 3-5, it can be seen that the signal portion portions must travel down one more Wilkinson arm when being combined than when traveling straight to their respected detectors. Because of this, compensation is necessary in e3.3 in order to give the actual angle. This compensation is dependent on the length of connection lines and efficiency of the splitters. This compensation will be covered in chapter IV.

D. Computational Considerations

As stated above, this circuit is not stand alone, but is only the front end for an impedance detector. It only serves to isolate and combine the signals. Three additional parts are needed in order to make this device a full replacement for an impedance measurement device.

The first part is a signal source, or driver. Ideally, this would be a surface mount, voltage controlled oscillator. Its role will be to generate the signal which will be split, reflected, isolated and measured.

The second part needed are three power detectors. These power detectors are connected to the three outputs of the measurement and comparison section of the device. They act to give a DC voltage which is proportional to the signal incident at each port. Ideally these would be surface mount diode detectors, whose price could widely range based upon required accuracy and range.

The third part is the microcontroller. The DC signals from the detectors must be processed somewhere. The local oscillator must be controlled by some means. And, the data gathered and processed must be interfaced with some peripheral system, such as a

computer, a network, humans, etc. Ideally, this microcontroller would be a series of surface mount chips.

For the purpose of testing the functionality of this device, the signal source will be simulated using Agilent's Advanced Design System and an equation based simulator designed in National Instrument's LabView. This is also the program that will serve to do all data processing and calculations.

E. References Cited

[1] Chao-Wei Wang, Kuen-Hua Li, Chin-Jay Wu, and Tzyh-Ghuang Ma, "A Miniaturized Wilkinson Power Divider with Harmonic Suppression Characteristics Using Planar Artificial Transmission Lines", Asia-Pacific Microwave Conference 2007, Dec 11-14 2007

[2] Liang-Hung Lu, Member, IEEE, Yu-Te Liao, and Chung-Ru Wu, A Miniaturized Wilkinson Power Divider With CMOS Active Inductors", IEEE Microwave and Wireless Components , vol. 15, no. 11, pp. 775-777, November 2005

[3] H Oraizi, A -R Sharifi, "Design and optimization of broadband asymmetrical multisection Wilkinson power divider", IEEE Transactions on Microwave Theory and Techniques, vol. 54, issue 5, pp. 2220 – 2231, May 2006

[4] L Chiu, T Y Yum, Q Xue, C.H. Chan, "A wideband compact parallel-strip 180/spl deg/ Wilkinson power divider for push-pull circuitries", vol.16, issue 1, pp. 49-51, January 2006

IV. Equation Based CAD Design and Analysis

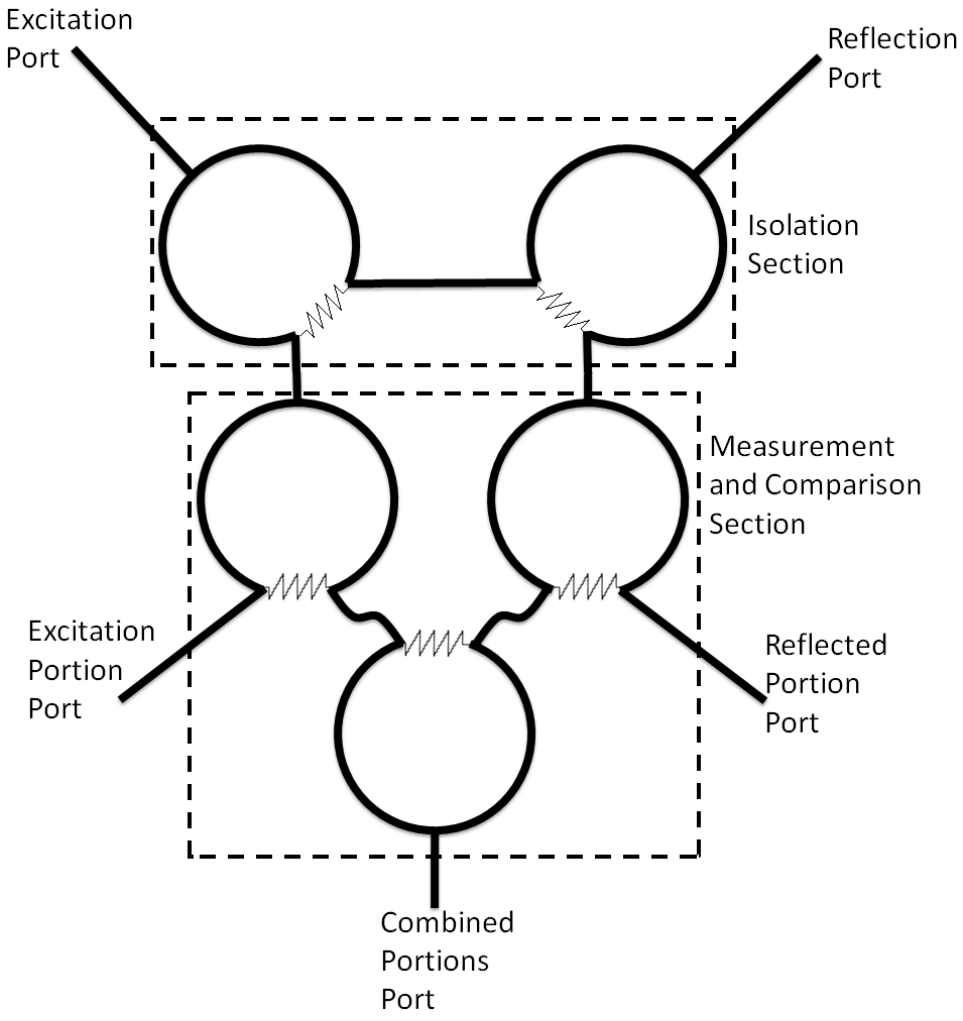

Figure 4-1 COMPLETE W-BCRCD CIRCUIT Complete Wilkinson Power Divider Based Reflection Coefficient Detector, or W-BCRCD, circuit design with both an isolation section, and a measurement and comparison section.

Presented previously have been the driving motivation and concept behind the novel design of an RCD. Presented herein are the design and testing of that device. This detector includes both the isolation section, and the measurement and comparison section conceptualized in chapter III. The complete Wilkinson power divider based complex reflection coefficient, or W-BCRCD, can be seen in Figure 4-1.

The design process was conducted using Agilent's Advanced Design System (ADS). An operating frequency of 2.5 GHz, and microstrip with a low relative permittivity have been chosen in order to keep the W-BCRCD large enough for ease of prototyping. Chapters V and VI will cover the CAD design of the circuit, fabrication and testing. Chapter VII will cover other methods of circuit design.

A. Ideal Equation-Based Simulation

The initial design is built using equation-based elements and the ideal characteristics of a Wilkinson power divider. These characteristics include: input and outputs matched to a 50 ohm line; -3 dB of gain between the input and the outputs; and near complete isolation between the output ports. In order to keep the isolation large, but still model a realistic Wilkinson, an isolation of 60 dB will be used. It also includes 90 degrees of phase shift between the input and outputs. Figure 4-2 shows an equation-based model built upon the ideal characteristics.

Figure 4-3 shows the detector design using equation-based Wilkinson models. Similar to Figure 4-1, the two Wilkinson models on top comprise the isolation section, and the three Wilkinson models on the bottom are the measurement and comparison

section. From this point forward, port 1 will be associated with the excitation signal input; port 2 will be the excitation signal portion output; port 3 will be the combined portions output; port 4 will be the reflected signal portion output; and port 5 will be the reflection port which connects to the device/material being tested.

Table T4-1 shows the S-Parameters to ports 2, 3, 4 and 5 from port 1. This is the same as the gain from port 1 to the other ports. Because of the symmetry of the design S(2,1) is the same as S(4,5), S(3,1) is the same as S(3,5), and S(4,1) is the same as S(2,5).

From the table it can be seen that ports 2 and 3 receive a different amount of power from port 1. As mentioned in chapter III, it is necessary for ports 2 and 3 to receive the same amount of power from port 1 in order for e3.3 to apply. The same holds true for ports 4 and 3 receiving power from port 5.

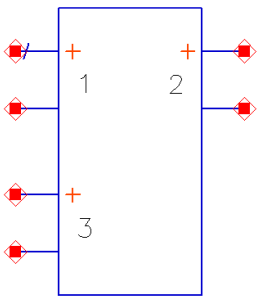

S3P_Eqn
S3P1

S[1,1]=dbpolar(-60,180)	S[3,1]=dbpolar(-3,90)
S[1,2]=dbpolar(-3,90)	S[3,2]=dbpolar(-60,180)
S[1,3]=dbpolar(-3,90)	S[3,3]=dbpolar(-60,180)
S[2,1]=dbpolar(-3,90)	Z[1]=50
S[2,2]=dbpolar(-60,180)	Z[2]=50
S[2,3]=dbpolar(-60,180)	Z[3]=50

Figure 4-2 EQUATION BASED WILKINSON POWER DIVIDER MODEL An Equation based, ideal Wilkinson power divider represented in Agilent's Advanced Design System. 'dbpolar(m,n)' converts an input of decibels (m) and degrees (n) into a complex value.

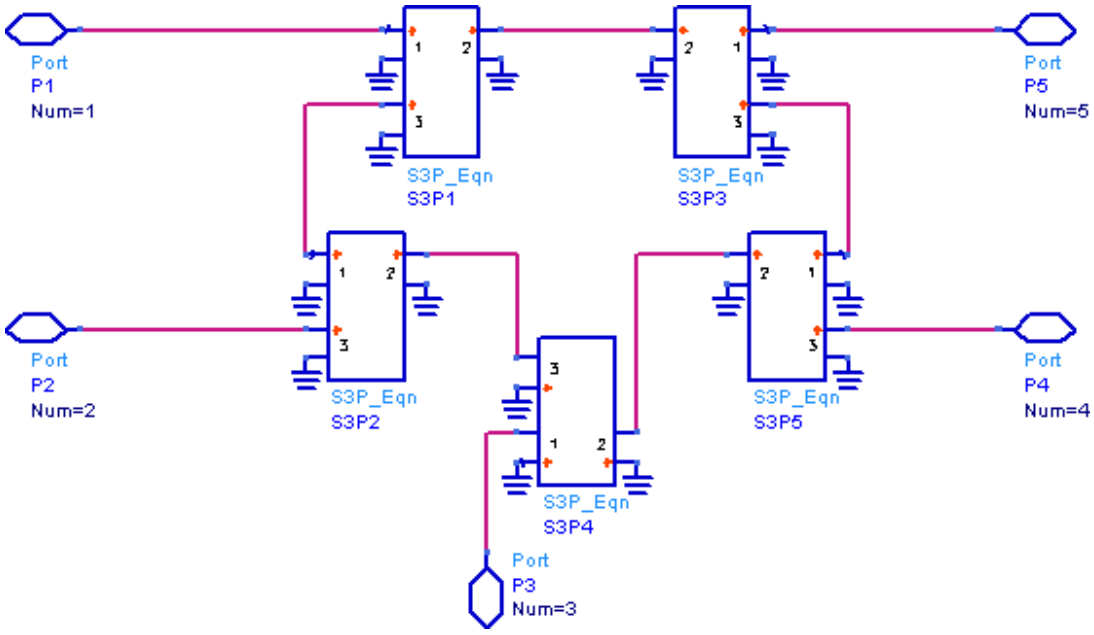

Figure 4-3 EQUATION BASED W-BCRCD SCHEMATIC Equation-Based, ideal Wilkinsons dividers linked together to create an ideal model for the W-BCRCD.

Table T4-1 EQUATION-BASED W-BCRCD S-PARAMETERS S-Parameters for the ideal equation-based W-BCRCD. These parameters are represented in dB/degrees.

freq	S(2,1)	S(3,1)	S(4,1)	S(5,1)
2.500 GHz	-6.000 / 180.000	-9.009 / -90.000	-66.004 / -1.403E-14	-5.996 / 180.000

B. Phase Compensation

Table T4-1 shows that there is a greater gain from port 1 to port 2 than there is from port 1 to port 3. E3.3 assumes that ports 2 and 4 receive the same amount of power from their sources as does port 3. Therefore, a correction needs to be made to the values at ports 2 and 4 for e3.3 to work. The compensation for port 2 can be found by

$$\frac{S_{31}}{S_{21}} = \alpha \qquad \text{(e4.1)}$$

where S_{21} is the gain from port 1 to port 2, S_{31} is the gain from port 1 to 3, and α is the port 2 compensation amount.

Because of the symmetry of the design, e4.1 can also be used for the compensation at port 4. This assumption can only be used in the CAD stage of the design as perfect symmetry is realized. In practice a separate compensation value will be needed for ports 2 and 4. The port 4 compensation can be found by

$$\frac{S_{31}}{S_{41}} = \beta \qquad \text{(e4.2)}$$

where S_{31} is the gain from port 5 to port 4, S_{41} is the gain from port 5 to 3, and β is the port 4 compensation amount. These compensations will be used in e3.3 in order to ensure that all three ports are receiving the same ratio of power from their respective sources.

When the compensation is applied, e3.3 becomes

$$\Phi = 180 - \cos^{-1}\left(\frac{(\alpha \times a)^2 + (\beta \times b)^2 - c^2}{2(\alpha a)(\beta b)}\right) \quad \text{(e4.3)}$$

With the assumption of symmetry, α is equal to β and e4.3 can be rewritten as

$$\Phi = 180 - \cos^{-1}\left(\frac{(\alpha \times a)^2 + (\alpha \times b)^2 - c^2}{2\alpha^2(a)(b)}\right) \quad \text{(e4.4)}$$

C. Magnitude Compensation

According to e2.3, if port 5 is left open then the magnitude of the signal found at port 2 should be equal to that at port 4 due to complete reflection, or a reflection coefficient of 1. However, because the excitation signal travels through two extra Wilkinson dividers before it gets reflected, the power at port 4 is less. This can be seen in tables T4-2 and T4-3 where in both cases the signal at port 4 is about 6dB less than that at port 2.

Table T4-2 EQUATION-BASED W-BCRCD S-PARAMETERS WITH SHORT CIRCUIT TERMINATION The ratio of power received at ports 2, 3, and 4 from an excitation signal at port 1 due to short circuit termination at port 5.

freq	S(2,1)	S(3,1)	S(4,1)
2.500 GHz	0.501 / 180.000	0.532 / -90.000	0.251 / 180.000

Table T4-3 EQUATION-BASED W-BCRCD S-PARAMETERS WITH OPEN CIRCUIT TERMINATION The ratio of power received at ports 2, 3 and 4 from an excitation signal at port 1 if due to open circuit termination at port 5.

freq	S(2,1)	S(3,1)	S(4,1)
2.500 GHz	0.501 / 180.000	0.177 / -90.000	0.252 / -1.404E-14

By analyzing figure 4-1, it can be seen that this extra -6 dB of gain comes from the path from port 1 to port 5. In order to make an accurate measurement of the reflection coefficient's magnitude, a compensation for the power at port 4 is needed. The compensation can be found by

$$\frac{S_{21}}{S_{45}S_{51}} = \gamma \tag{e4.4}$$

where S_{51} is the gain from port 1 to port 5, S_{45} is the gain from port 5 to port 1, S_{21} is the gain from port 1 to port 2, and γ is the compensation amount. Plugging this into e2.3 yields

$$\Gamma = \frac{\gamma \times S_{41}}{S_{21}} \tag{e4.5}$$

This compensation, along with the phase compensation of the last section, will be used in calculating the results for the equation-based model of the detector.

D. Simulation Results

For visualizing the accuracy of the reflection coefficient detector, the results will be graphed on a Smith chart. This is done so that the accuracy can be seen across the full range of possible reflections*. X and Y will represent the real and imaginary parts of the actual reflection coefficient at port 5 respectively; and Z will represent the error between the actual value and the reflection coefficient's perceived value; that is the value which would be calculated from the power found at the outputs. The reflection coefficient phase error will be shown in degrees. The reflection coefficient magnitude error will use the form

$$\left| \, |\Gamma|_{real} - |\Gamma|_{meas} \, \right| = \, |\Gamma|_{error} \tag{e4.6}$$

where $|\Gamma|_{meas}$ is the detector's perceived magnitude of the reflection coefficient, $|\Gamma|_{real}$ is the actual magnitude of the reflection coefficient, and $|\Gamma|_{error}$ is the magnitude error of the reflection coefficient. The reflection coefficient total error will be measured using a vector error found by the form

$$\left| \, |\Gamma|_{meas} \, \times e^{i \times \Phi_{meas}} - \, \Gamma_{real} \, \right| = |\vec{\Gamma}|_{error} \tag{e4.7}$$

* The full range of reflection is from a reflection coefficient of magnitudes 0 to 1, and phase -180 to 180 degrees. This is using the assumption that all devices and/or materials which will be tested are passive.

where $|\Gamma|_{meas}$ is the measured magnitude of the reflection coefficient, Φ_{meas} is the measured phase of the reflection coefficient, Γ_{real} is the complex value of the actual reflection, and $|\vec{\Gamma}|_{error}$ is the vector error. For a more complete definition of the vector error and what it represents see Appendix A.

Figures 4-4a and 4-4b both show the phase error found in the detector. The lower half of the Smith chart is located at or near 0 degrees of error. The upper half spirals upward from 0 to 360 degrees of error. This error is due to the fact that the law of cosines is only capable of returning an absolute value for the phase of the reflection coefficient. The worst-case error occurs when the reflection is 90 degrees and the calculated value is -90 degrees. This problem will be addressed, along with possible solutions, in the following section.

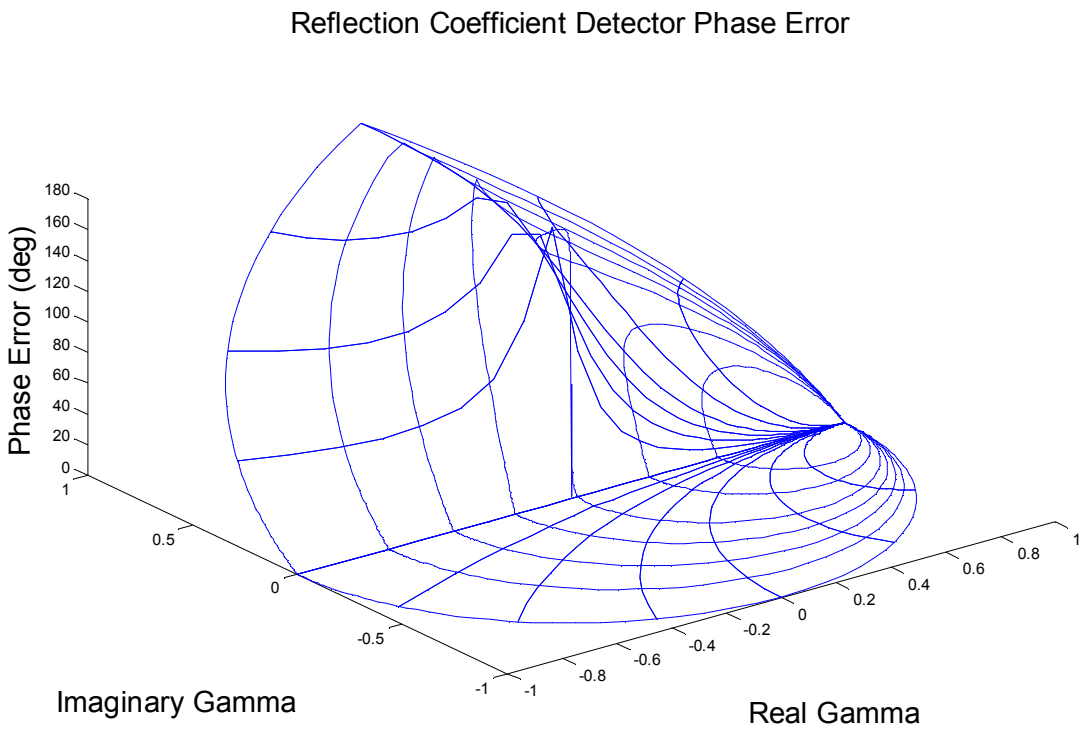

Figure 4-4a W-BCRCD PHASE ERROR A The phase error of the reflection coefficient detector using equation-based Wilkinson dividers plotted in the Γ plane.

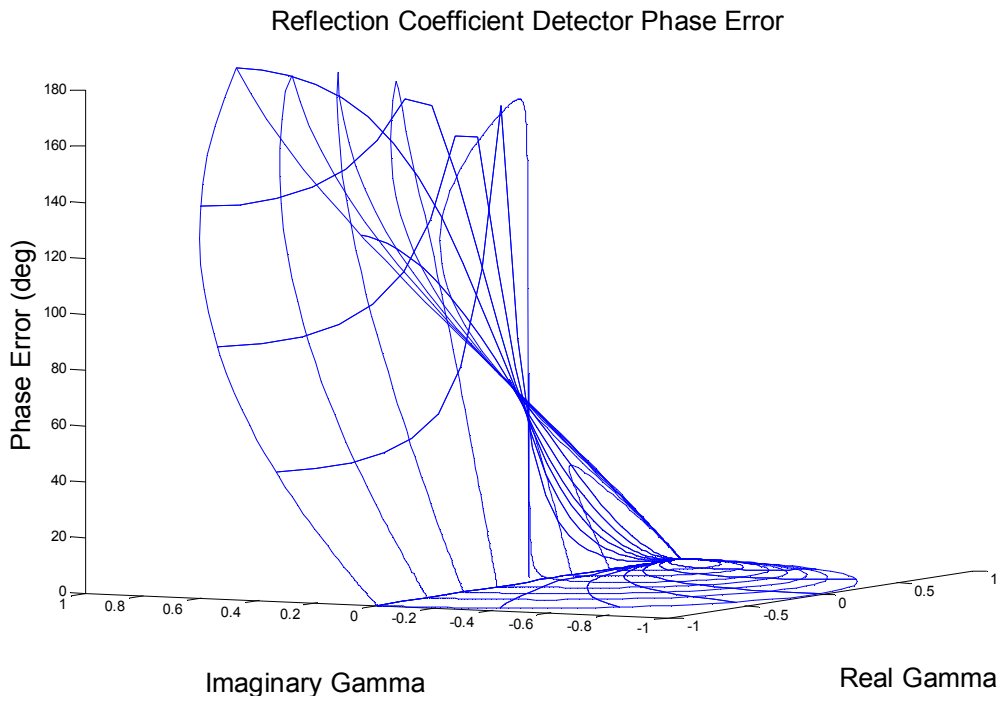

Figure 4-4b W-BCRCD PHASE ERROR B The phase error of detector using equation-based Wilkinson dividers plotted in the Γ plane. This is the same graph from figure 4-4a shown at a different angle.

Figures 4-5a and 4-5b both show the magnitude error found in the detector. The maximum error occurs at the 0 reflection point, and has a magnitude of 0.002. This error is due to the fact that the Wilkinson dividers do not give perfect isolation. So, even if there is no signal being reflected back at port 5, some of the signal from port 1 still leaks through to port 4.

There is also a phase based error which can be seen. Figure 4-5 shows that at +90 and – 90 degrees there is very little error, and the error is at its maximum at 0 and 180 degrees. As will be shown in chapter V, this phase based error is strongly correlated with the amount of isolation found between ports 1 and 4.

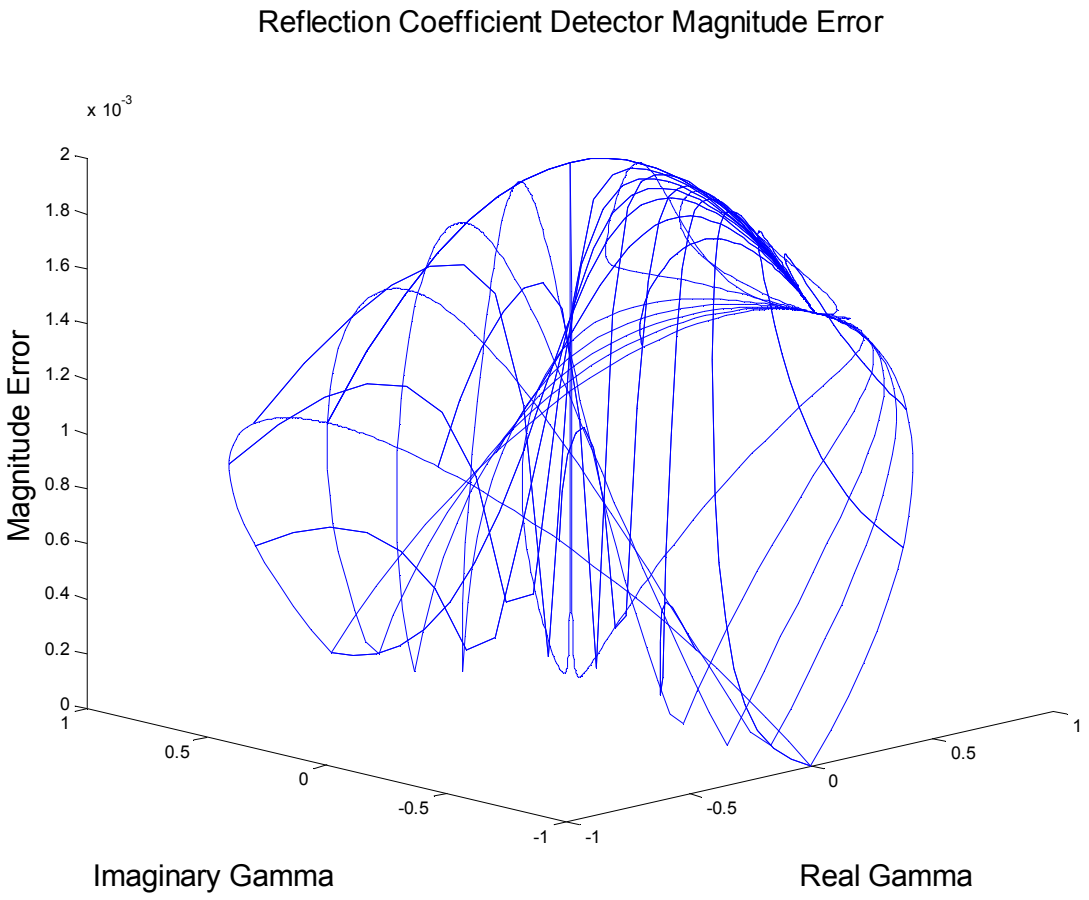

Figure 4-5a W-BCRCD MAGNITUDE ERROR A The magnitude error of the reflection coefficient detector using equation-based Wilkinson dividers plotted in the Γ plane.

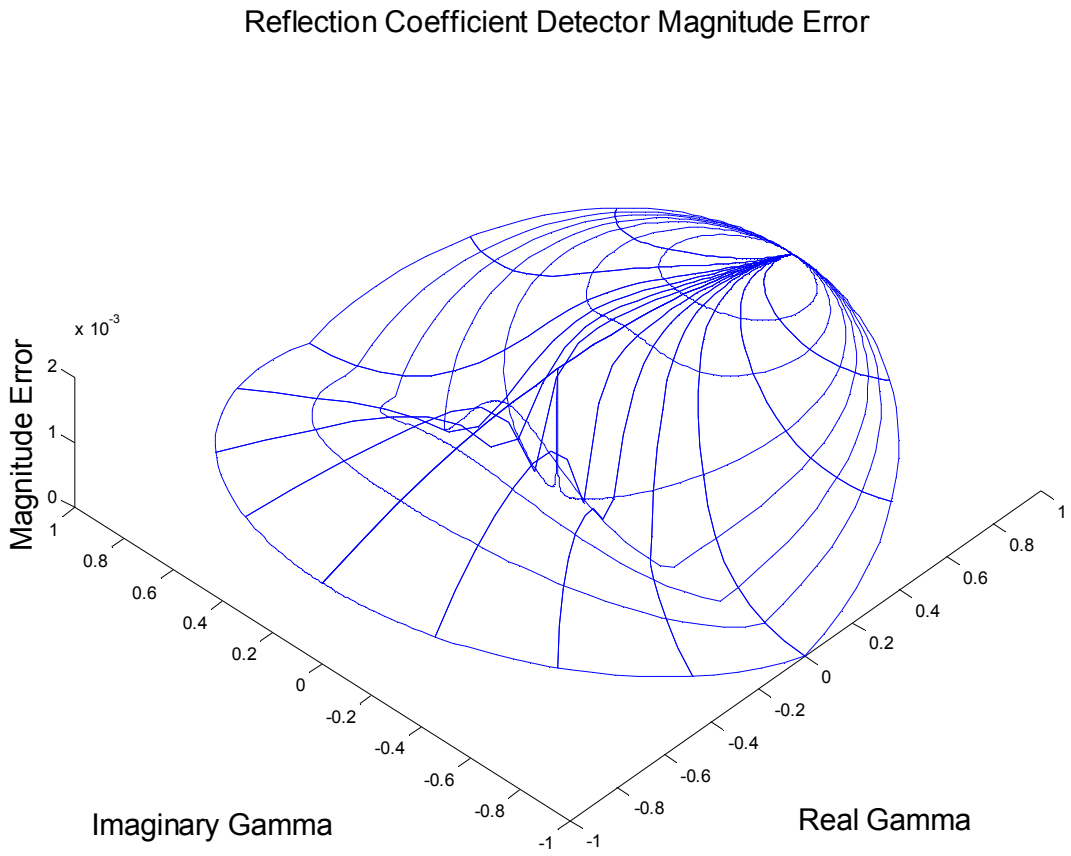

Figure 4-5b W-BCRCD MAGNITUDE ERROR B The magnitude error of detector using equation based Wilkinsons plotted in the Γ plane. This is the same graph from figure 4-5a shown at a different angle.

Figures 4-6a and 4-6b both show the vector error found in the detector. As it can be seen, the lower half of the Smith chart has a very low error, while the upper half has a phase dependent error. Since the error of the magnitude is very small, and the error due to the law of cosines shortcoming is very high, only the phase error can be seen.

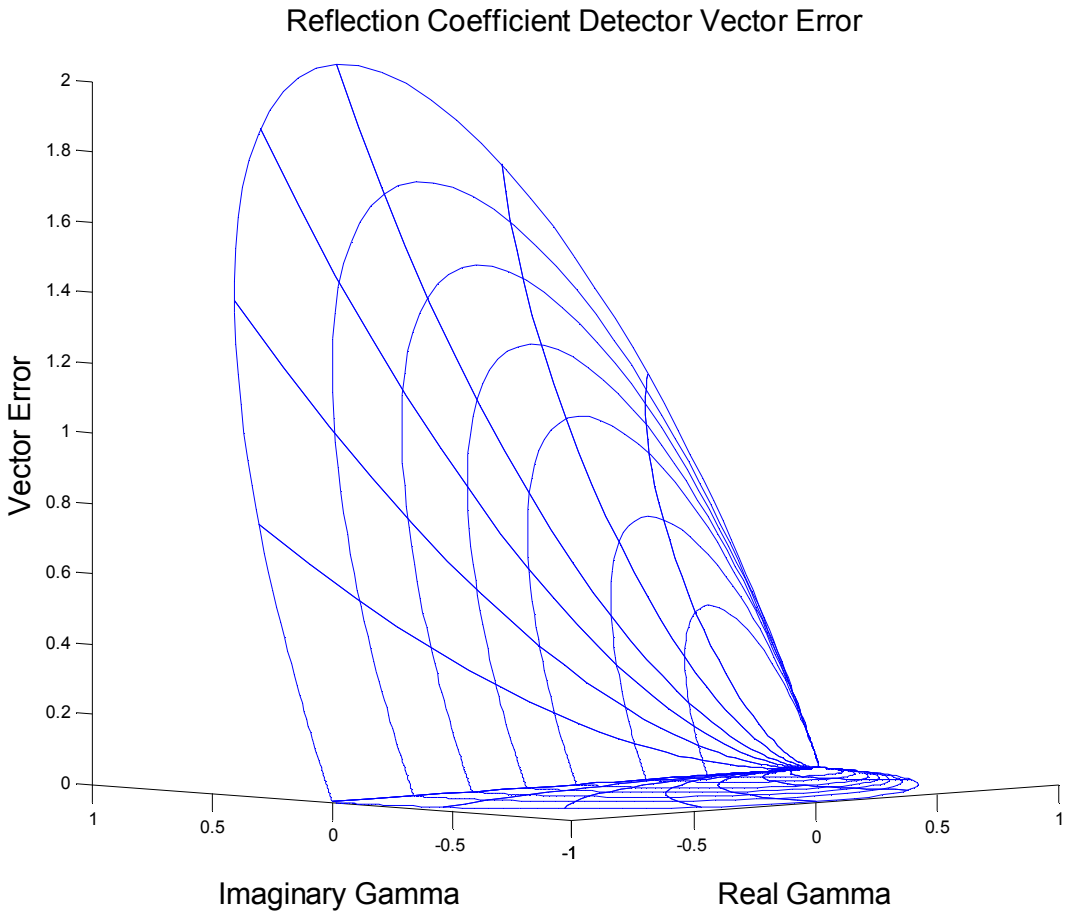

Figure 4-6a W-BCRCD VECTOR ERROR A The vector error of the reflection coefficient detector using equation-based Wilkinson dividers plotted in the Γ plane. Note that the error is mostly caused by the phase error seen in figures 4-4a and 4-4b. An error of 2 means that the measured value has no correlation with the actual reflection coefficient value.

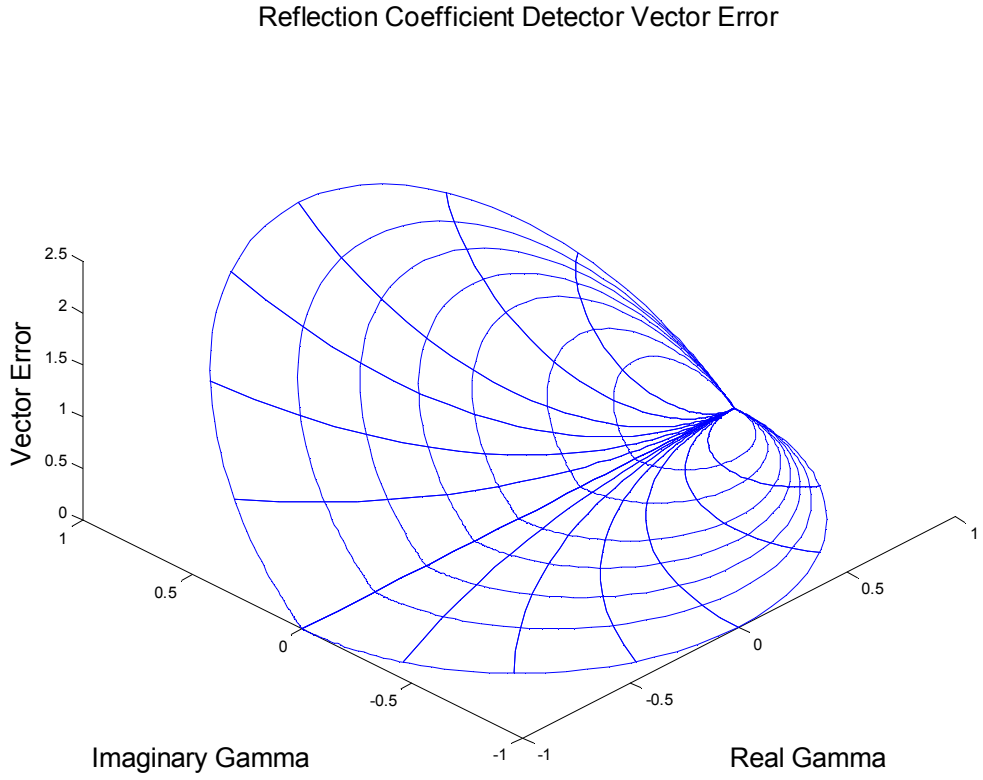

Figure 4-6b W-BCRCD VECTOR ERROR B The vector error of the reflection coefficient detector using equation-based Wilkinson dividers plotted in the Γ plane. This is the same graph from figure 4-6b shown at a different angle.

E. Correcting for Law of Cosines

The main limitation in the design at this point is in the fact that only an absolute phase can be obtained using the law of cosines and the phasor combinations. However, since this problem occurs due to a lack of distinction between + and – phase, the problem can be fixed.

It can be corrected for by shifting the phase of the reflected signal. This can be done by using a probe which can change length. This would in turn change the signal's phase. It can also be done by using a series of switches and transmission lines of different length, which again changes the signal's phase shift. Or, it can be done using a standard quadrature phase shifter, or technology which allows for variable, reciprocal phase shifting[1]. For any of these methods, the actual phase can be found by shifting the reflection signal's phase, and monitoring which way the measured value of phase changes. If it changes with the shift in phase, then the correct sign is detected. If it shifts in the opposite direction, then the incorrect sign is detected.

The problem can also be addressed using narrow bandwidth frequency shifting. Comparing the change of frequency to the change in the reflection coefficient's phase can determine the sign of the phase. See appendix C for more information.

Despite the method, if the knowledge of the sign is applied to the data taken in section D, it would result in the vector error graph shown in figures 4-7a and 4-7b. Figures 4-8a and 4-8b show the phase error. It can be seen that the phase is still the largest contributing factor in the vector error since figure 4-5a shows the minimum magnitude error at the same places where the vector error, figure 4-7a, and phase error, figure 4-8b, are at their maximum.

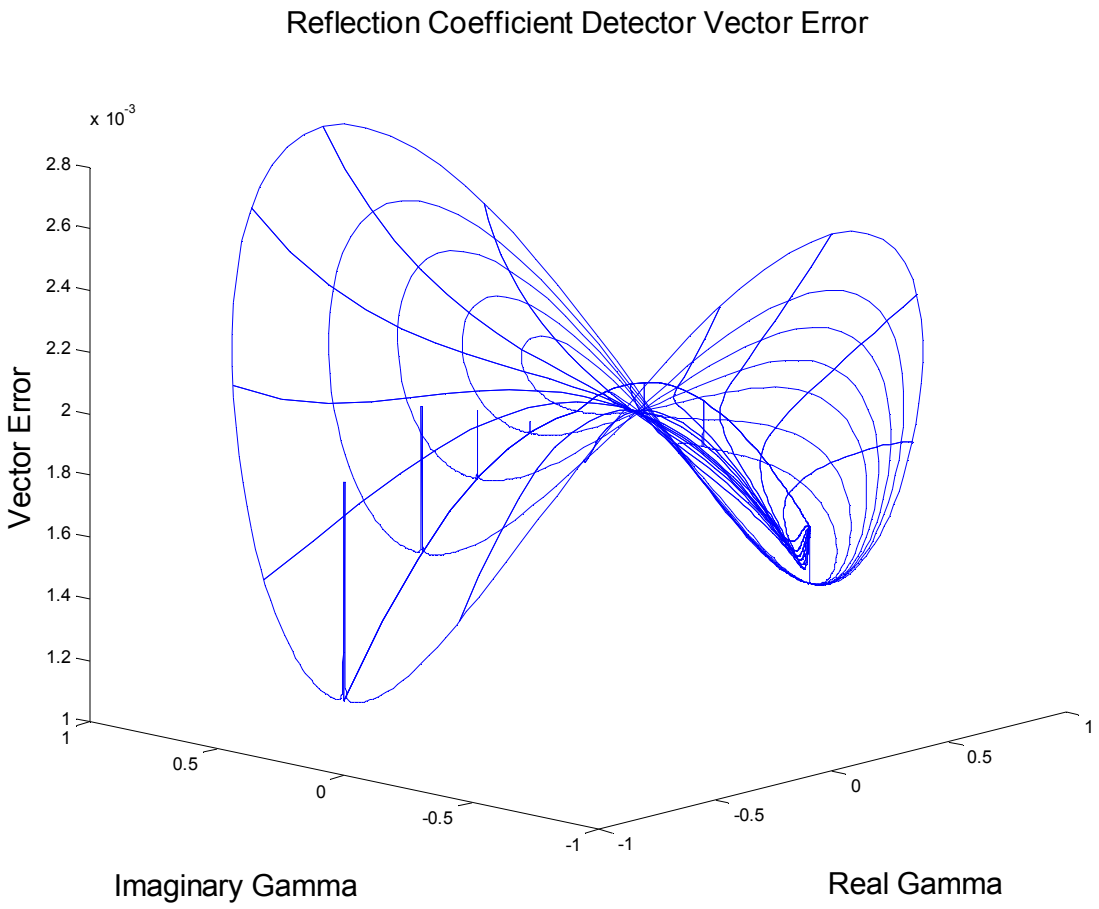

Figure 4-7a W-BCRCD CORRECTED VECTOR ERROR A The vector error of the reflection coefficient detector using equation-based Wilkinson dividers with phase sign correction. Note that the minimums and maximums do not correspond with figures 4-5a and 4-5b, which means that the vector error is still mostly based on the phase error.

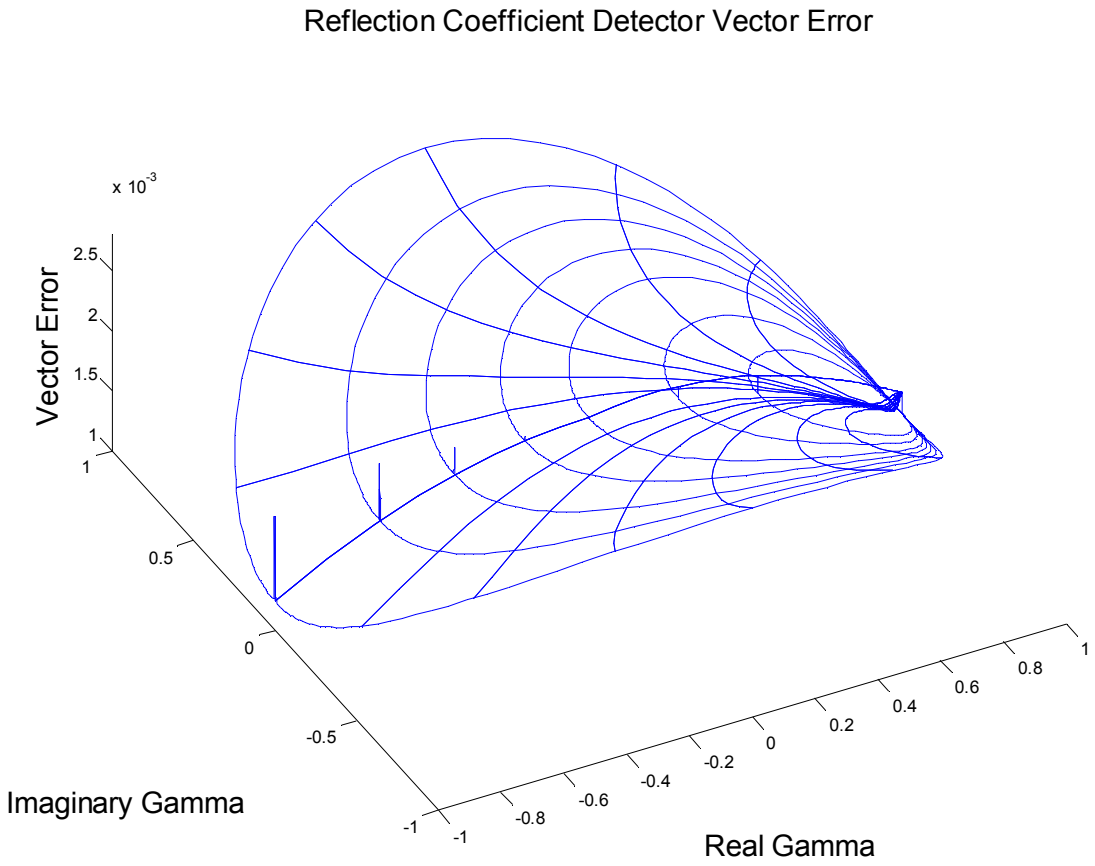

Figure 4-7b W-BCRCD CORRECTED VECTOR ERROR B The vector error of the reflection coefficient detector using equation-based Wilkinson dividers with phase correction. This is the same graph from figure 4-7a shown at a different angle.

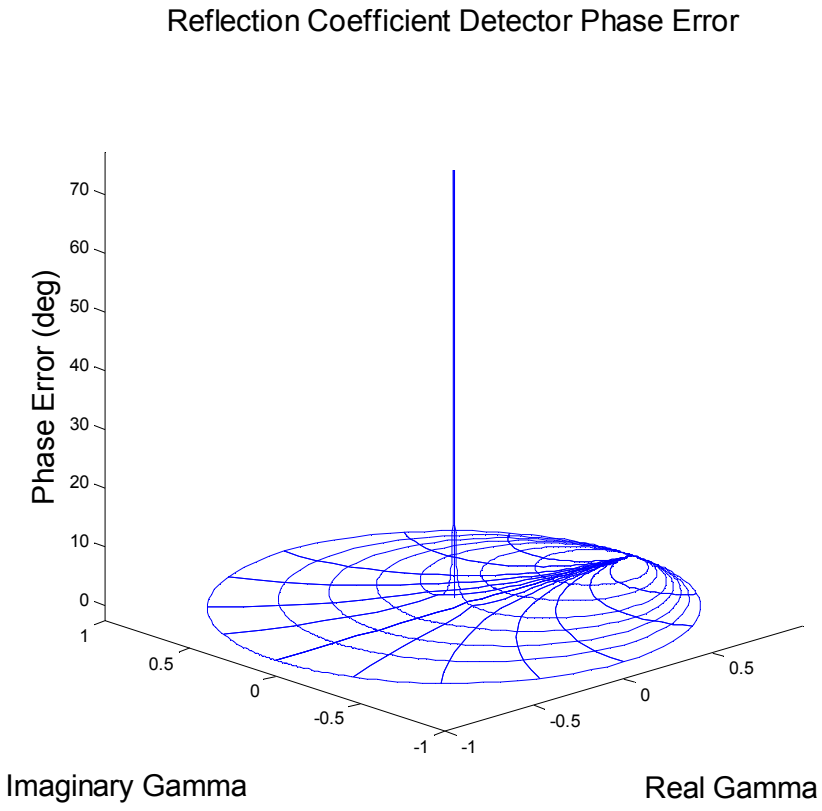

Figure 4-8a W-BCRCD CORRECTED PHASE ERROR A The phase error of the reflection coefficient detector using equation-based Wilkinson dividers with the phase sign correction.

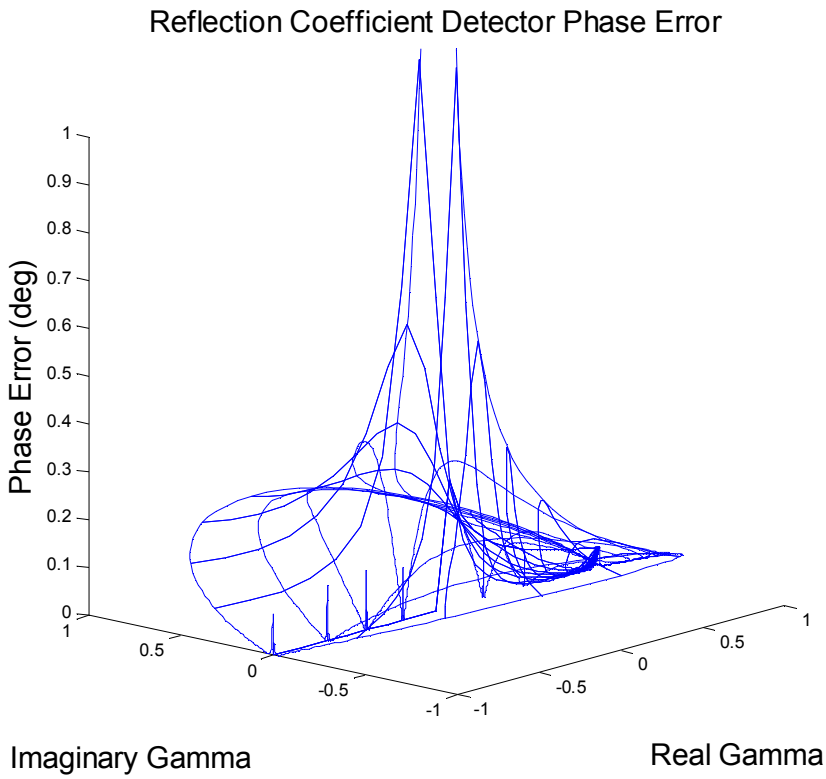

Figure 4-8b W-BCRCD CORRECTED PHASE ERROR B The phase error of the reflection coefficient detector using equation-based Wilkinson dividers with phase correction. This is the same graph from figure 4-8a shown at a different scale.

When using phase correction the vector error ranges between .001 and .0028. As will be shown later, this error is most likely due to the finite isolation between certain ports. Therefore, the isolation of the more realistic models and the fabricated prototype should play a large role in the accuracy of the design.

F. References Cited

[1] Mamdouh M I Saadoun, Nader Engheta, “A reciprocal phase shifter using novel pseudochiral or ω medium”, Microwave and Optical Technology Letters, vol. 5, issue 4, pp. 184 – 188, January 2007

V. Ideal and Parasitic CAD Simulation and Analysis

In chapters III and IV, certain innate problems in the reflection coefficient detector design were addressed. These included extra loss due to different signal paths in the circuit, and a lack of distinction between capacitive and inductive loading at the reflection port. From this point on it will be assumed that the necessary steps have been taken to account for these errors.

Presented herein is the design and analysis of an ideal and realistic model for the reflection coefficient detector. These models will be built, like the equation based models, using Agilent's Advanced Design System. The ideal model will use ideal transmission lines, 'TLines', and ideal lumped elements. The simulation model will be done using parasitic microstrip models and parasitic lumped element models (Modelithics CLR Library).

The use of a low dielectric constant microstrip and a center frequency of 2.5 GHz are chosen for ease of fabrication and testing. Later models can theoretically be built at any RF frequency. Stripline or microstrip with a higher relative permittivity can also be used in order to adjust for the size and function of the design.

A. Ideal Transmission Line Design

A Wilkinson power divider is built using two quarter wave transformers and a resistor. The quarter wave transformers are built in parallel, connected together at one end and connected by the resistor at the other. These transformers are designed to match the devices' reference impedance, 50 ohms in this case, to twice the characteristic, 100 ohms. This will make the point at which they join, the input, appear as a 50 ohm load; and make the point at which they connect to the resistor, the output, also appear as a 50 ohm. This means the quarter wavelength transmission lines must have a characteristic impedance of 70.71 ohms.

Figure 5-1 shows the ideal transmission line design of the Wilkinson. Port 1 is the input port, while ports 2 and 3 are the output ports. Extra lengths of transmission line have been added to the inputs and outputs in order to make the design more representative of the final design which will need interconnects and feed lines. Figure 5-2 shows the resulting S-Parameters. Because of the symmetry of the design, the gain from port 1 to port 2, S21, is the same as the gain from port 1 to port 3, S31; and the reflection at port 2, S22, is the same as the reflection at port 3, S33. From these parameters it can be seen that the Wilkinson is well matched to 50 ohms at all ports, and has a significant amount of isolation between the two output ports.

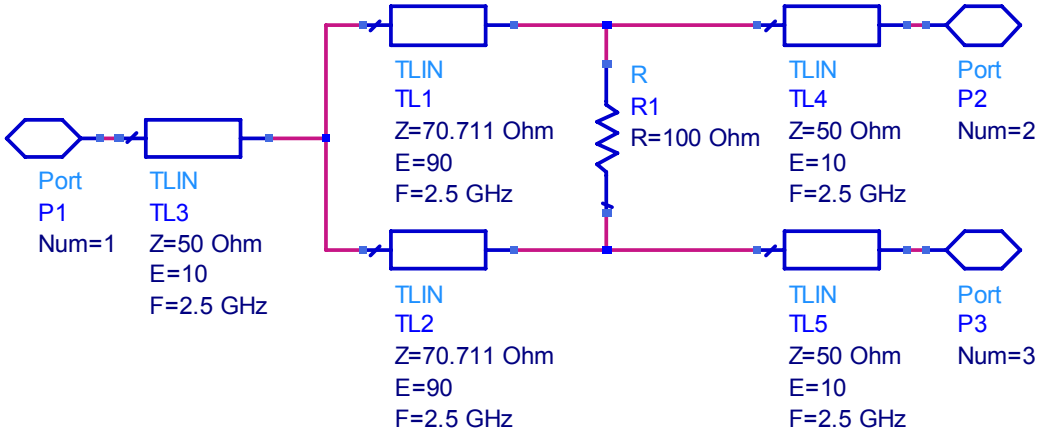

Figure 5-1 IDEAL T-LINE WILKINSON POWER DIVIDER A Wilkinson power divider composed of ideal transmission line elements matched to a 50 ohm system. Port 1 is the input; port 2 and 3 are the outputs; and TL1 and TL2 are the quarter wave transformers.

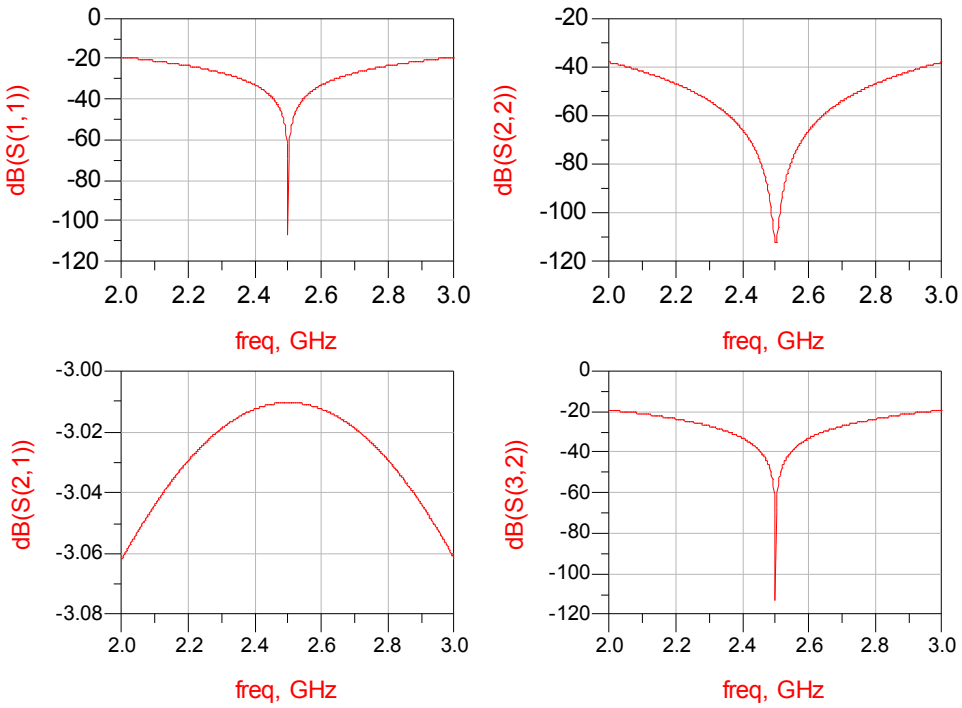

Figure 5-2 IDEAL T-LINE WILKINSON POWER DIVIDER S-PARAMETERS S-Parameters of the Wilkinson power divider in figure 5-1 around its center frequency, 2.5 GHz. Due to symmetry, ports 2 and 3 are interchangeable, i.e. S(2,1) is the same as S(3,1).

Figure 5-3 shows the complete detector design using the ideal transmission line Wilkinson dividers from figure 5-1. Each divider is easily identified as the five loops created by two transmission lines and a resistor. Figure 5-4 shows the resulting gain to each port from port 1. It shows that ports 2, 3 and 5 all receive close to the expected amount of signal power relative to each other; while port 4 is well isolated. Using these graphs and the symmetry of the design, it can be seen that ports 2 and 4 receive almost their entire power from their respective sources, i.e. port 2 from the excitation port, and port 4 from the reflected port.

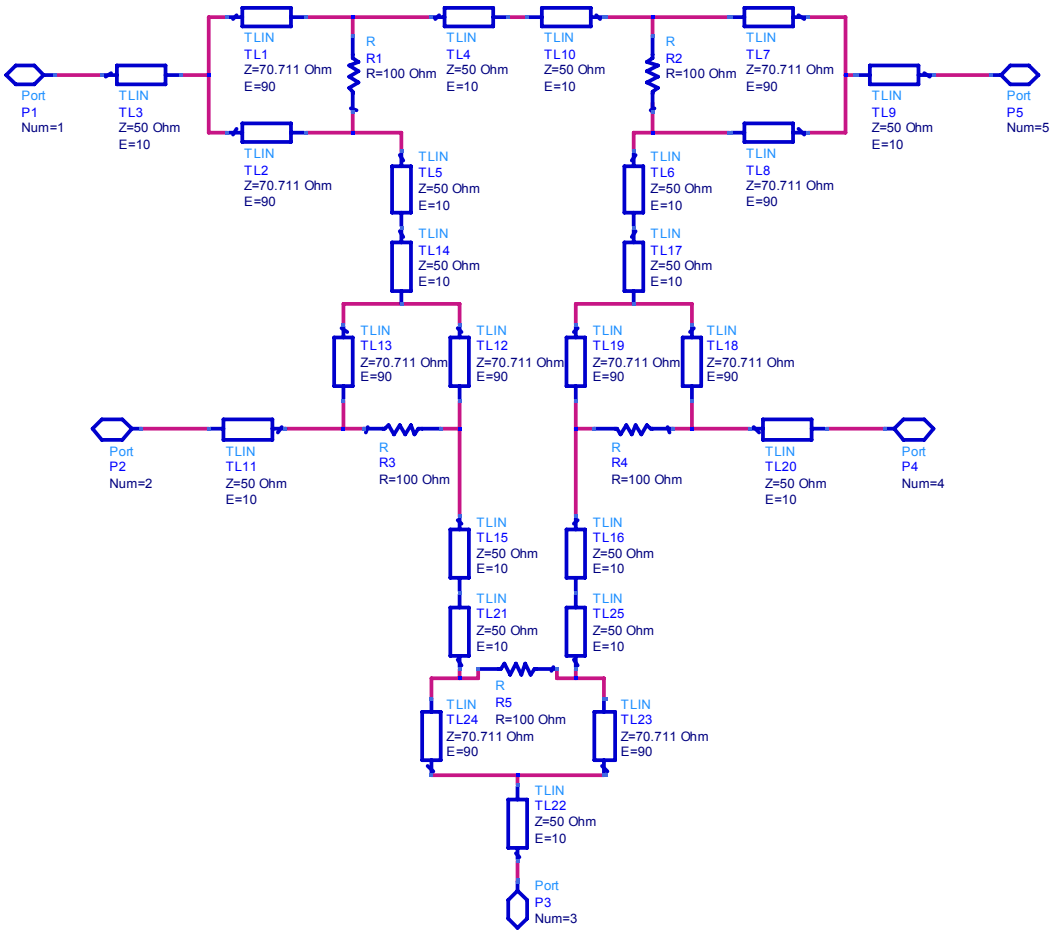

Figure 5-3 IDEAL T-LINE W-BCRCD Full detector circuit design using ideal transmission line Wilkinson power dividers. The five Wilkinson dividers can be identified by two transmission lines and a resistor.

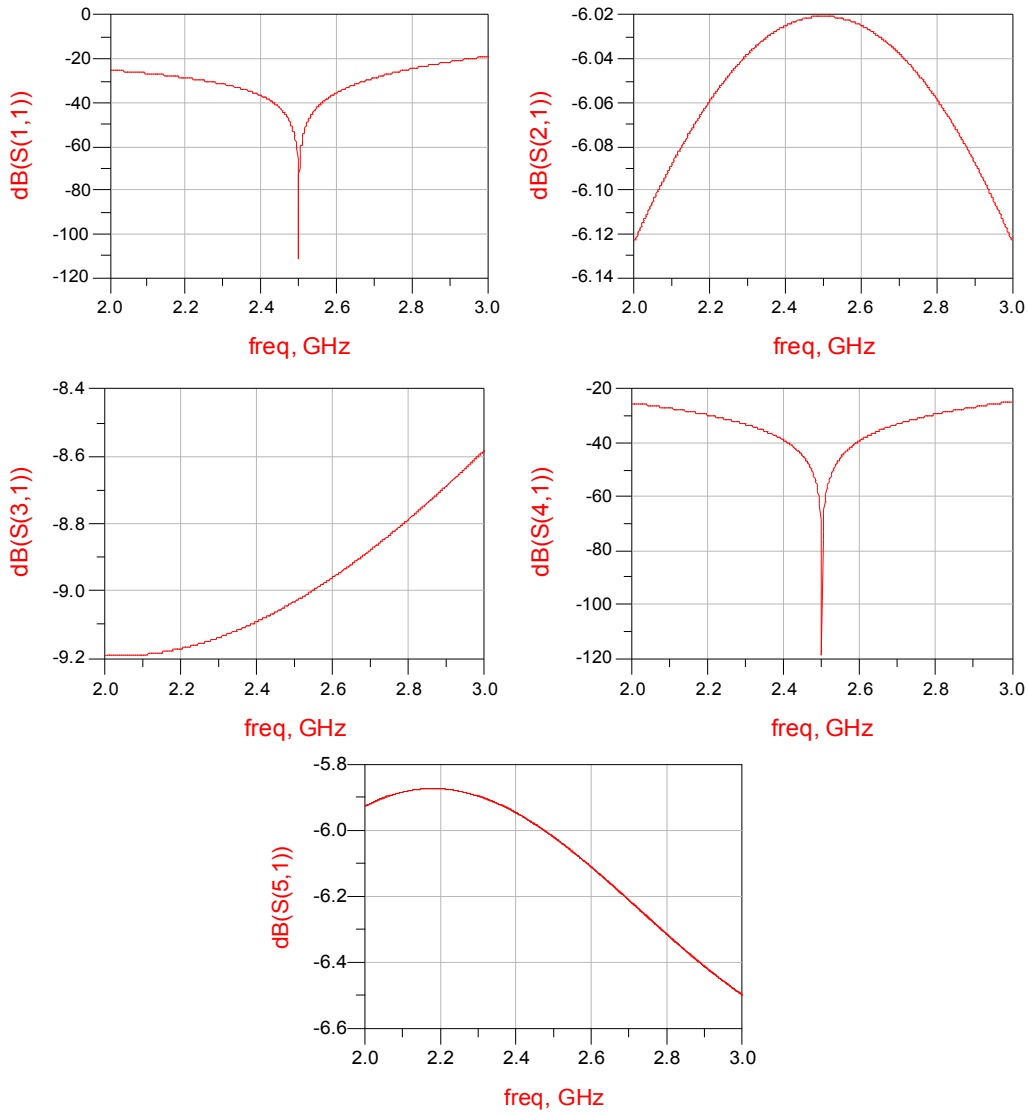

Figure 5-4 IDEAL T-LINE W-BCRCD S-PARAMETERS Gain (in dB) from port 1 to port 1 (upper-left), port 2 (upper-right), port 3 (middle-left), port 4 (middle-right), and port 5 (bottom) for the full detector seen in figure 5-3.

Figures 5-5, 5-6 and 5-7 show the phase error, magnitude error, and vector error, respectively. As in chapter IV, these errors are defined as the absolute difference between the actual value and the calculated value for all values of reflection at port 5. Notice that the error in figure 5-4 follows nearly a straight line. At the same time, notice how much

less the error is in figure 5-4 than in figure 4-8b. The magnitude error, seen in figure 5-6, has a maximum error of 4.7E-6. This is almost 3 orders of magnitude less than the minimum error of the equation based model, at 1e-3. As will be shown later, this is most likely due to the amount of isolation between ports 1 and 4.

Because of the low phase error and magnitude error, figure 5-7 shows the ideal transmission line model to have a very low vector error. The maximum errors occur along the same line that is defined in figure 5-5, showing that once again the majority of the error occurs due to the phase.

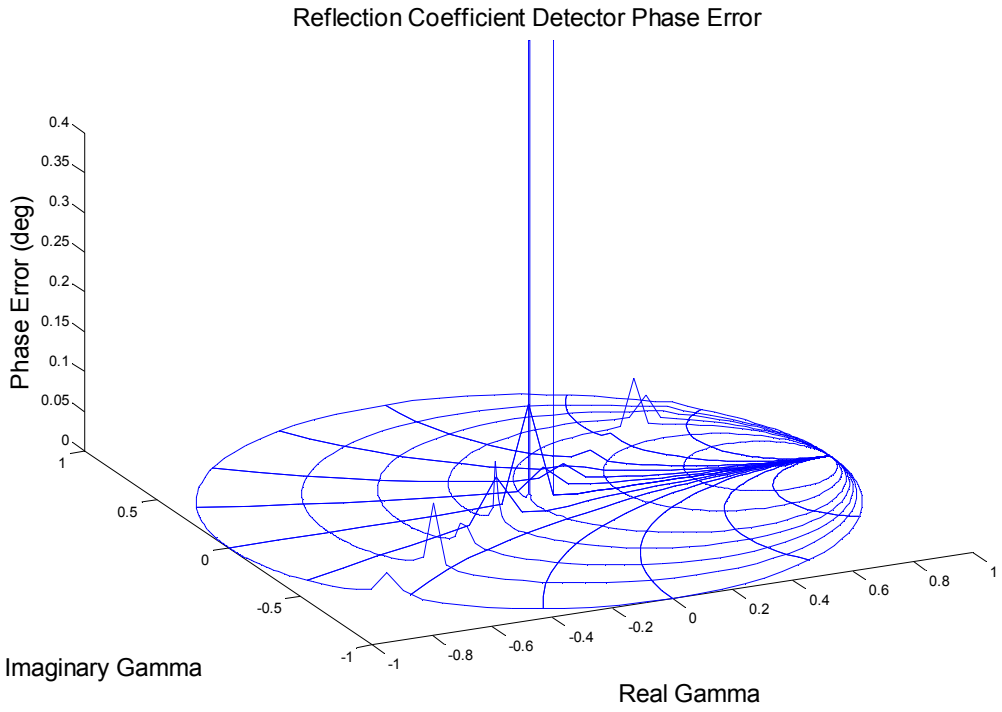

Figure 5-5 IDEAL T-LINE W-BCRCD PHASE ERROR The phase error of the reflection coefficient detector using ideal transmission line Wilkinson power dividers.

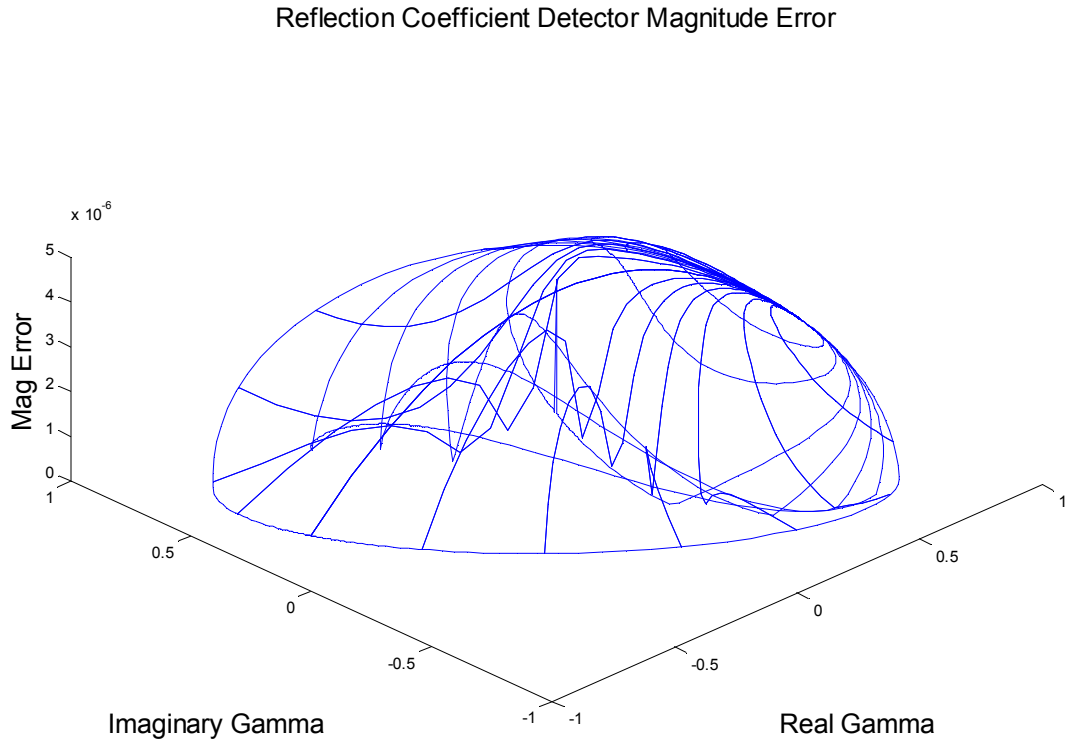

Figure 5-6 IDEAL T-LINE W-BCRCD MAGNITUDE ERROR The magnitude error of the reflection detector using ideal transmission line Wilkinson power dividers. The error maximum of 4.7E-6 occurs at the origin.

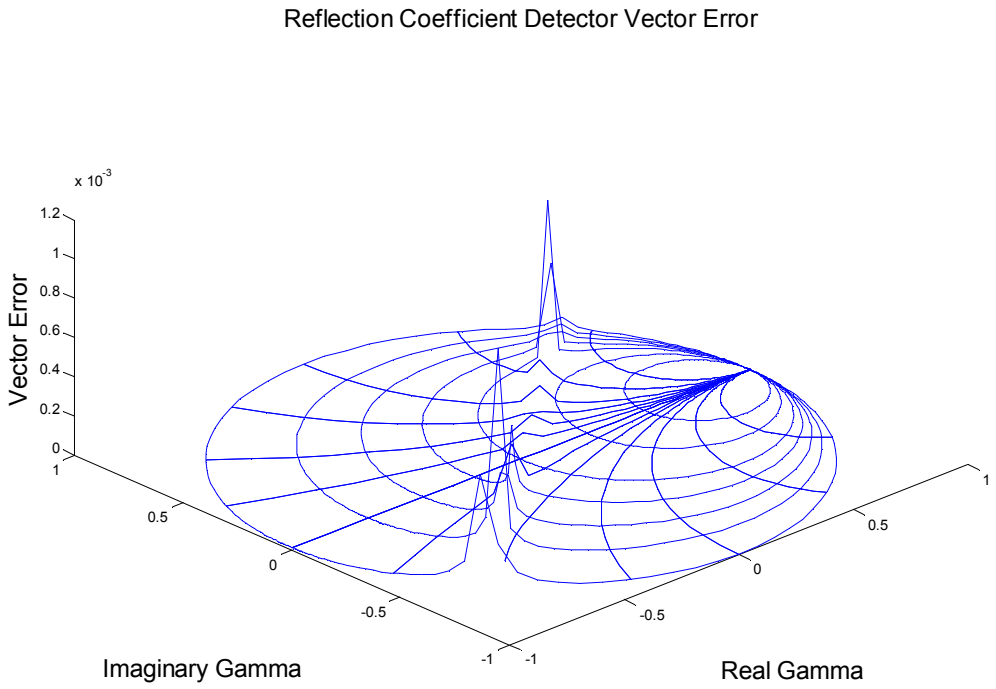

Figure 5-7 IDEAL T-LINE W-BCRCD VECTOR ERROR The vector error of the reflection coefficient detector using ideal transmission line Wilkinson power dividers. The maximum errors of about 1E-3 occur along a straight line which runs through the origin.

The error seen in all three plots is still mostly likely due to the finite isolation between ports 4 and 1, or the finite return loss seen at port 5. This is most noticeable from figures 5-5 and 5-7 where the error occurs along a straight line which runs through the origin. This is the line at which the return loss or leaked signal most notably interferes with the reflected signal or the reflected signal portion. Comparing Table T4-1 and figure 5-4, it can be seen that the ideal model has a higher return loss at the input port (which is the same for port 5) and greater isolation between ports 4 and 1, than the equation based model. This directly correlates to a decrease in the error for the ideal case.

This increase in isolation from the equation-based model to the ideal model is due to the isolation in the dividers being set at 60 dB. In order to make the equation based model more representative of the ideal model, the isolation could be set to a higher value for the individual dividers. As will be shown later, adjusting this isolation will also adjust the error.

B. Parasitic Microstrip Model

As stated in section A, a Wilkinson power divider is constructed from two quarter wave transformers connected together at one end and connected by a resistor at the other end. Figure 5-8 shows a Wilkinson power divider constructed using parasitic transmission line models, and a parasitic lumped element resistor model (KOA_RK73B1J, using the Modelithics model KOA_0603_101). Notice that the quarter wave transformers are made using eight transmission line elements each. This is so that they make a complete circle and properly connect at the resistor.

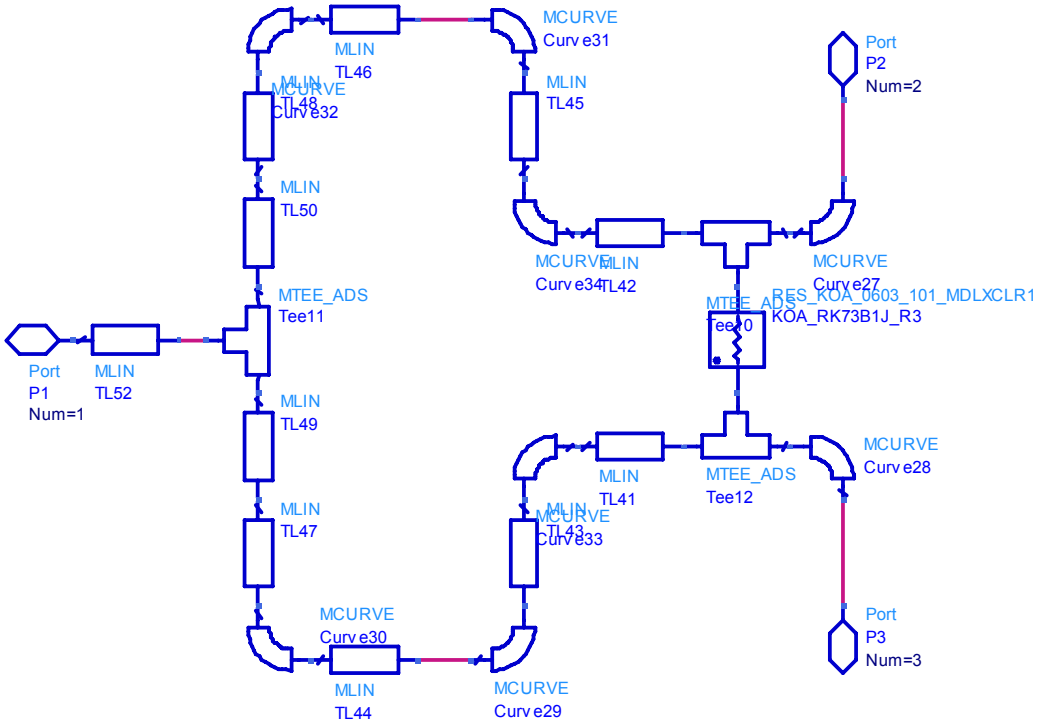

Figure 5-8 PARASITIC T-LINE WILKINSON POWER DIVIDER Parasitic transmission line implementation of a Wilkinson power divider.

Table T5-1 MICROSTRIP BOARD SPECIFICATIONS FOR W-BCRCD Table showing the substrate properties being used in the parasitic model. These are the same parameters that will be used for the prototype.

Substrate Thickness	Relative Permittivity	Relative Permeability	Conductor Conductance	Conductor Thickness	Dielectric Loss Tangent
60 mil	3.6	1	59e6 S/m	1.4 mil	0.003

The lengths and widths of the transmission lines in the Wilkinson divider are based on the substrate properties shown in table T5-1. The final layout of the divider can be seen in figure 5-9. The quarter wave transformers are easily identified as they are thinner than the 50 ohm lines at the input and outputs. The transmission gain, from port 1 to ports 2 and 3, and the isolation gain, from port 2 to port 3, can both be seen in figure 5-10.

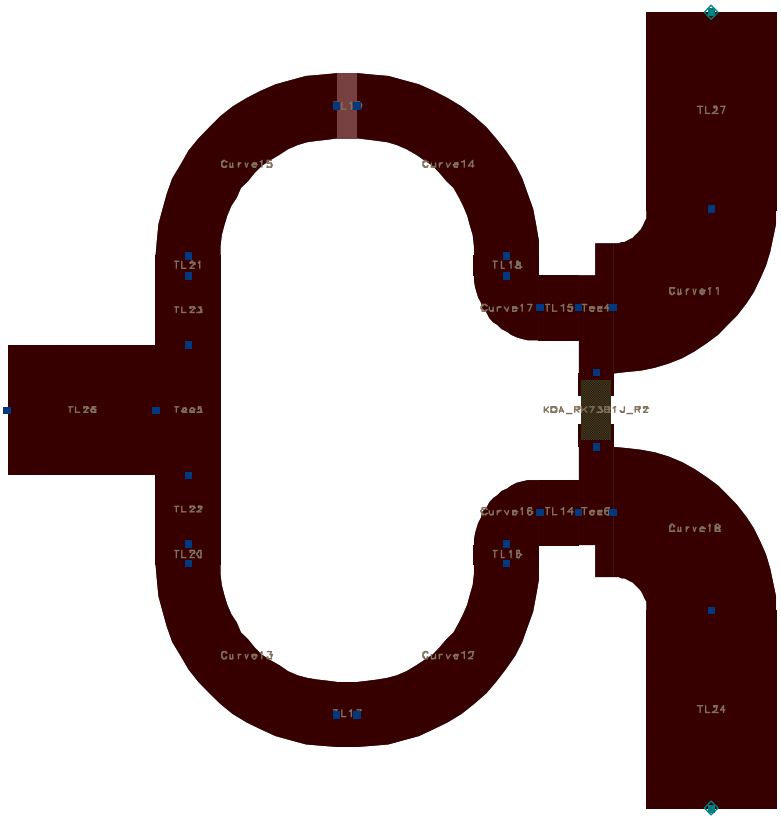

Figure 5-9 SIMULATED T-LINE WILKINSON POWER DIVIDER Conductor level representation of Wilkinson power divider shown in figure 5-8.

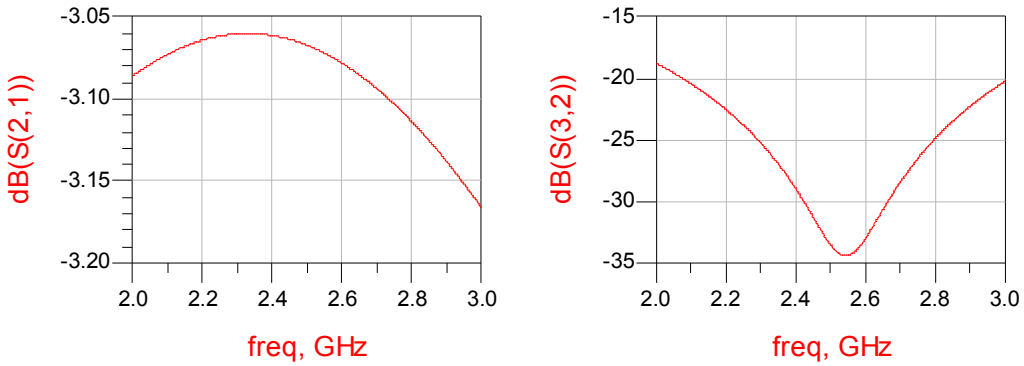

Figure 5-10 PARASITIC T-LINE WILKINSON POWER DIVIDER S-PARAMETERS

Transmission and isolation parameters for the Wilkinson power divider shown in figure 5-8

Figure 5-11 shows the full schematic of the CRCD using the Wilkinson divider designed in figure 5-8. As with figure 5-3, the five Wilkinson dividers are easily identified as the five loops created from transmission line and a resistor. The S-Parameters of this and the past two CRCDs can be seen in figure 5-12. Note that the parasitic model has significantly less isolation, S41, which correlates with the increase in error. Also note that the input reflection at port 1, S11, due to the symmetry of the device, is the same as the reflection at port 5, S55.

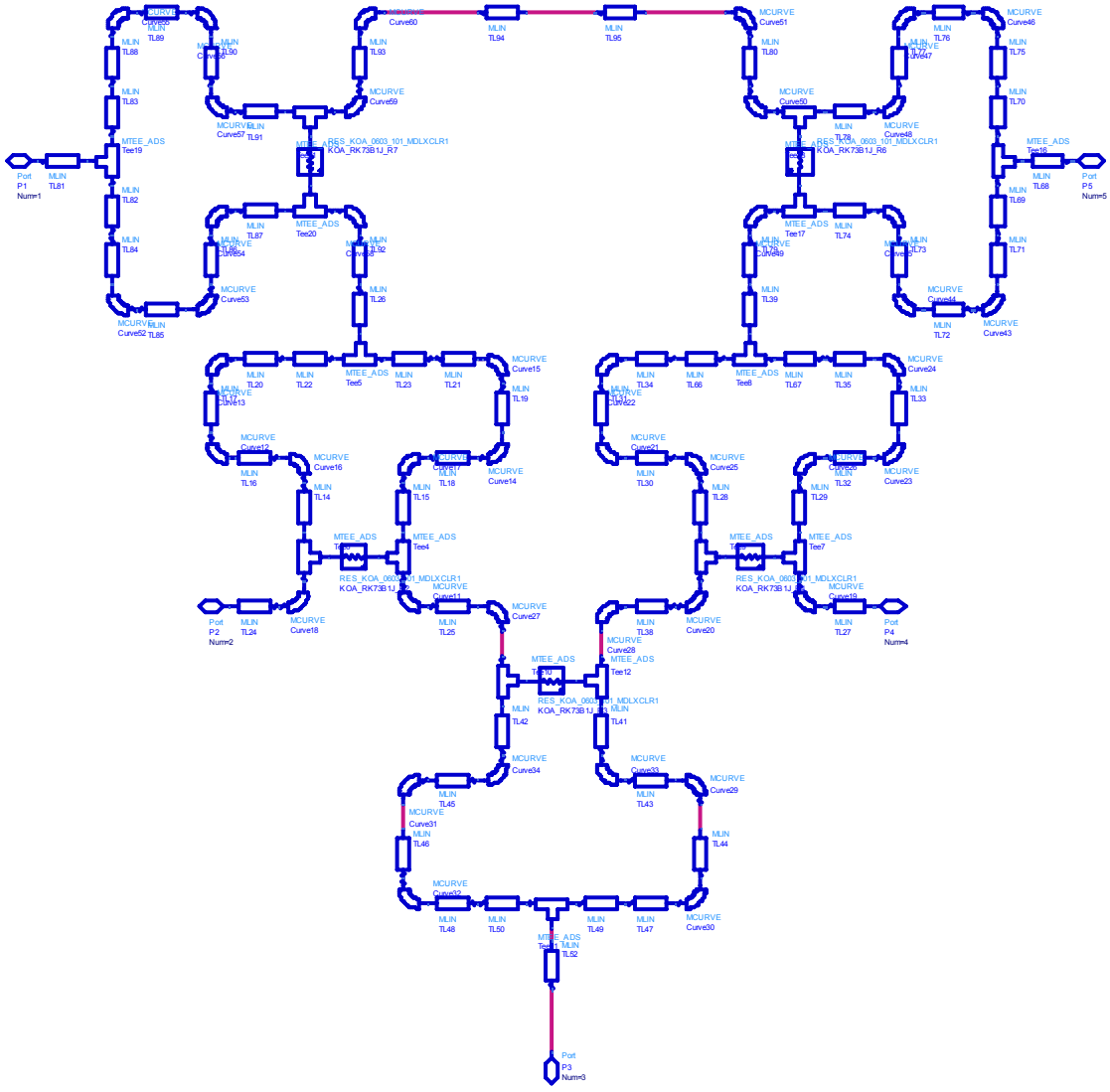

Figure 5-11 PARASITIC T-LINE W-BCRCD Full schematic of reflection coefficient detector using parasitic microstrip transmission line models and parasitic surface mount lumped element resistors.

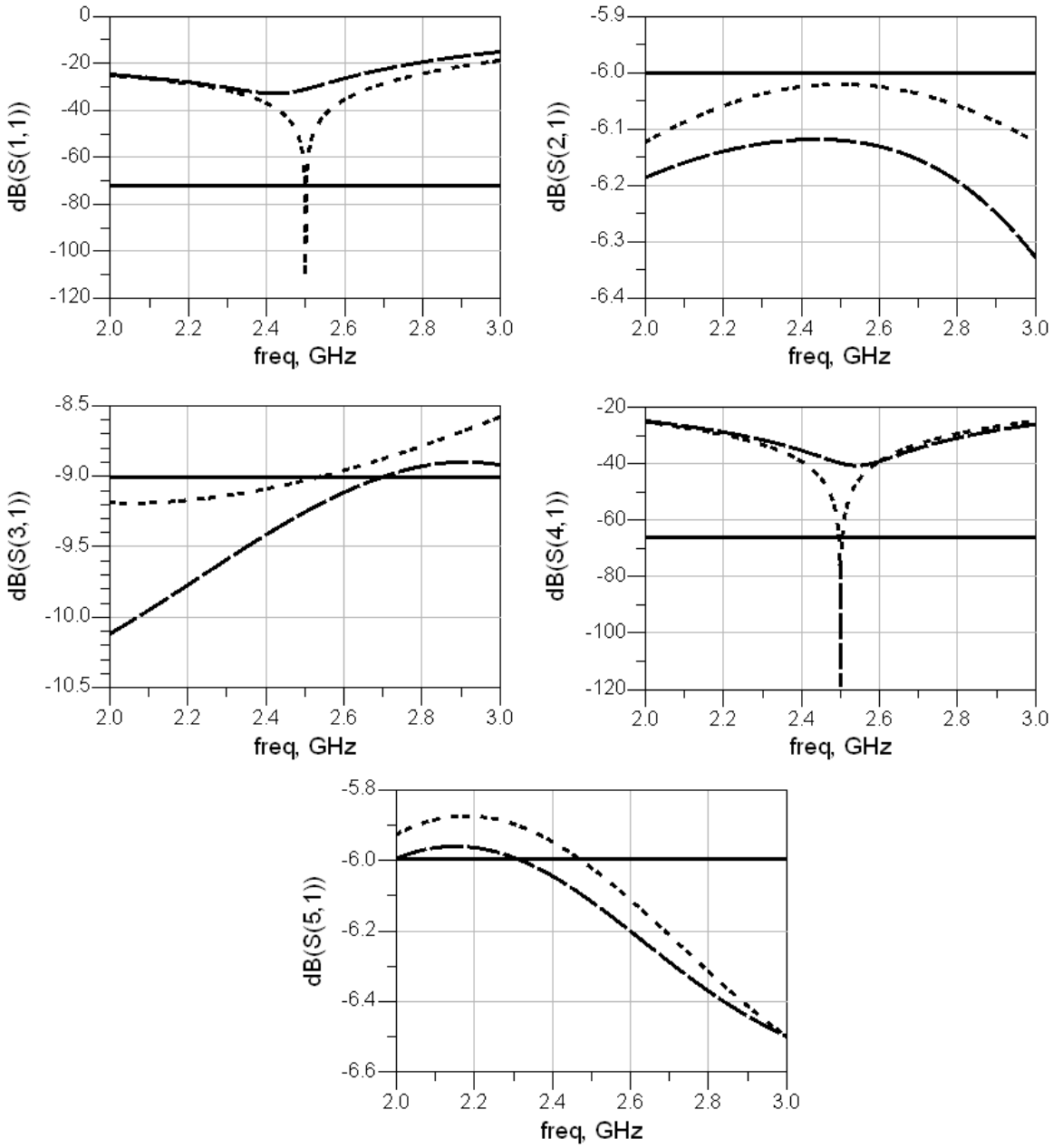

Figure 5-12 PARASITIC T-LINE W-BCRCD S-PARAMETERS S-Parameters of parasitic model (dashed line), ideal transmission line model (dotted line), and equation based model (solid line) W-BCRCDs.

Figures 5-13, 5-14 and 5-15 show the error of the parasitic design for different values of reflection at port 5. As with the past two designs, it can be seen that the vector

error is affected more by the phase error than the magnitude error. Notice the drastically higher error in the parasitic model than either the equation based or ideal transmission line based models. This corresponds, again, with the isolation found between port 1 and 4.

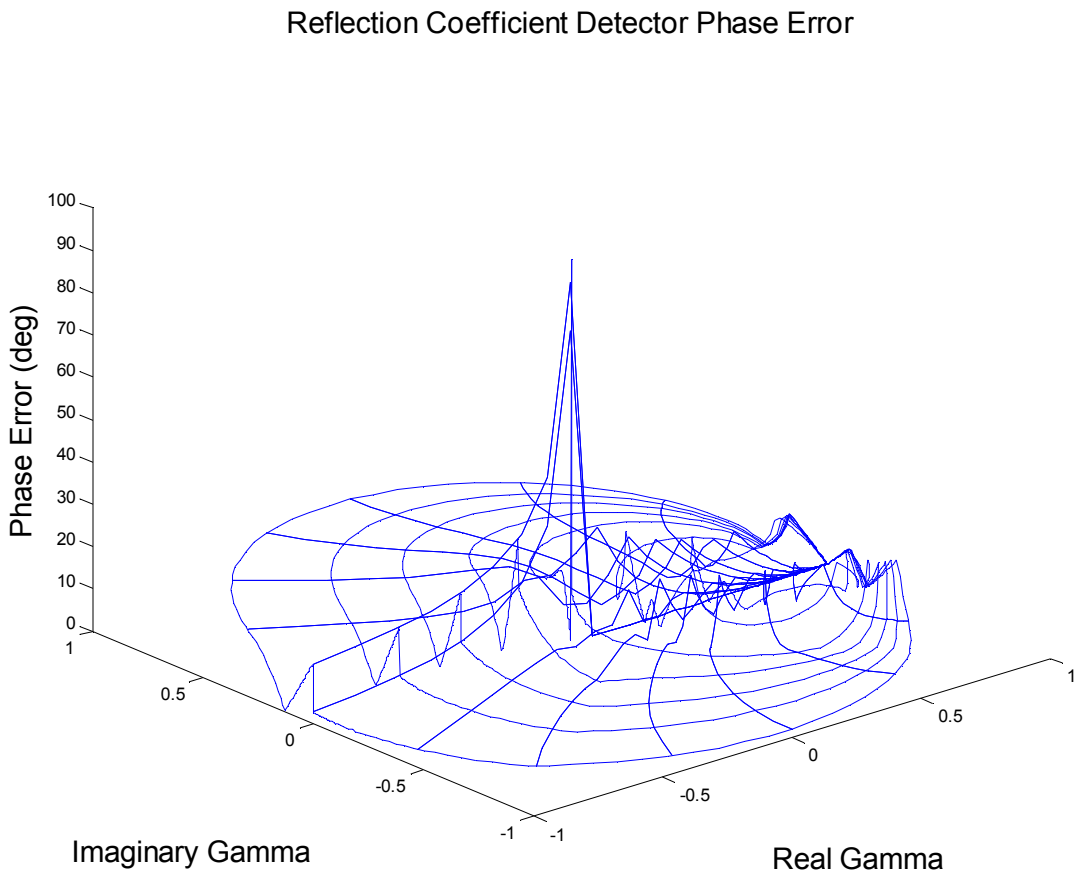

Figure 5-13 PARASITIC T-LINE W-BCRCD PHASE ERROR The phase error of the reflection coefficient detector using parasitic microstrip transmission line models and parasitic surface mount lumped element resistor models.

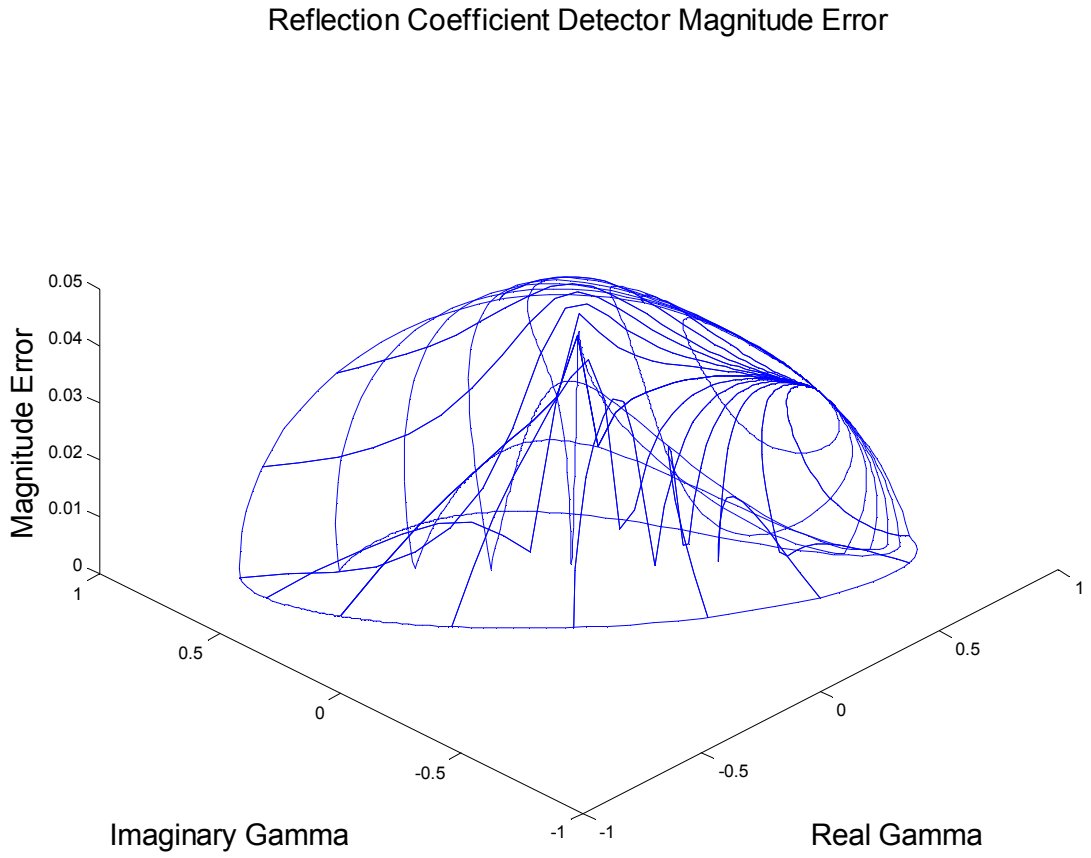

Figure 5-14 PARASITIC T-LINE W-BCRCD MAGNITUDE ERROR The magnitude error of the reflection coefficient detector using parasitic microstrip transmission line models and parasitic surface mount lumped element resistor models.

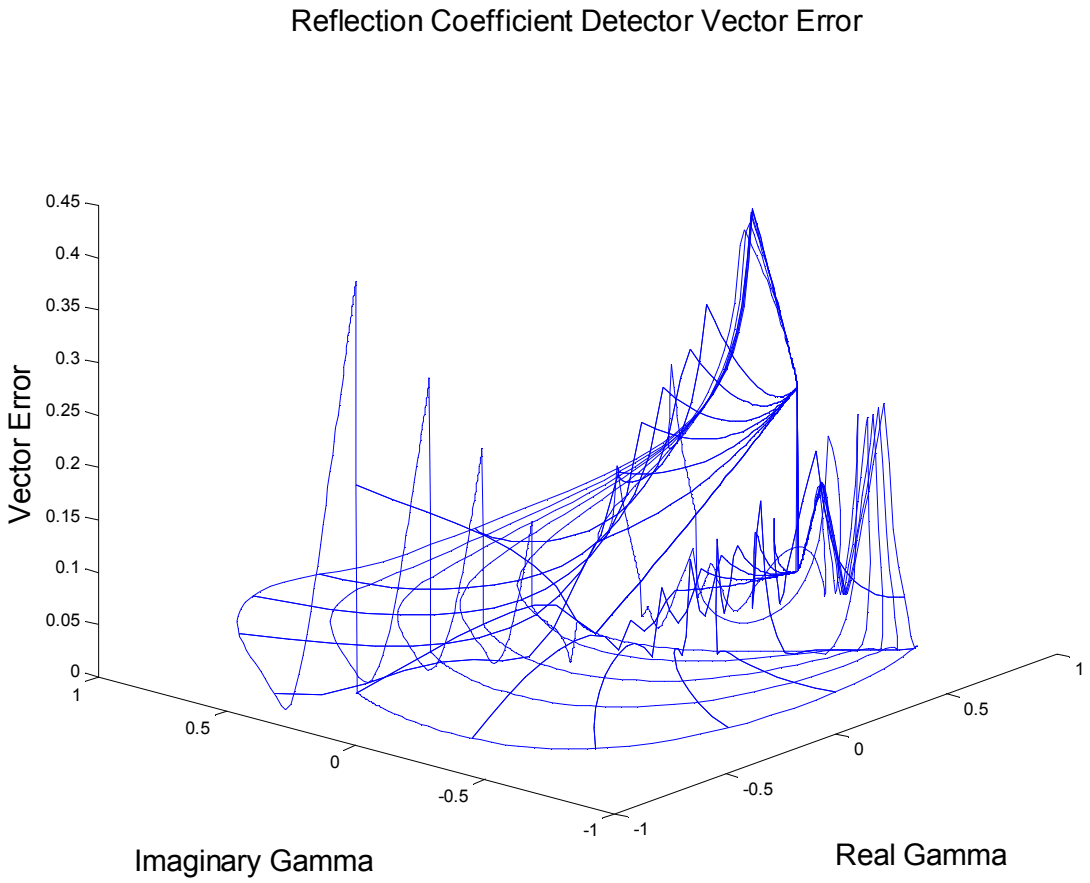

Figure 5-15 PARASITIC T-LINE W-BCRCD VECTOR ERROR The vector error of the reflection coefficient detector using parasitic microstrip transmission line models and parasitic surface mount lumped element resistor models. Notice the drastically higher error seen across the design, and the wide regions of higher error located at three different regions across the Smith chart.

C. Error Analysis

In all three CAD models, there has been an error which is based upon the phase of the reflection found at port 5. This error is likely caused by either imperfect isolation between the input ports, 1 and 5, and the measurement ports, 2 and 4, or a finite return loss at port 5. This conclusion comes from

$$S'_{rec,send} = S_{rec,send} + \frac{S_{rec,term} \times S_{term,send} \times \Gamma}{1-(S_{term,term} \times \Gamma)} \quad \text{(e5.1)}$$

where $S_{rec,send}$ is the gain between a transmitting port and a receiving port of a system, $S_{rec,term}$ is the gain between a terminated port and a receiving port, $S_{term,send}$ is the gain between a transmitting port and a terminated port, $S_{term,term}$ is the input reflection on a terminated port, Γ is the output reflection on a terminated port, and $S'_{rec,send}$ is the gain between a transmitting port and a receiving port when another port is terminated in a mismatched load.

E5.1 represents how much power is received at the measurement port from the excitation signal port when the reflection port is terminated in some mismatched load. The excitation port is represented by the sending port, the reflection port by the terminated port, and the measurement port by the receiving port. Ideally, all the power at port 4 should come from the second half of e5.1 so that none of the excitation signal directly interferes with the reflected signal portion. However, since S41 is not zero there will always be interference from the excitation signal.

The magnitude of the power received at port 4 should also be independent of the phase of the reflection at port 5. However, as can be seen in the second term of e5.1, the denominator changes with gamma. The impact of this change is determined by S(5,5).

Figures 5-16, 5-17 and 5-18 show the impact of the isolation between port 1 and 4 and the input reflection at port 5 on the vector error. The data in these figures were created by changing the magnitude of the isolation and reflection in the parasitic transmission line model's data file. Comparing figure 5-16 and figure 5-14 shows a significant decrease in the error of the device across the Smith chart; and thus a strong correlation between the isolation and total error.

Figure 5-16 was created by decreasing the gain between ports 4 and 1 by 60 dB. Figure 5-17 was created by decreasing the reflection coefficient at port 5 by 60 dB. Figure 5-18 was created by decreasing both S(4,1) and S(5,5) by 60 dB. The choice of 60 dB was so that there would be a significant change without completely removing all gain.

Notice that there is no noticeable change between figures 5-14 and 5-17, nor between 5-16 and 5-18. This shows that the magnitude of the reflection at port 5 plays little to no role in measurements. At the same time, figure 5-16 shows a very drastic change from 5-14. Therefore, in the fabrication of this device, the most important parameter to design towards should be the isolation.

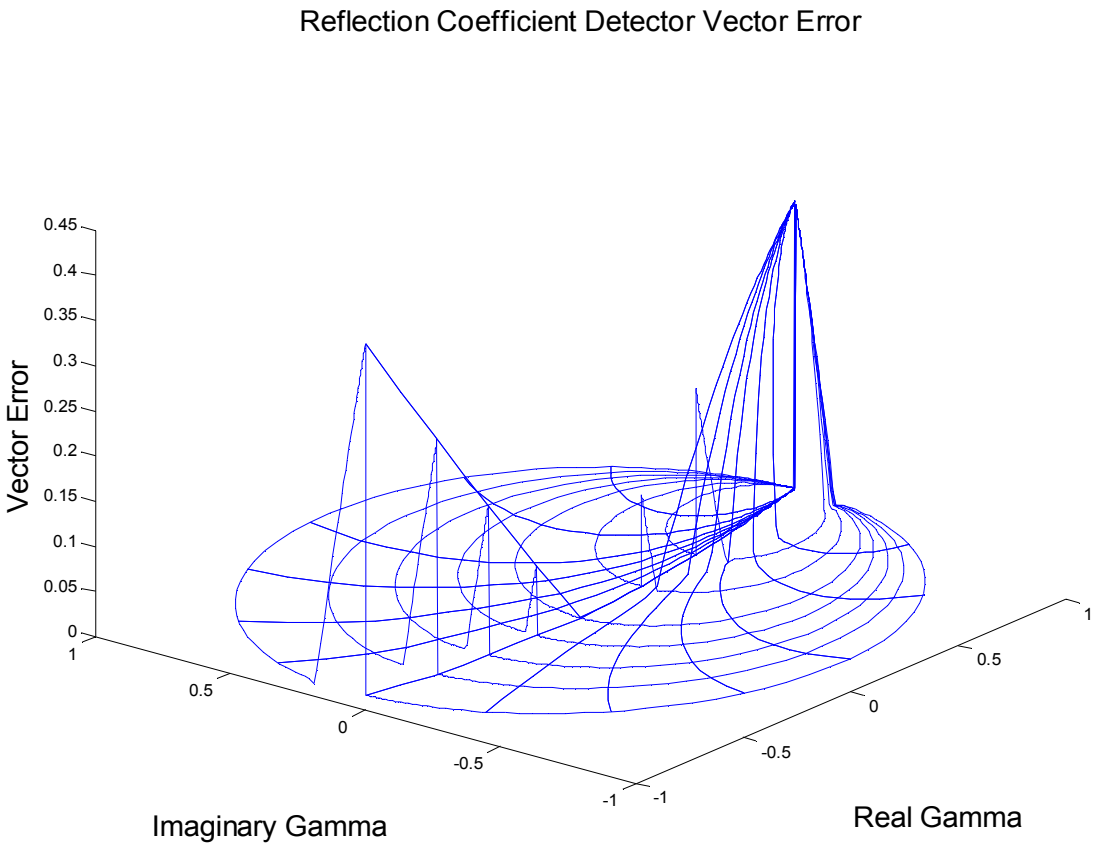

Figure 5-16 PARASITIC T-LINE W-BCRCD VECTOR ERROR WITH HIGH ISOLATION The vector error of the parasitic transmission line model of the reflection coefficient detector if the isolation between ports 1 and 4 were to be increased by 60 dB with no other changes to the design.

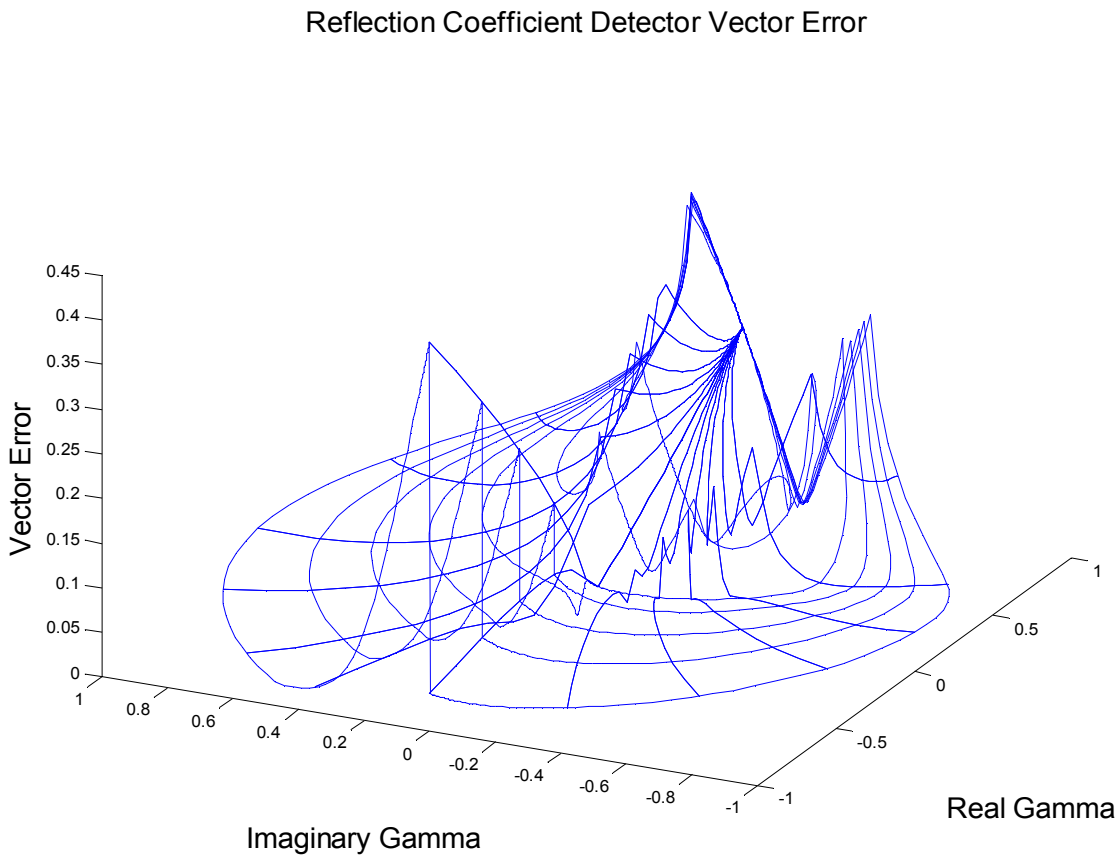

Figure 5-17 PARASITIC T-LINE W-BCRCD VECTOR ERROR WITH LOW INPUT REFLECTION The vector error of the parasitic transmission line model of the reflection coefficient detector if the input reflection found at port 5 were to be decreased by 60 dB with no other changes to the design.

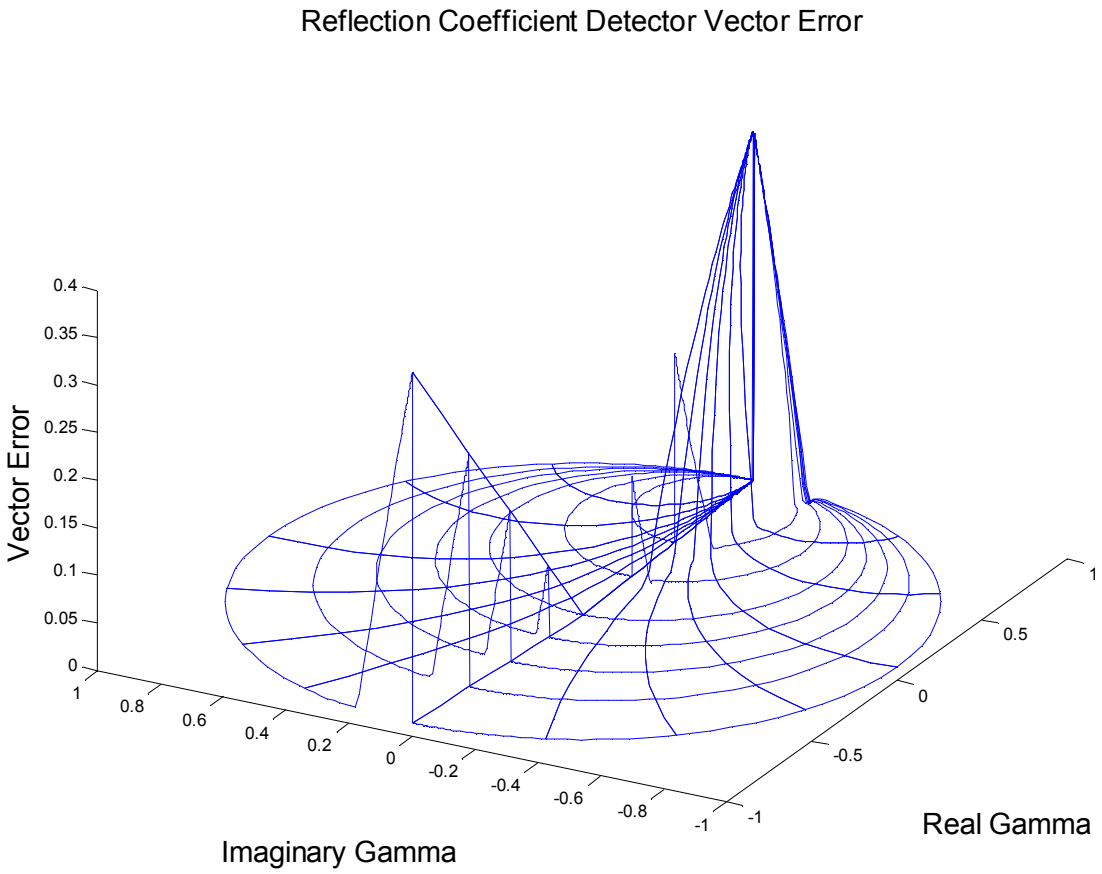

Figure 5-18 PARASITIC T-LINE W-BCRCD VECTOR ERROR WITH HIGH ISOLATION AND LOW INPUT REFLECTION The vector error of the parasitic transmission line model of the reflection coefficient detector if the isolation between ports 1 and 4 were to be increased by 60 dB and the input reflection found at port 5 were to be decreased by 60 dB with no other changes to the design.

VI. Prototype Analysis

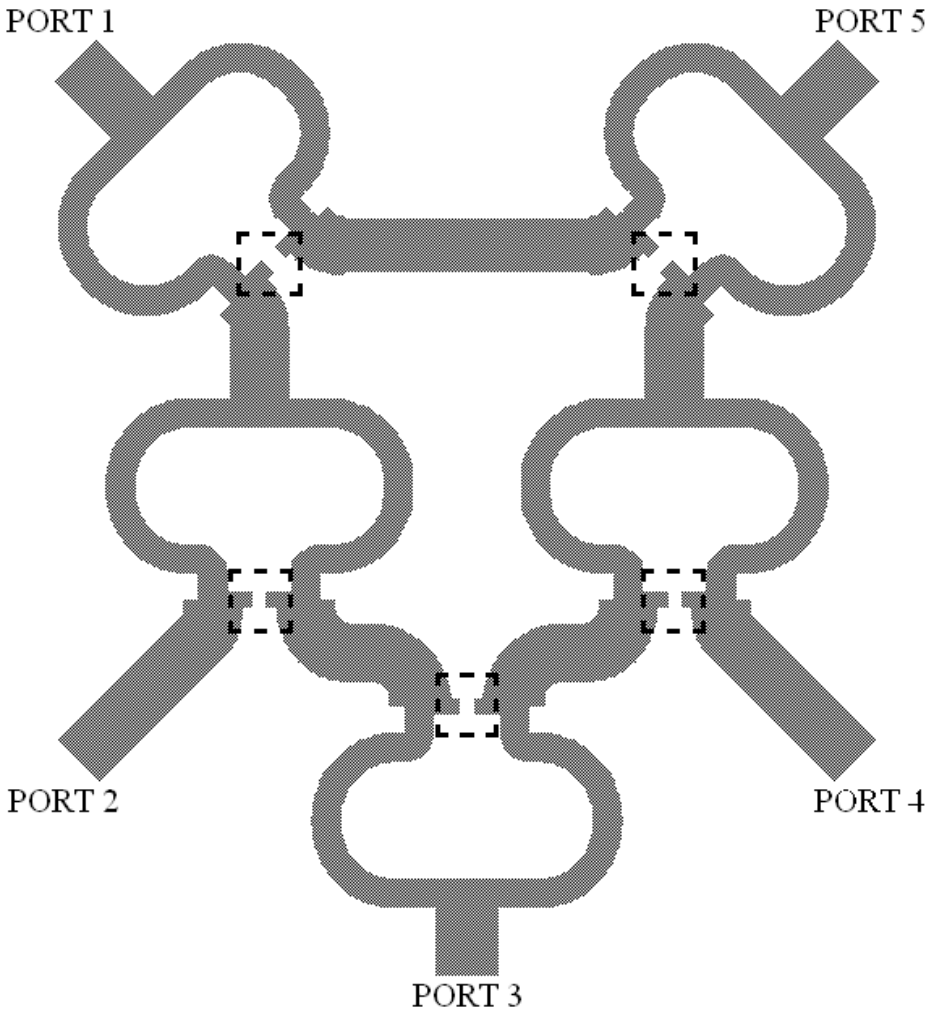

Figure 6-1 MICROSTRIP W-BCRCD CIRCUIT DIAGRAM The microstrip implementation of a W-BCRCD drawn out using Agilent's Momentum 2.5D electromagnetic simulator. The dashed boxes represent the location where surface mount resistors are placed.

Presented previously has been the development of concepts behind the Multi-Wilkinson Power Divider Based Complex Reflection Coefficient Detector, or W-BCRCD. This was followed up with computer simulations of the device's functionality. It has been observed that certain corrections need to be made to the design in order to account for ports receiving unequal power and for limitations in the usage of the law of cosines. Through these simulations it has been observed that there exists a correlation between S41 and the devices overall accuracy.

Presented herein will be the testing and analysis of the first generation prototype. The prototype is based upon the parasitic transmission line model simulated in Agilent's Advanced Design System. It is built on microstrip board having the characteristics stated in table T5-1, and using KOA 100 ohm 5% tolerance thick film, surface-mount resistors. The topography of the design can be seen in figure 6-1, where the pattern for the top conducting layer is shown. The dashed boxes show the gaps where the resistors are mounted. The fabricated prototype can be seen in figure 6-2, where it is shown connected to a 4-port network analyzer.

The analyzer in use, shown in figure 6-2, has 4-ports. Therefore when making S-Parameter measurements, one port needs to be terminated in a 50-ohm load. In this figure, port two is terminated in a wide-band 50-ohm load.

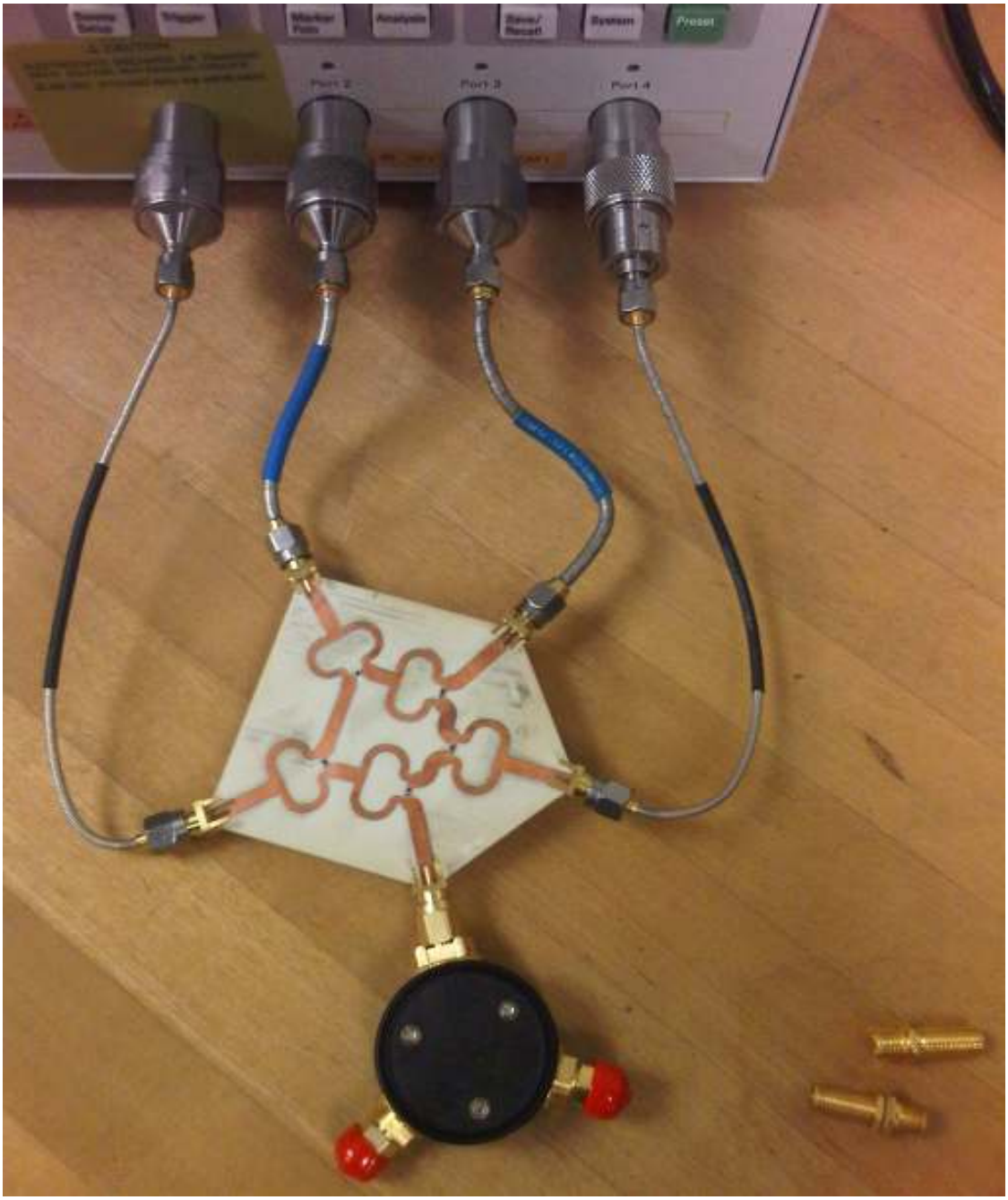

Figure 6-2 MICROSTRIP W-BCRCD CIRCUIT CONNECTED TO 4-PORT VNA

Picture of fabricated Wilkinson W-BCRCD connected to a 4-port network analyzer. Going around clockwise starting at the top port, the ports of the W-BCRCD are numbered 5, 4, 3, 2 and 1 respectively. Port 2 is terminated with a broadband 50-ohm load.

A. S-Parameter Measurement and Simulated Analysis

The W-BCRCD is a five port device, having an excitation input port (port 1), reflection port (port 5), an excitation signal portion measurement port (port 2), a reflected signal portion measurement port (port 4), and a combined signal portions measurement port (port 3). In order to measure the S-Parameters of the device using an available 4-port vector network analyzer, three separate sets of measurements were made. For each measurement, 4 out of 5 of the ports were connected to the network analyzer while one port was terminated in a 50-ohm broad-band load. This setup can be seen in figure 6-2, where port 2 is the terminated port. The missing S-Parameters from the first measurement were found in the subsequent measurements.

Figure 6-4 shows the resulting S-Parameters. In every measurement up to this point only certain S-Parameters were shown. This was due to the symmetry of the device, where port 5 and port 1, along with ports 2 and 4 were interchangeable (i.e. S54 was the same as S12, S52 was the same as S14, S11 was the same as S55, S31 was the same as S53, etc.). In the fabricated W-BCRCD, this assumption is lost due to three main factors.

First, the resistors used have a 5% tolerance. This means, most likely, each resistor in the circuit will have a different value; and therefore, each Wilkinson divider will have finitely different S-Parameters. Second, the connectors at each port are hand-soldered on. Since each port will have its own geometry for the solder joint, the connection will vary by some amount at each port. Third, there are points in the substrate which were etched into during fabrication. The non-uniformity of these etchings leads to non-uniformity in the performance of each Wilkinson.

Because of the lack of symmetry, it cannot be assumed that S21 and S45 have the same ratio to S31 and S35, respectively. This assumption was made in past chapters where α and β, from e4.1 and e4.2, were assumed to be equal. Now, e4.3 must be used instead of e4.4.

From the graphs in figure 6-3, it can be seen that at the center frequency there is 34 dB of isolation between ports 4 and 1, and 37 dB isolation between ports 5 and 2. This is less than all three of the simulations (66 dB for equation based model, 119 dB for the ideal transmission line model, and 40 dB for the parasitic microstrip model). As was shown, limited isolation is strongly correlated to points of inaccuracy.

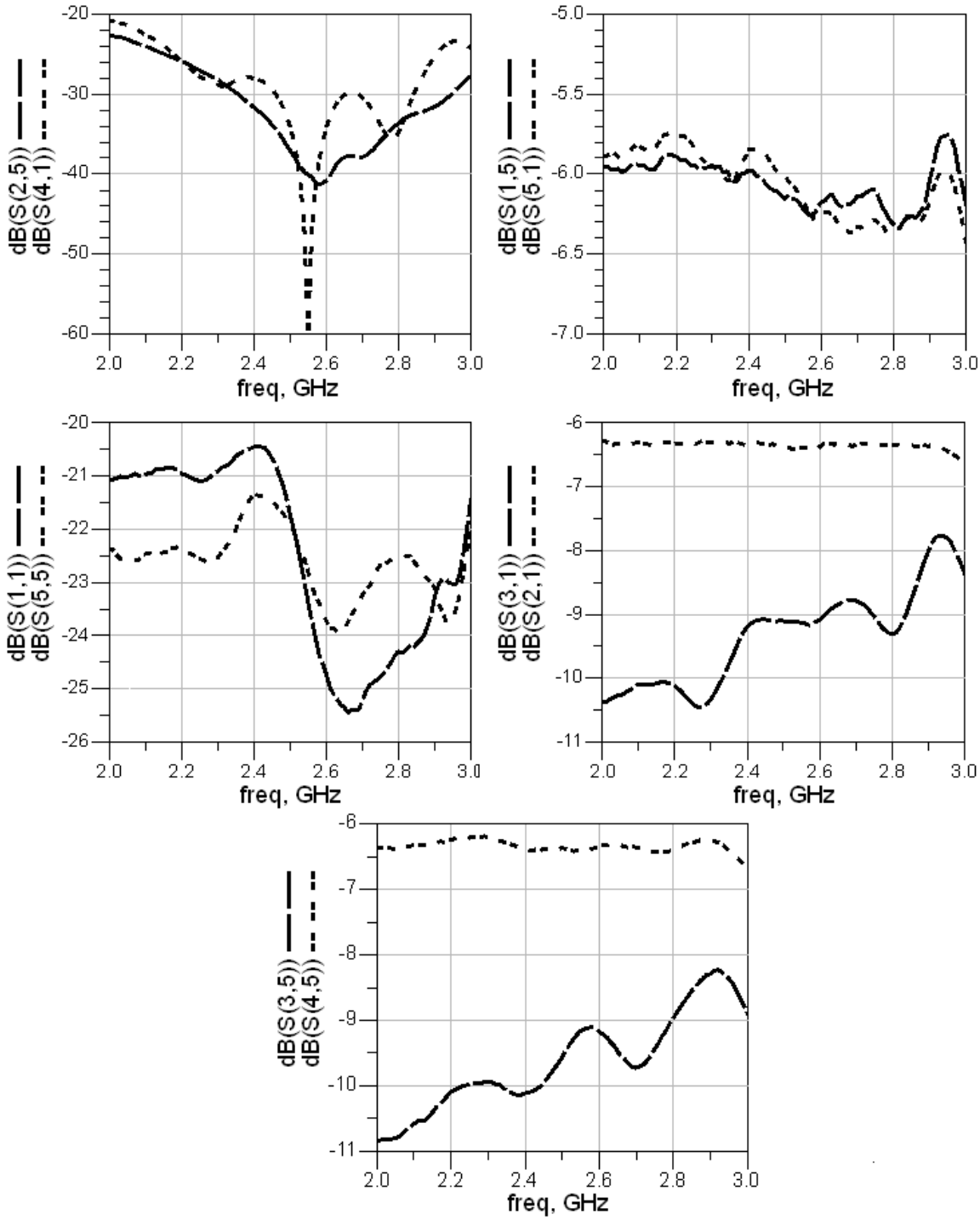

Figure 6-3 MICROSTRIP W-BCRCD S-PARAMETERS S-Parameters of the fabricated W-BCRCD. Due to resistor values, connector solder joints and substrate etching the W-BCRCD can no longer be assumed to be symmetric.

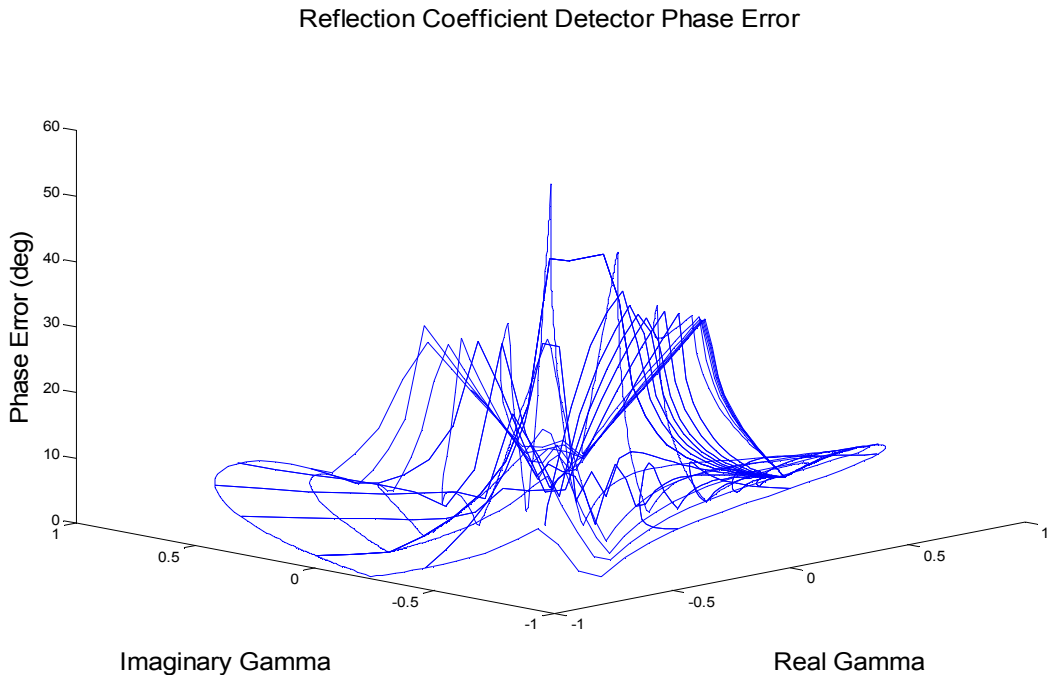

Figure 6-4 MICROSTRIP W-BCRCD PHASE ERROR Phase error of the W-BCRCD versus reflection coefficient at port 5. The detector has a maximum phase error of 52 degrees at the center, and a maximum phase error of 39 degrees away from the center.

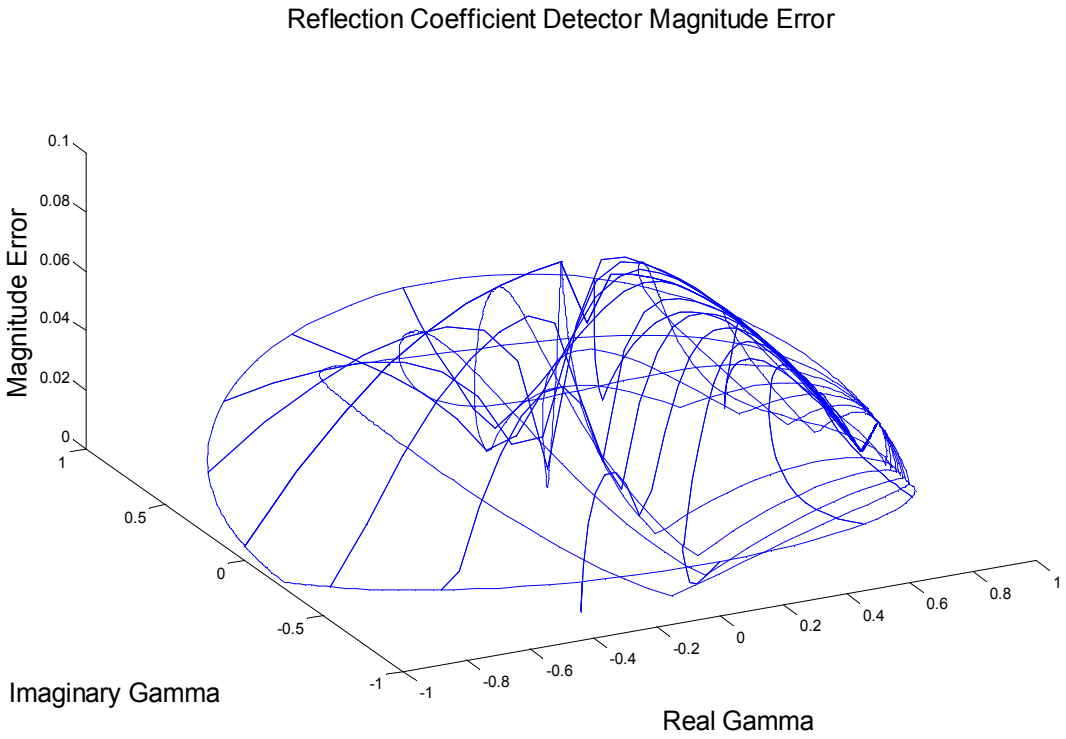

Figure 6-5 MICROSTRIP W-BCRCD MAGNITUDE ERROR Magnitude error of the W-BCRCD versus reflection coefficient at port 5. The detector has a maximum magnitude error of .082.

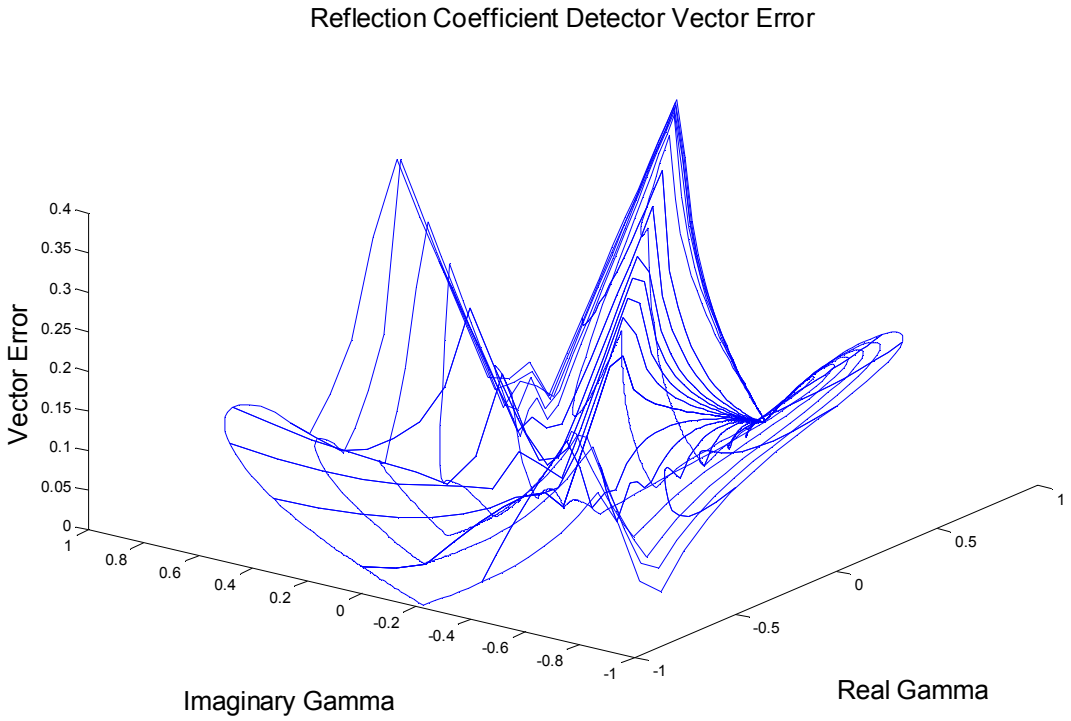

Figure 6-6 MICROSTRIP W-BCRCD VECTOR ERROR Vector error of the W-BCRCD versus reflection coefficient at port 5. The detector has a maximum vector error of 0.39. Like in the simulated designs, the vector error follows the phase error more than the magnitude error.

Figures 6-4, 6-5 and 6-6 show the phase error, magnitude error and vector error, respectively, of the W-BCRCD prototype. As is to be expected, the vector error is relatively high in comparison to the equation-based and ideal transmission line models. The error falls into the same range as that of the parasitic model, even though the parasitic model has higher amount of isolation. The difference being that the parasitic model is more predictable as the error jumps in three narrow regions, while the prototype shows more randomness. This can be seen in figure 6-7.

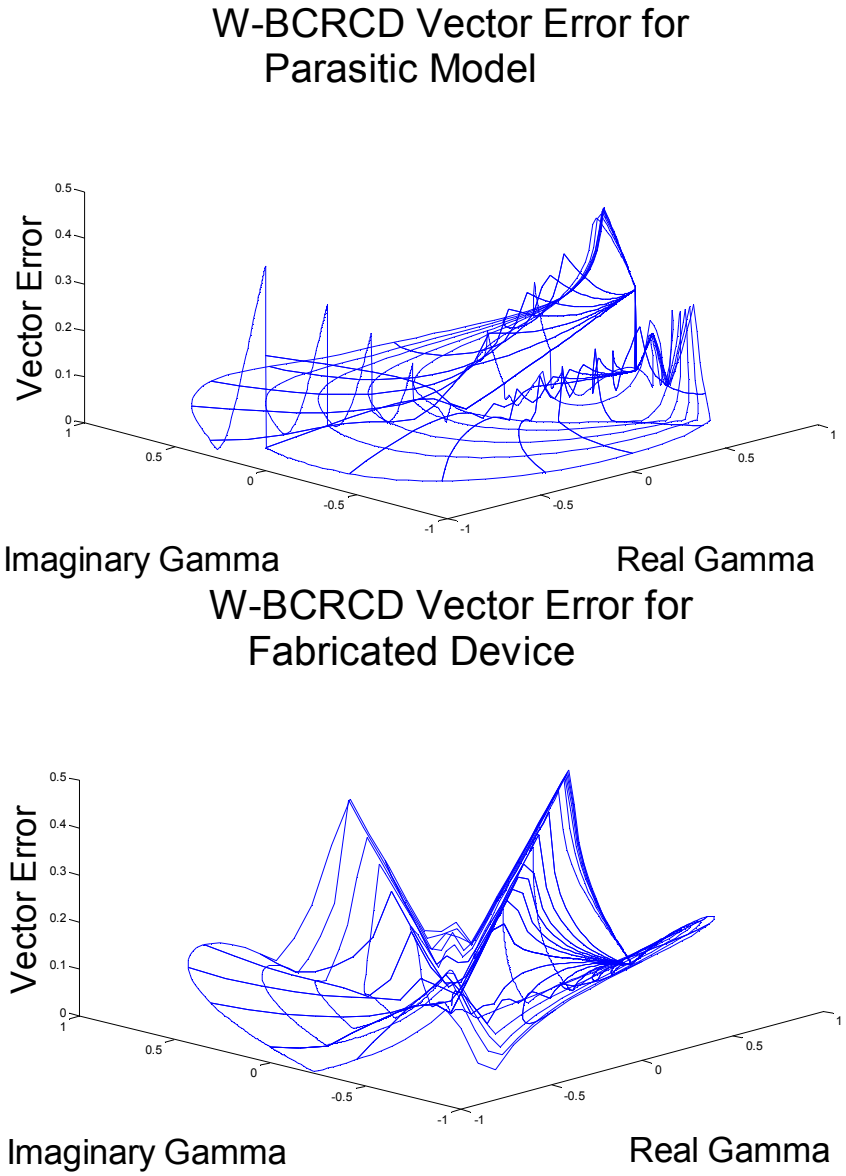

Figure 6-7 COMPARISON OF W-BCRCD PARASITIC AND FABRICATED VECTOR ERROR Side-by-side comaprison of the randomness of the W-BCRCD vector error for the parasitic model (left), and the prototype (right).

B. Off Frequency Analysis

From figure 6-3 it can be seen that there is an increase in the isolation between ports 4 and 1 as the device moves away from its center frequency of 2.5 GHz, towards 2.55 GHz. At the 2.55 GHz point the prototype gives an isolation of 60 dB between ports 4 and 1, and 40 dB isolation between ports 5 and 2. Figures 6-8, 6-9 and 6-10 show the resulting phase error, magnitude error, and vector error of the device if the operating frequency were to be shifted to 2.55 GHz.

As is to be expected with the higher isolation, the maximum phase error away from the center is about 11 degrees, as opposed to the 2.5 GHz operating point which gave a maximum error of 39 degrees. The vector error also shifted from having a maximum error of 0.39 to 0.18. In the shifted frequency, very little of the total error even goes above 0.08. However, the vector error still shows the same amount of randomness as the vector error at 2.5 GHz.

The magnitude error is a little different as its maximum value went up with the frequency shift, from a maximum of 0.082 to a maximum error of 0.090. However, the error high points of error fall into well defined regions based upon phase, and thus less random.

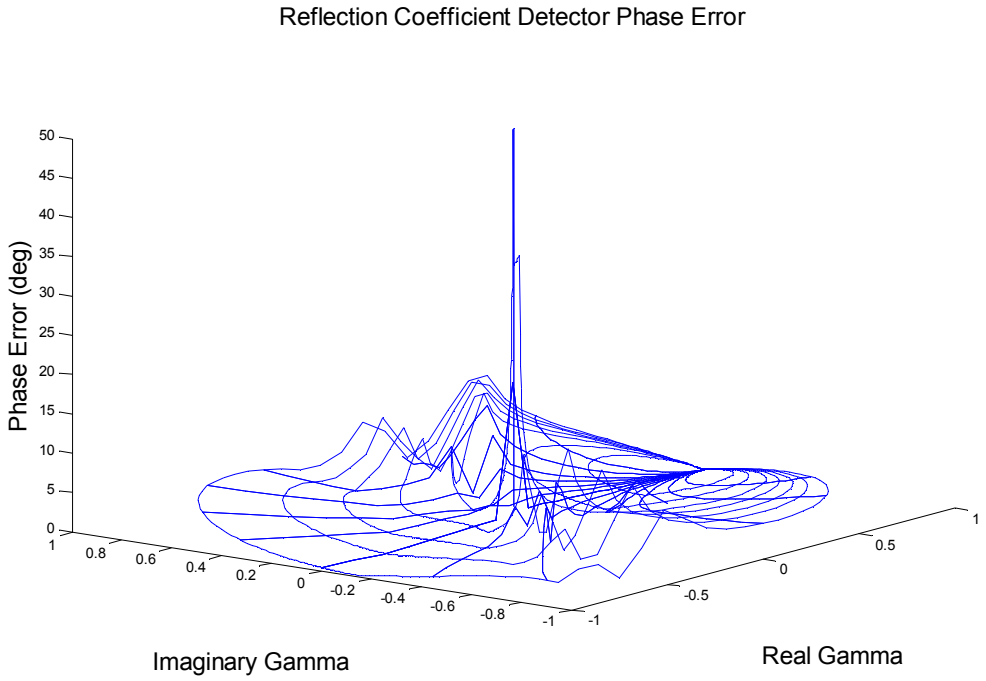

Figure 6-8 W-BCRCD PHASE ERROR AT 2.55 GHZ Phase error of the W-BCRCD with a center frequency of 2.55 GHz. At this frequency the detector has a maximum phase error of 52 degrees at the center, and a maximum phase error of 11 degrees away from the center.

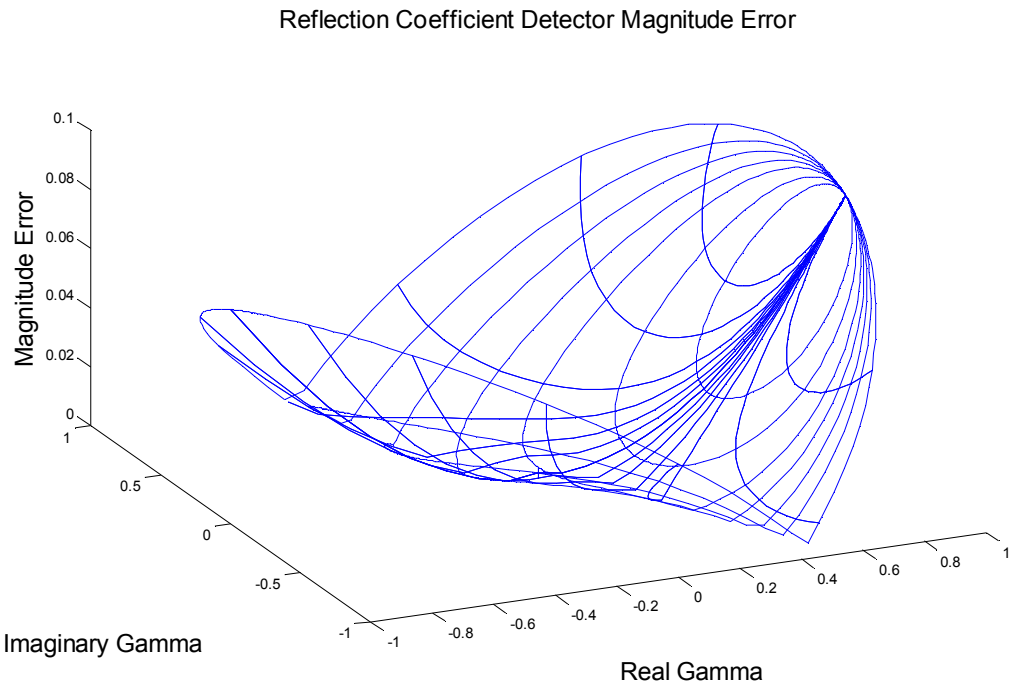

Figure 6-9 W-BCRCD MAGNTIUDE ERROR AT 2.55 GHZ Magnitude error of the W-BCRCD with a center frequency of 2.55 GHz. The detector has a maximum magnitude error of 0.09 at this frequency.

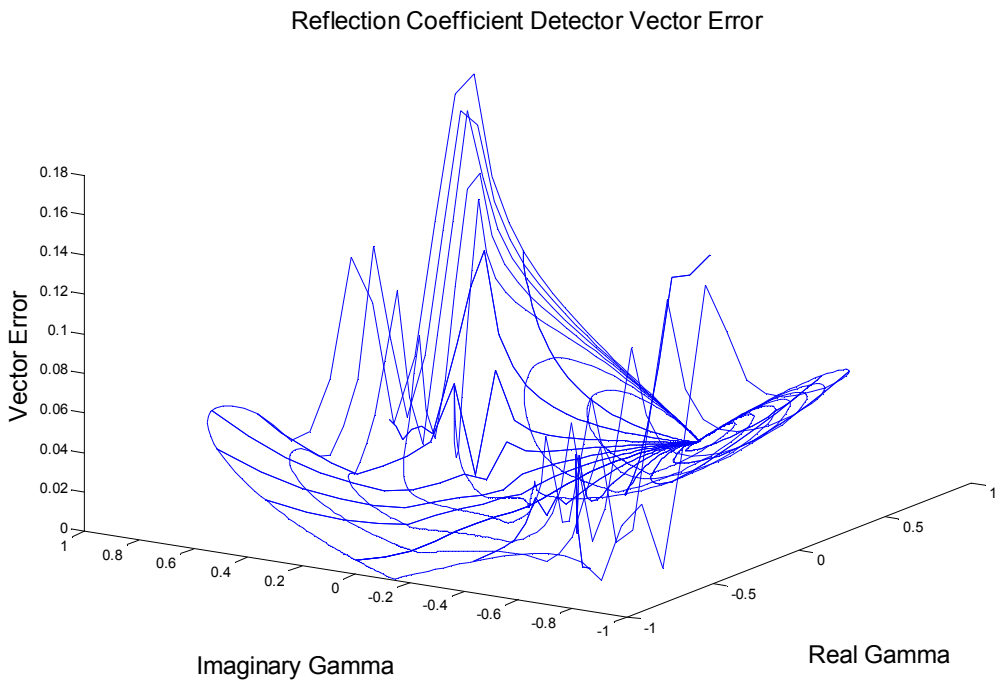

Figure 6-10 W-BCRCD VECTOR ERROR AT 2.55 GHZ Vector error of the W-BCRCD with a center frequency of 2.55 GHz. The detector has a maximum vector error of 0.18 at this frequency.

Since it can be seen that the performance of the W-BCRCD can change drastically from one frequency to another, it is worthwhile to look at the frequency response of the error. For this, the focus will be kept on the vector error, since it incorporates both the phase and magnitude errors. Also, since a high maximum error does not necessarily imply high inaccuracy, the analysis will be done using the average error over the entire Smith chart. How the average error is calculated is shown in appendix B. Figure 6-11 shows the average error for an 8% bandwidth around the center frequency.

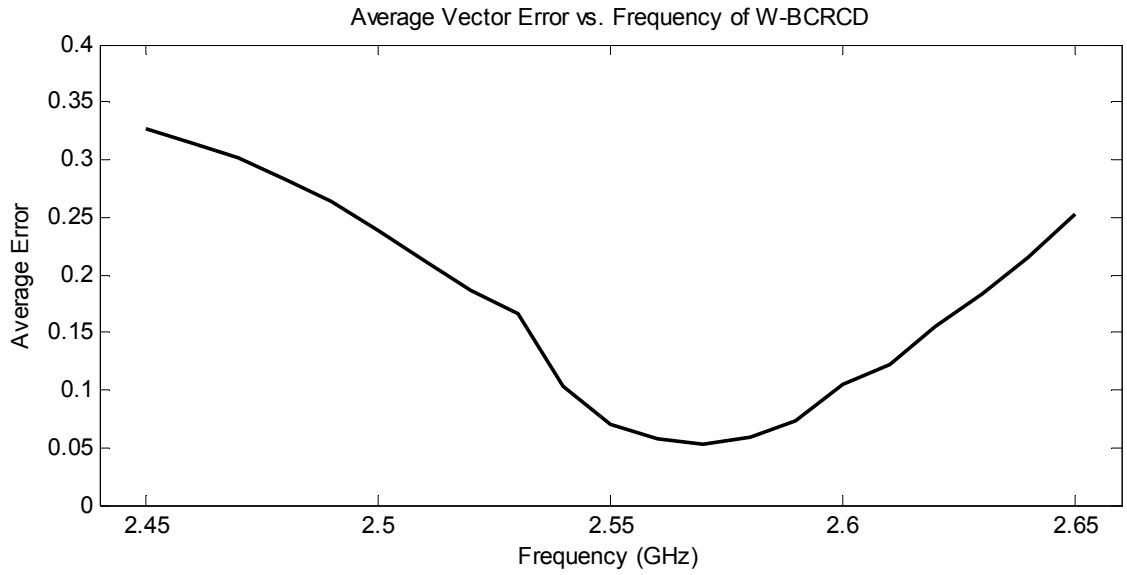

Figure 6-11 W-BCRCD VECTOR ERROR VS FREQUENCY The average vector error the W-BCRCD from 2.45 to 2.65 GHz. The minimum average error of 0.05 occurs at 2.57 GHz; with a bandwidth of 2.4% below an error of 0.1.

As was shown earlier, there exists greater accuracy at 2.55 GHz than at the center frequency of 2.5 GHz. However, unlike what was assumed from the isolation graph shown in figure 6-3, the minimum average error does not occur at 2.55 GHz, but at 2.57 GHz. Figure 6-12 shows the vector error of the W-BCRCD operating at 2.57 GHz.

The isolation decreases by about 20 dB from 2.55 to 2.57 GHz, and none of the other S-Parameters make much of a change. There is a drop in S(5,5); but chapter V showed that the magnitude of the input reflection at port 5 had little effect on the overall performance. Since the magnitudes of the S-Parameters do not explain why there is an improvement from 2.55 to 2.57 GHz, there is most likely an issue in phase interference. As the frequency changes, the wavelength of the signals, and therefore the phase shift

through the circuit, changes. At 2.57 GHz, there must be a set of leaked signals that line up perfectly to cancel each other out.

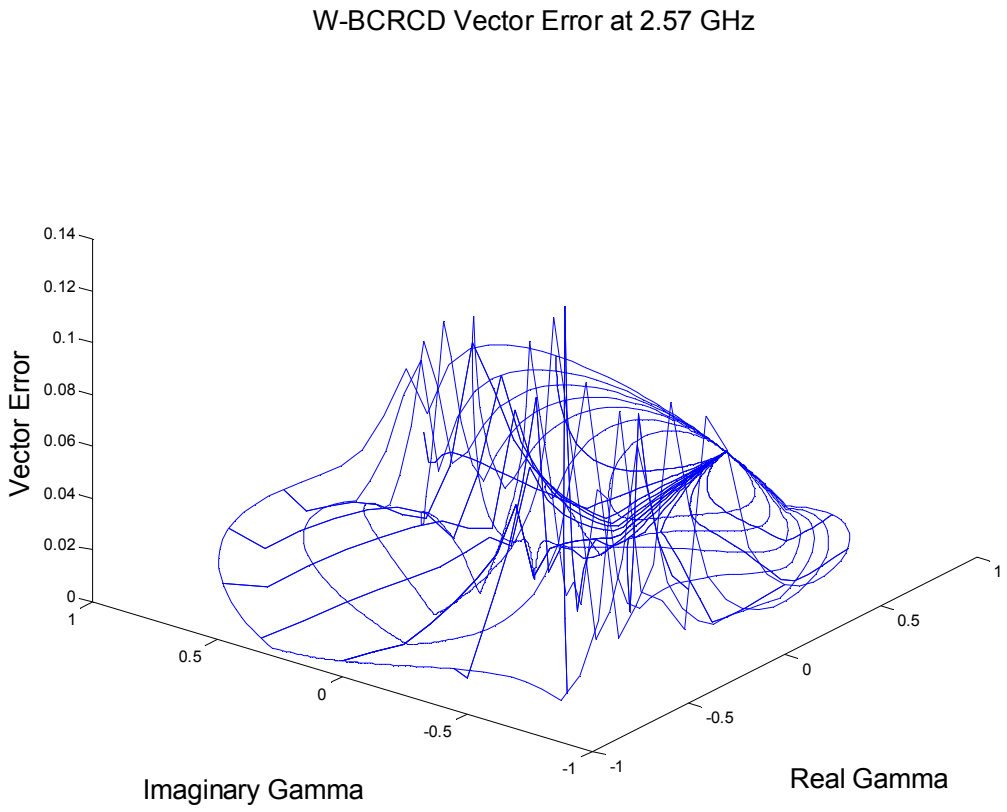

Figure 6-12 W-BCRCD VECTOR ERROR AT 2.57 GHZ The vector error of the W-BCRCD operating at 2.57 GHz. At this frequency there is an average error of 0.052, which is a 26% decrease in average error over the operating frequency of 2.55 GHz; and a 78% decrease over the operating frequency of 2.5 GHz.

C. Analysis Conclusions

The prototype has shown there will be some finite amount of error, even in the best working model. However, there are regions of the graph that are very flat with constant error; and, then there are regions, defined by phase, which have a very high error. This shows that the error is phase based. At the same time, shifting the frequency has been shown to change the accuracy of the W-BCRCD. And, shifting the frequency changes the wavelength of the test signal, and therefore the phase of the signal received at any given port.

From this, it can be concluded that the device has a high amount of potential. There exists the possibility that the error of the measurement could be drastically reduced by just taking multiple measurements at different frequencies; and making the conclusion based upon multiple measurements instead of one. Or, as mentioned in chapter IV section E, the reflected signal could be shifted by some amount through the use of a phase shifter, or transmission lines of variable length. Since the error appears to be phase based, possibly shifting out of the region of error could lead to a more accurate measurement, both for the phase and magnitude calculation.

More exactly, if the probe or material which causes the shifting has the ability to shift by small discrete values over a wide range, the phase could be shifted until the measured phase changes directly with the value of the shifting phase. This would be the region of highest accuracy. With the use of a simple calibration, such as TRL, and a phase shifting method, such as adjustable probe of quadrature phase shifter, in essence the points of major error could be removed from measurement.

The prototype has also shown that some amount of calibration is needed. The compensations that have been discussed, through chapters III, IV and V, all need to be done through the use of a standard. First, in order to test the isolation at port 4 from port 1, a calibration needs to be done using a matched 50 ohm termination at port five. This will also allow for the calculation of e4.1. Similarly, an open or short at port 5 will allow for a calculation to be done on the isolation between ports 2 and 5; as well as allowing the calculation of e4.2.

Now due to the points of high inaccuracy placed around the edges of the Smith Chart, it may also be prudent to use other calibration standards, such as a capacitor or inductor. These standards would correct for if the open and/or short loads fell into the regions of low accuracy. The capacitive and inductive loads would be in regions of high accuracy in this case.

However, the capacitive and inductive loads would be unnecessary if the probing port used a phase shifter. During calibration the phase shifter could simply move the open and short out of the inaccurate regions.

VII. Alternative Designs, Possible Applications, and Future Work

Chapters III through VI have shown presented a novel design and method for making electrical properties measurements. This has involved the conceptualization, design and analysis of a Wilkinson Power Divider Based Reflection Coefficient Detector. Through the design it has been shown that, with some inaccuracy and limitation, these measurements can be done without the use of expensive and bulky instruments, such as network analyzer.

This design has been done in the hope that it may broaden the applications in which measurements, normally constrained to well funded, immobile systems, can now be done in a broad manner of scenarios.

A. Alternative Designs

Because this design is very much based upon Wilkinson power dividers, and therefore very dependent upon the driving signal's wavelength, this device is very easily scalable. The wavelength of the signal is

$$\lambda = \frac{1}{2\pi \times f \times \sqrt{\varepsilon_{er}\varepsilon_0\mu}} \quad \text{(e7.1)}$$

Where λ is the wavelength of the excitation signal, f is the frequency in Hz of the excitation signal, ε_{er} is the effective relative permittivity of the microstrip board, ε_0 is the permittivity of free space, and μ_0 is the permeability of free space.

The specific substrate that was chosen for the microstrip, the usage of microstrip, and the center frequency of 2.5 GHz were all chosen because it kept the board large enough to make fabrication of the prototype easy. However, as can be seen in e7.1, the board is easily made smaller by increasing the operational frequency, using stripline instead of microstrip as it will increase the effective relative permittivity, using a substrate of higher relative permittivity, or by using a thinner substrate which will also increase the effective relative permittivity.

Other then size reduction, the board could be design to be a fully impedance measurement device, instead of just a reflection coefficient detector. This is done by adding surface mount diode detectors at each of the three measurement ports, adding an oscillator to the circuit, and maybe even adding some surface mount analog-to-digital converters and a microcontroller. All of these changes could be done based upon the required specifications of the application in which it will be implemented.

B. Possible Applications

As was mentioned in chapter I, the primary applications for this device are those which require higher frequency, complex measurements, but are not capable, nor conducive, to the use of network analyzers. These include applications which require

compact, light weight, cheap, and/or low power in order to make the appropriate measurements.

These applications can include bio-sensors. When monitoring a living organism, you want a system that is as non-invasive as possible. It would be a little ridiculous to have to strap a network analyzer on the back of a person in order to keep real-time track of that person's vitals; not to mention the extension cord. Instead it would be more practical to have a device similar to a wrist watch which is small and light weight. Also, when monitoring a large organism, such as a human being, there may be a need to track vitals at different points in the body. Once again, it could become costly and even more cumbersome to place probes all over the body. However, the Wilkinson Power Divider Based Complex Reflection Coefficient Detect could very easily be set-up as patches placed around the body. Other than the size, the relative cost of a single detector makes the dispersion of several of them across a system still cheaper than a network analyzer.

Other applications could include material testing, and system testing. When searching for imperfections in a dielectric, or when measuring changes in the input impedance of a transceiver, it is more important to note changes, and magnitudes in those changes, in the electrical properties than it is to measure an exact value of impedance or permittivity. For applications like these, where accuracy becomes less of an issue, this detector would excel greatly.

Of course, as has been reiterated multiple times earlier, this device is ideal for any application which requires higher frequency measurements (>300 MHz) testing of electrical properties in materials, loads, system, etc., but is limited by either size, cost,

power, or weight. And, being unconstrained as it is, this device has more possible applications than can be listed or thought of.

C. Future Work

In this paper, the functionality of the reflection coefficient detector has been tested through simulation. For each design, from equation based to prototype, the method of determining the phase, magnitude and vector error has been through the use of the device's S-Parameters and computer simulation. In order to further the innovation of this device it is necessary to make physical measurements. This will include the use of a signal generator, three coaxial diode detectors and an impedance tuner.

While making these measurements it will also be necessary to create a calibration technique for the device. This will include the design of a series of impedances, most likely an open circuit, short circuit, and broad-band load, but could also include a shunt capacitor or inductor. The advantage to using extra calibration loads would be to correct for the lack of distinction in the sign of a measured angle. This calibration would also include measuring power outputs on the three measurement ports in order to account for the compensations that were discussed earlier in this paper.

There is also a necessity to build a phase shifter into the design. In both of the prototype error calculations, and in the parasitic model error calculations, there were seen very distinct regions of high error. Because these regions are so well defined by regions of phase, it would be simple to remove them from the measurements by sampling shifting the reference plane to a point of stability on the Smith Chart.

As far as the creation of a second and third generation prototype, different variances could be attempted. First would be to try out the miniaturization, and broadband techniques discussed earlier in this chapter. After that, fully functional impedance measurement devices could be built using the design, which would include the use surface mount detectors and voltage sources, along with some sort of attached microcontroller.

Eventually, the device will be implemented in an applicable system. This system can range from any of the possibilities listed in the previous section. Most likely the device will first be used in a probing system for measuring the relative permittivity of dielectrics.

Bibliography

Pozar, David M, “Microwave Engineering Third Edition”, ©2005 John Wiley & Sons, Inc., ISBN 0-471-44878-8

Appendices

Appendix A: Understanding Vector Error

For every value of passive impedance that can be placed on the probing port of the reflection coefficient detector, there is a corresponding reflection coefficient value. Figure A-1 shows how a normalized impedance corresponds to a value of reflection.

When making measurements, using the reflection coefficient detector, there will always be some finite amount of difference between the reflection coefficient value found at the probing port, and the measured reflection coefficient value. This is the error of the device. For example, if an impedance of 1 + j*1 (normalized to the devices characteristic impedance) is found at the probing port, then a value of 0.649+ j*0.817 may be measured. In terms of reflection, this would be a reflection coefficient of 0.447∟63.4º with a measured value of 0.483 ∟86.9º. Figure A-2 shows the two points on the Smith chart. Figure A-3 represents the value of reflection for each of the normalized impedances. The circles represent the magnitude of the reflection coefficient; and the lines represent the phase of each reflection coefficient.

This error can be defined in three different ways. It could be defined as the difference between the magnitudes of the actual value and the measured value of the reflection coefficient. 1+j*1 has a magnitude of 0.447, and 0.649+ j*0.817 has a magnitude of 0.483. Therefore, at this value of reflection, there would be a magnitude error of 0.036. It could be defined as the difference between the actual value and measured value of the angle of the reflection coefficient. 1+j*1 has an angle of 63.4 º, and 0.649+ j*0.817 has an angle of 86.9 º. Therefore, at this value of reflection, there would be a phase error of 23.5 º. Figure A-3 shows the regions of magnitude error and phase

error. If given a magnitude error of 0.036 and a phase error of 23.5 º, an actual reflection coefficient value of 0.447∟63.4º could read out any value in between the two circles and in between the two lines.

The third method in defining the error would be to define a total error, which incorporates both the phase and the magnitude. This is done by finding the absolute distance between the actual value and the measured value. For an actual reflection coefficient of 0.447∟63.4º and a measured reflection coefficient of 0.483 ∟86.9º, the absolute distance between them would be 0.2. This absolute distance is denoted as the vector error.

If the normalized impedance of 1+j*1 were given a vector error of 0.2, then the measured value could lie on any point within a circles of radius 0.2 around the point 1+j*1. Figure A-4 shows the error region which encompasses all the possible values that may be measured.

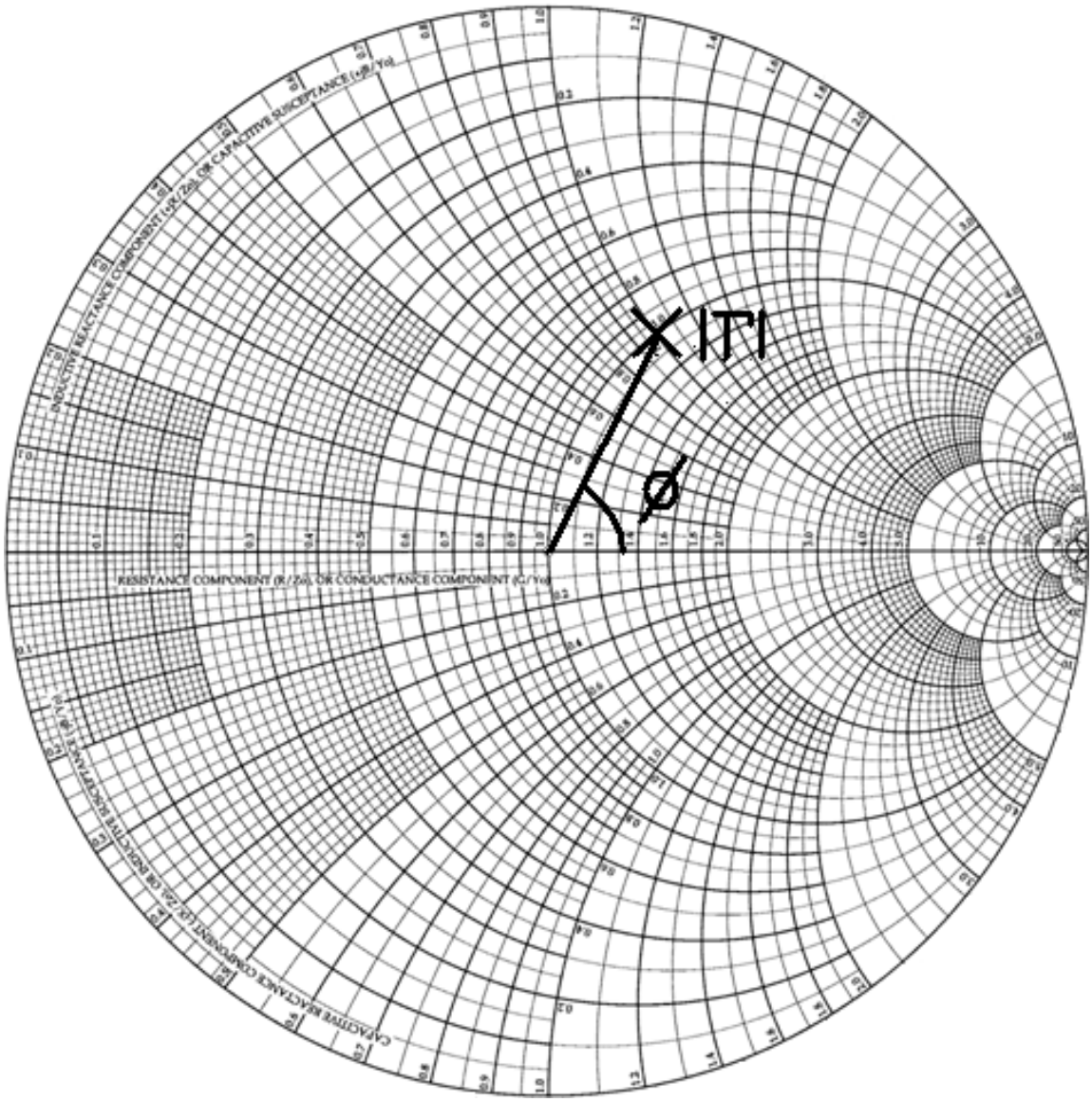

Figure A-1 SMITH CHART WITH PHASE AND MAGNITUDE OF A GIVEN GAMMA Picture of normalized, impedance-based Smith chart with a reflection coefficient value being represented. The value of reflection is denoted by its magnitude distance from the center and its phase. Each value of reflection corresponds to a given normalized impedance value. Here a gamma of $0.447 \angle 63.4^{\circ}$ corresponds to a normalized impedance of 1+j*1.

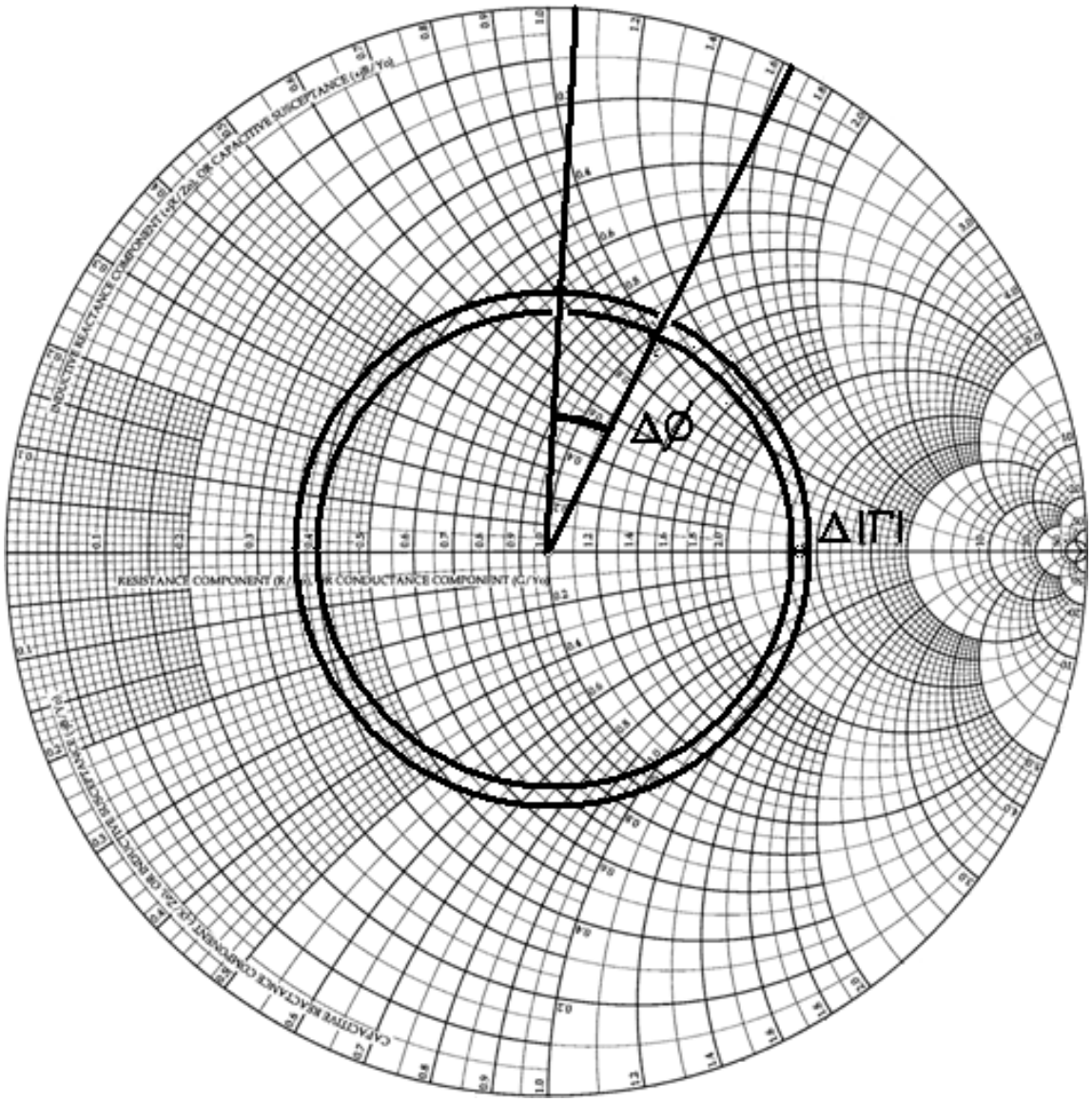

Figure A-2 SMITH CHART WITH PHASE AND MAGNITUDE DIFFERENCE BETWEEN ACTUAL GAMMA AND MEASURED GAMMA Picture of normalized, impedance-based Smith chart showing the magnitude and phase error between the normalized impedances 1+j*1 and 0.649+ j*0.817. The inner circle and right-most line represent the phase and magnitude, respectively, of 1+j*1; the outer circle and left-most line represent the phase and magnitude, respectively, of 0.649+ j*0.817.

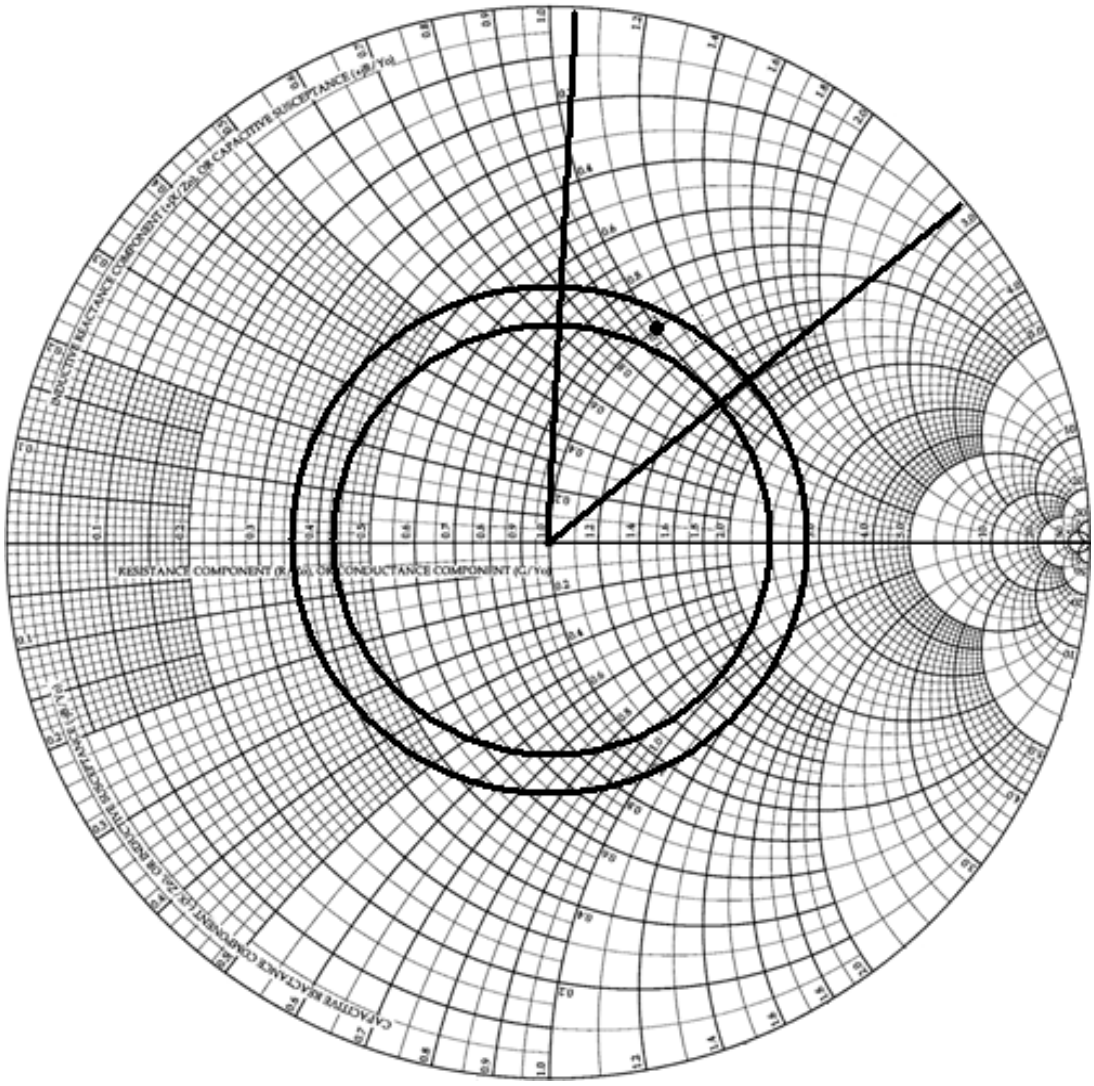

Figure A-3 SMITH CHART WITH PHASE AND MAGNITUDE OF GIVEN GAMMA'S FULL MAGNITUDE AND PHASE ERROR Picture of a normalized, impedance-based Smith chart with a defined region of phase error and magnitude error. For the normalized impedance of 1+j*1, the two circles encompass all the possible measured values if it had a reflection coefficient magnitude error of 0.036. The two lines encompass all the possible measured values if it had a phase error of 23.5º.

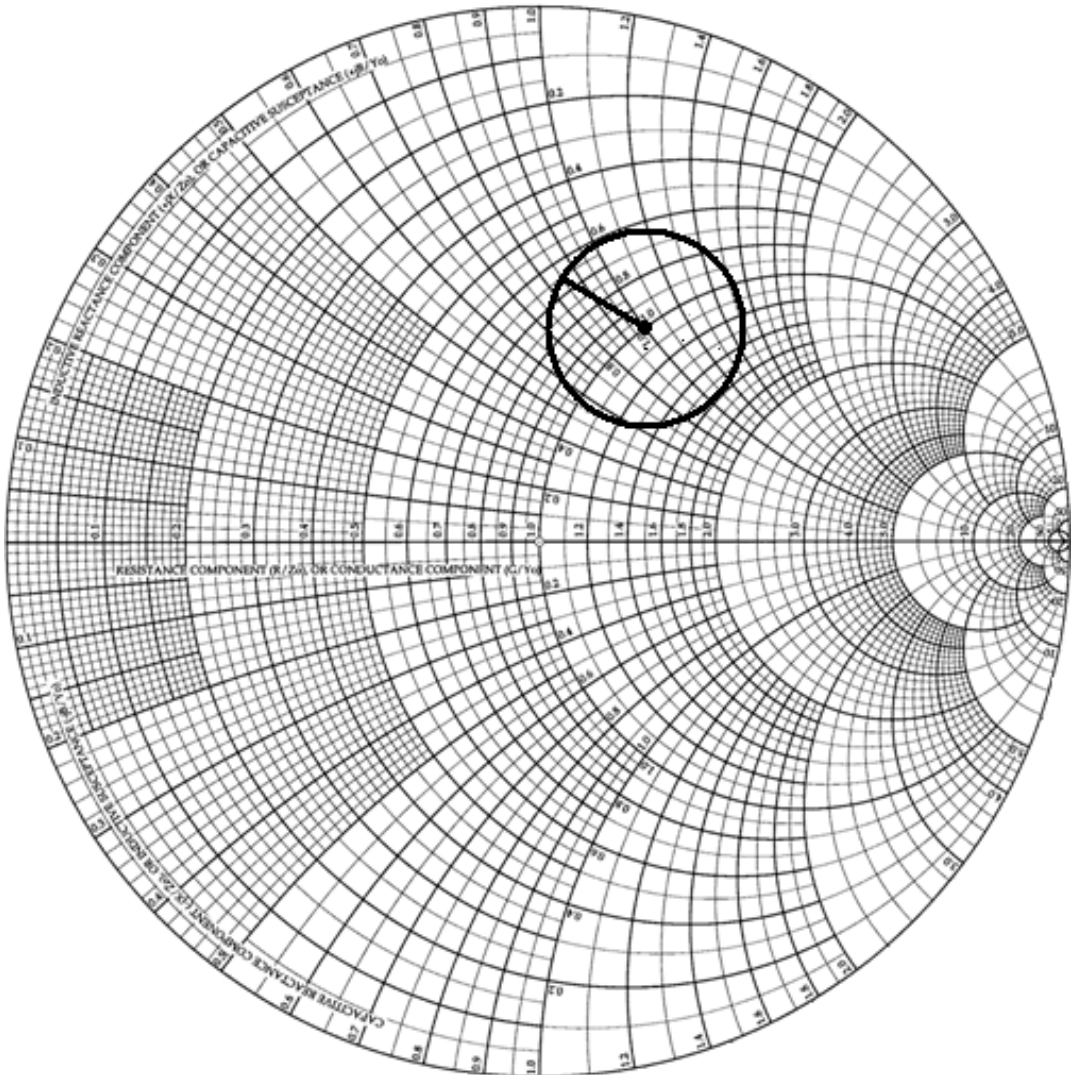

Figure A-4 SMITH CHART WITH TOTAL PHASE ERROR OF ACTUAL GAMMA

Picture of a normalized, impedance-based Smith chart with region of error based upon an actual load normalized impedance of 1+j*1 and a vector error of 0.2. The circle encompasses all possible values that may be measured based upon this load and vector error.

Appendix B: Defining Average Error

In order to perform frequency based analysis of the W-BCRCD, it is necessary to assign a numeric value to its performance. This value needs to quantitatively show the overall performance of the device. Therefore, this value is derived by calculating the average error of the entirety of the Smith Chart containing all Γ's $\leq$ 1.

This is first done by drawing a set of centric circles in the Γ-plane, which can be seen in fig B-1. The largest circle has a radius of 1. This corresponds to the circle on the Smith chart which represents a real impedance of zero. Like in the 3-D Smith chart plots from chapters IV, V and VI, the concentric circles are drawn into a third dimension. The z-axis represents the vector error at any given value of reflection coefficient. A concentric circle graph of vector error for the W-BCRCD at 2.57 GHz can be seen in fig B-2.

The area under each circle is found using Simpson's extended rule of integration. The volume between each circle is found by then multiplying that area by 2π and the separation between each circle. The volume under all the circles put together is then calculated by using Simpson's rule again. Finally, the average error is calculated by dividing the previous value by the area of the concentric circle graph; which due to the largest ring having a radius of 1 comes out to 2π.

This process is repeated, increasing the number of concentric circles and the number of points per circle each time, until the average area converged to within 3 digits of the largest non-zero digit.

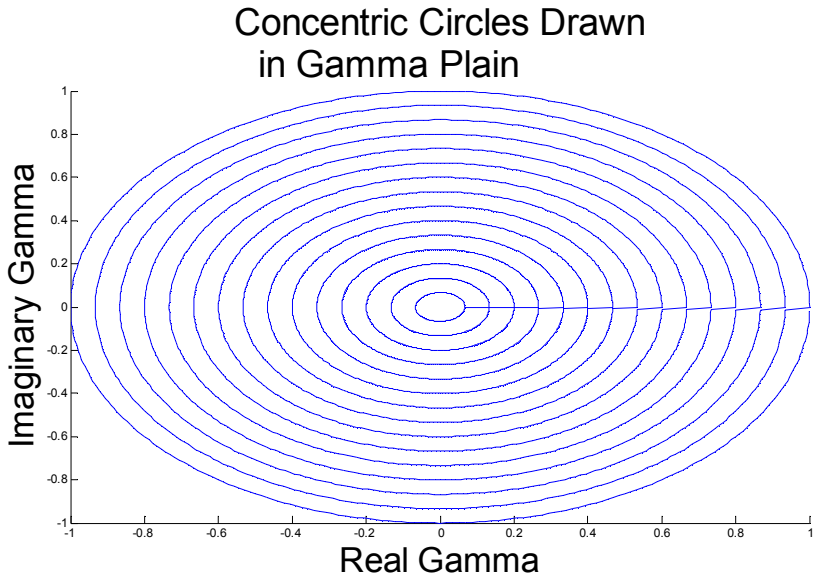

Figure B-1 CONCENTRIC CIRCLES IN GAMMA PLANE Concentric circles drawn in the gamma plain with the largest circle having a radius of 1. If overlaid with a Smith chart, the largest circle would overlay the real impedance equal to 0 line.

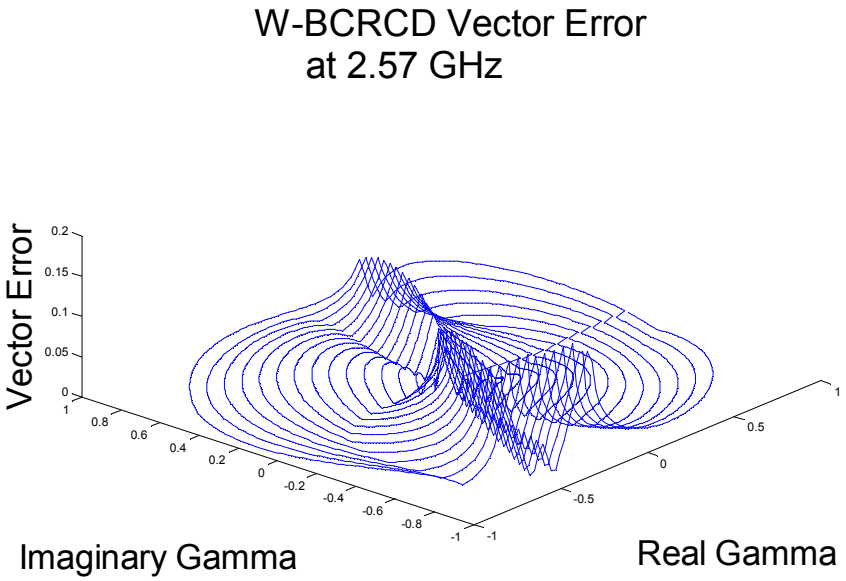

Figure B-2 CONCENTRIC CIRCLES IN GAMMA PLANE WITH W-BCRCD VECTOR ERROR The concentric circles from fig B1.1 drawn with a z-axis, which represents the vector error of the W-BCRCD at 2.57 GHz. The average height of all the circles is the average vector error of the device at this frequency.

Appendix C: Measurement and Calibration through Phase Shifting

In the design of the WBCRCD, there are two main problems which were found. The first has to do with the law of cosines. When calculating an angle using this method, the device is only able to calculate an absolute angle, i.e. it cannot distinguish the sign of the angle. The second problem is found in the performance of the realistic model and prototype. In both of these, there exist regions on the Smith chart which exhibit large amounts of error.

Both of these problems have the potential to be fixed using a single method: phase shifting. Between the testing port of WBCRCD and the object which is being tested, there is a need for some length of transmission line to connect the two. This length of transmission line could be converted into a phase shifter. This could be done through the use of a phase shifting circuit, the use of switches which guide the signal down different lengths of transmission line, the use of a low attenuating material with variable phase shifting capabilities, or some other means.

When a measurement of an object is made, the WBCRCD will read out a certain phase. This phase will always be in the range of 0 to 180 degrees. The object's actual reflection coefficient's phase shift has the potential to be in the range of -180 to 180 degrees. This problem arises because the equations used to determine the phase only return an absolute value of phase, not the sign of the phase.

The sign of the phase shift could be found my simply adjusting the phase by a known amount. If one of the methods mentioned above were used then the sign could be

determined by how the measured phase shifts in turn with the phase shifter's phase. An example would be if a device has a measured reflection coefficient phase shift of 45 degrees. A phase shifter, placed in between the measurement port of the WBCRCD and the probe connected to the measured device, could make a shift of positive 20 degrees. If the measured value of phase goes from 45 to 65 degrees, then we know that the sign of the phase is positive. If, however, the measured phase were to change from 45 degrees to 25 degrees with a positive 20 degree phase shift in the phase shifter, then it would conclude that the actual reflection coefficient phase is -45 degrees. This then solves the issue of only being able to read out a positive angle.

When a measurement of an object is made, there is a chance that the reflection phase shift falls into one of two regions of high error. Figure C-1 shows those regions. To the benefit of the device however, these regions are phase bound. This means that simply changing the measured phase will change the accuracy of the measurement. Also, outside of these regions, the WBCRCD has a consistent and low level of error. Shifting the phase could be used to both show whether the measured phase falls into a region of high error, and to move the measured phase into a region of low error for calculating the phase shift.

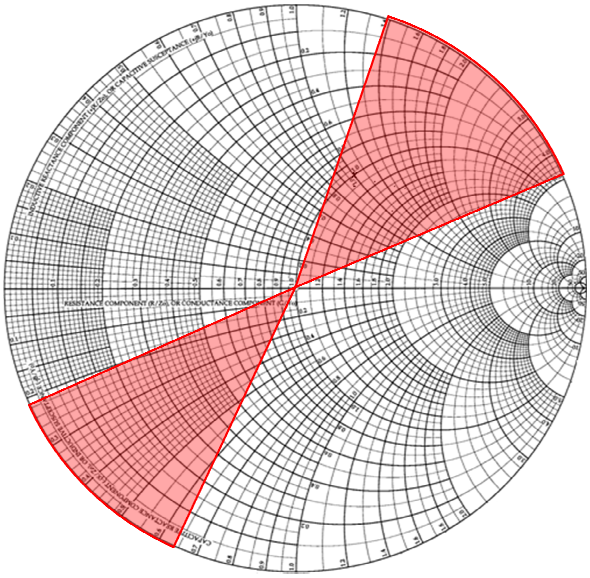

Figure C-1 PHASE BOUND REGIONS OF HIGH ERROR The two regions where the highest levels of inacuracy are found in the parasitic model and the generation 1 prototype. Notice that the regions are bound by lines of constant phase.

As an example, the material which has a measured phase of 45 degrees will be used again. And once again, the phase will be shifted by positive 20 degrees. If the measured phase shifts by positive 20 degrees, it is known that the measurement is made in a region of low error and high stability, and that the sign is positive. If the measured phase shifts by negative 20 degrees, it is known that the measurement is made in a region of low error and high stability, but that the sign is negative. If the phase shifts by a drastically different amount, or does not shift at all, it can be concluded that the

measurement is in a region of high error. In this case, the phase should be shifted another 20 degrees until the measurement falls into one of the first two cases.

Therefore, phase shifting allows for drastically increased amount of accuracy. This is done through both correcting for the law of cosines and by, for all practical purposes, removing the regions of high error.

Now, for the section of transmission line in between the measurement port and the object being measured, there will be innate phase shifting and attenuation. Also, within the WBCRCD itself, there will be unaccounted phase shifting and attenuation. All of these values will come into play in the calculating of measured reflection coefficient, for both the phase and the magnitude. To account for these values, a calibration will need to be done.

The standard calibration of an open, short and load will be most useful in calculating these values. However, due to the problems addressed above, just using these standards by themselves would not necessarily give the correct information. In order to account for the absolute phase issue and the high error region issue, phase shifting should also be incorporated. It will work in much the same way as the sign can be found and the measurement could be moved to a region of higher accuracy.

At the same time, these calibration measurements could be used to calibrate the phase shifters. It will be necessary for all three of the mentioned methods of phase shifting to calculate exactly how much phase shifting occurs versus how much is meant to occur.

About the Author

James Cooper was born in Bradenton, Florida and spent most of his childhood in the neighboring city of Palmetto. He received his B.S. and M.S. in Electrical Engineering at the University of South Florida. In the fall of 2010, he will be pursuing his Ph.D. at the Georgia Institute of Technology. He began his work in Wireless and Microwave engineering as a sophomore in his undergraduate studies under Dr. Thomas Weller. Since that time, he has authored one publication and co-authored two more. He has also orally presented at one conference and four workshops.

Upon entering graduate school, James was awarded with an NSF fellowship through the University of South Florida. This fellowship involved working closely with local elementary schools in order to bring high level engineering concepts to the classroom. Upon completion of his M.S., James was awarded with the NSF Graduate Research Fellowship for pursuing his Ph.D.